THE UNIVERSITY OF MICHIGAN

INDUSTRY PROGRAM OF THE COLLEGE OF ENGINEERING

# DISPERSION COEFFICIENTS FOR GASES FLOWING IN CONSOLIDATED POROUS MEDIA

Max Wilhelm Legatski

A dissertation submitted in partial fulfillment
of the requirements for the degree of
Doctor of Philosophy in the
University of Michigan
Department of Chemical and Metallurgical Engineering
1966

February, 1966

IP-729

# ACKNOWLEDGEMENTS

The author wishes to express his appreciation to the many people who have contributed to this work. Their advice, interest, patience, and moral support have been instrumental in the completion of this manuscript.

Professor Donald L. Katz, as chairman of the committee, has been generous with his advice and assistance. His astute guidance has enhanced this manuscript.

Associate Professor Robert H. Kadlec has contributed unselfishly of his time and ability. His guidance during critical stages of the experimental work was an important factor in the development of the experimental and mathematical techniques ultimately employed.

Professor M. Rasin Tek has contributed materially to this dissertation by his donation of both time and moral support.

Associate Professor Herman Merte, Jr., and Assistant Professor James O. Wilkes have offered helpful criticisms and suggestions.

Messrs. Cleatis Bolen, John Wurster, Peter Severn, Robert Reed, Douglas Connell, and Elmer Darling of the Chemical and Metallurgical Engineering Department provided valuable assistance in the construction of experimental apparatus.

The Michigan Gas Association has made this manuscript possible by providing a generous fellowship during four years of graduate study.

Mr. William H. McDougald provided valuable assistance in constructing an instrumentation and control system for the experimental apparatus.

Continental Oil Company and the United States Bureau of Mines provided core samples used in the experimental work.

Professor G. Brymer Williams, Mr. L. Karl Legatski, Mr. L. Kent Thomas, and Mr. Finis E. Carleton, III have provided valued advice and moral support.

The Industry Program of the College of Engineering has done an excellant job of producing this manuscript in its final form.

My parents have made this work possible by their unselfish financial and moral support during the past 26 years.

My wife, Pat, and my son, Scott, to whom this manuscript is dedicated, are due particular gratitude. Their inspiration, confidence, moral support, and patience have made this dissertation not only possible, but worthwhile.

TABLE OF CONTENTS

LIST OF FIGURES

LIST OF FIGURES CONT'D



LIST OF FIGURES - APPENDICES

# LIST OF TABLES

NOMENCLATURE

| Symbol | | Definition |
|---|---|---|
| $A$ | = | cross sectional area ($L^2$) |
| $a_p$ | = | particle radius (L) |
| $C$ | = | capacitance (microfarads) or concentration (vol. fr.) |
| $C_A$ | = | concentration of component A |
| $d_p$ | = | particle diameter (L) |
| $D, D_A$ | = | longitudinal or transverse dispersion coefficient ($L^2T^{-1}$) |
| $D_o, D_{A_o}$ | = | molecular diffusion coefficient ($L^2T^{-1}$) |
| $D_\ell, D_{A\ell}$ | = | longitudinal dispersion coefficient ($L^2T^{-1}$) |
| $D_t, D_{At}$ | = | transverse dispersion coefficient ($L^2T^{-1}$) |
| $f$ | = | fraction of void volume inaccessible to bulk flow |
| $F$ | = | electrical resistivity factor |
| $K$ | = | permeability ($L^2$) |
| $L$ | = | specimen length (L) |
| $\mathcal{M}_K$ | = | $\int_o^\infty (t-\mu)^K f(t)dt \Big/ \int_o^\infty f(t)\,dt$ $\quad (T^K)$ |
| $M'_K$ | = | $\int_o^\infty t^K f(t)dt$ $\quad (T^K)$ |
| $M_K$ | = | (scale factor) $\times M'_K$ $\quad (T^K)$ |
| $M$ | = | molecular weight |
| $m$ | = | power dependence of dispersion upon Peclet number |
| $P$ | = | pressure ($FL^{-2}$) |
| $Pe$ | = | Peclet Number, $d_p u/D_o$ or $u d_p \sigma/D_o$ |
| $q$ | = | injection rate ($L^3T^{-1}$) |
| $R$ | = | gas constant or resistance (megohm) |

| Symbol | | Definition |
|---|---|---|
| $Re$ | = | Reynolds Number |
| $r$ | = | radius (L) |
| $T$ | = | temperature |
| $t$ | = | time (T) |
| $t'$ | = | $t - \mu_{est.}$ (T) |
| $\bar{t}$ | = | mean residence time (T) |
| $u$ | = | interstitial velocity ($LT^{-1}$) |
| $\vec{V}$ | = | vector velocity ($LT^{-1}$) |
| $V$ | = | void volume ($L^3$) |
| $v$ | = | linear (superficial) velocity ($LT^{-1}$) |
| $v'$ | = | volumetric flow rate ($L^3T^{-1}$) |
| $v''$ | = | mixing cell volume ($L^3$) |
| $W$ | = | mass flow rate |
| $z$ | = | compressibility factor |
| $x,y,z$ | = | rectangular coordinates |
| $r,\theta,z$ | = | cylindrical coordinates |
| $r,\theta,\phi$ | = | spherical coordinates |
| $\beta$ | = | turbulence factor ($L^{-1}$) |
| $\phi$ | = | void fraction, or porosity |
| $\rho$ | = | density ($ML^{-3}$) |
| $\mu'$ | = | viscosity ($ML^{-1}T^{-1}$) |
| $\mu$ | = | mean residence time (T) |
| $\sigma$ | = | packing, or inhomogeneity, factor |
| $\sigma'$ | = | mass transfer coefficient |
| $\sigma_t^2$ | = | variance of f(t) about mean, $\mu$ ($T^2$) |
| $\Delta\sigma^2$ | = | relative variance change, $\Delta\sigma_t^2(u/L)^2$ |
| $\psi$ | = | particle sphericity |

# I. INTRODUCTION

Mixing of miscible fluids flowing through porous media has been studied extensively by the petroleum industry and by the chemical industry. Investigators in these fields have been concerned with the behavior of reservoir fluids during miscible secondary recovery operations and with the behavior of fluids flowing through packed columns. While the petroleum industry has studied dispersion in liquid systems flowing through both consolidated and unconsolidated porous media, the chemical industry has investigated both liquid and gaseous systems in unconsolidated porous media.

The gas storage industry, however, is interested in the behavior of gaseous systems flowing through consolidated porous media, a process which has not been studied extensively to date. In one case of interest, the United States Bureau of Mines is storing vast quantities of a rich helium-nitrogen gas in contact with a natural gas in a dolomite reservoir. Since the rich gas occupies only 15% of the total reservoir volume, it is essential that the extent of rich gas-natural gas mixing be predicted and understood as a function of rock properties, pressure, and rate of movement.

The natural gas companies of the midwest also have an important stake in the understanding of gas mixing. Natural gas from the southwest is commonly stored during the summer in depleted reservoirs in Michigan or aquifers in Illinois for later use during winter peak loads. A portion of the gas stored in such reservoirs will be entrapped and lost when the reservoir is finally abandoned. If it were

possible to use a cheaper gas (e.g. flue gas) as a cushion, the effective capital investment for the operation would be reduced considerably. There are also many occasions when it would be helpful to be able to predict gas mixing in the reservoir, such as in evaluating the stripping of liquids when recycling gas through the reservoir.

It was the purpose of this research to develop an understanding of gaseous mixing for flow through consolidated porous media, using both the existing literature and experimental measurements. Emphasis was placed upon an experimental technique for conveniently measuring the dispersion coefficient for a variety of gas systems and porous media and a range of flow rates.

## II. DISPERSION COEFFICIENTS; THEIR USE AND LIMITATIONS

It is pertinent, before discussing the experimental evaluation of dispersion coefficients, to survey the significance of these coefficients and the limitations implied by their use. It is the purpose if this section to make such a survey, and to briefly describe the ultimate use of dispersion coefficients.

### A. The Continuity Equations

For mass transfer due to bulk flow and diffusion, with no generation of a component by chemical reaction, the general equations for the conservation of mass in various coordinate systems may be written as follows:

1. General

Accumulation = bulk flow terms + diffusion terms (1)

2. Rectangular Coordinates

$$\frac{\partial C_A}{\partial t} = -\left(v_x \frac{\partial C_A}{\partial x} + v_y \frac{\partial C_A}{\partial y} + v_z \frac{\partial C_A}{\partial z}\right) + D_{A_0}\left(\frac{\partial^2 C_A}{\partial x^2} + \frac{\partial^2 C_A}{\partial y^2} + \frac{\partial^2 C_A}{\partial z^2}\right) \quad (2)$$

3. Cylindrical Coordinates

$$\frac{\partial C_A}{\partial t} = -\left(v_r \frac{\partial C_A}{\partial r} + \frac{v_\theta}{r} \frac{\partial C_A}{\partial \theta} + v_z \frac{\partial C_A}{\partial z}\right) + D_{A_0}\left[\frac{\partial}{r \partial r}\left(r \frac{\partial C_A}{\partial r}\right) + \frac{\partial^2 C_A}{r^2 \partial \theta^2} + \frac{\partial^2 C_A}{\partial z^2}\right] \quad (3)$$

4. Spherical Coordinates

$$\frac{\partial C_A}{\partial t} = -\left(v_r \frac{\partial C_A}{\partial r} + \frac{v_\theta}{r} \frac{\partial C_A}{\partial \theta} + \frac{v_\phi}{r \sin\phi} \frac{\partial C_A}{\partial \phi}\right) + D_{A_0}\left[\frac{\partial}{r^2 \partial r}\left(r^2 \frac{\partial C_A}{\partial r}\right) + \frac{\partial}{r^2 \sin\theta \partial \theta}\left(\sin\theta \frac{\partial C_A}{\partial \theta}\right) + \frac{\partial^2 C_A}{r^2 \sin^2\theta \partial \phi^2}\right] \quad (4)$$

5. Vector Notation

$$\frac{\partial C_A}{\partial t} = -\vec{V} \cdot \nabla C_A + D_{A_0} \nabla^2 C_A \quad (5)$$

where $C_A$ = concentration of component $A$, lb/cu. ft.

$x, y, z$ = rectangular coordinate directions, ft.

$D_{A_o}$ = diffusivity of component $A$ in solution, $ft^2/hr.$

$r, \theta, \phi$ = spherical coordinates, ft.

$r, \theta, z$ = cylindrical coordinates, ft.

$t$ = time, hours

$v$ = bulk flow velocity component, ft./hr.

$\vec{v}$ = vector velocity ($v_x, v_y, v_z$), ft./hr.

$\nabla$ = vector operator

In the usual context of molecular diffusion only, the symbol $D_{A_o}$ represents the molecular diffusivity of component $A$. For fluids flowing through a porous medium, the symbol $D_A$ may be used to represent a dispersion coefficient; the term "dispersion," as opposed to "diffusion," implies flow conditions. Further, the subscript "A" may be neglected if the identity of the diffusing gas is understood.

B. Longitudinal and Transverse Dispersion

It is also necessary to distinguish between a "transverse dispersion coefficient" and a "longitudinal dispersion coefficient" for flow through porous media. It has been found that the coefficient characterizing dispersion in the direction of bulk flow (longitudinal) can be an order of magnitude greater than the coefficient characterizing mixing perpendicular to the direction of flow (transverse)[10,43]. We shall use the subscripts "$\ell$" and "$t$" to denote longitudinal and transverse dispersion, respectively; this work is concerned with the determination of longitudinal dispersion coefficients.

To summarize, the nomenclature used throughout this report is as follows:

$D_o$ = molecular diffusion coefficient in the absence of a porous matrix,

$D_t$ = transverse dispersion coefficient, and

$D_\ell$ = longitudinal dispersion coefficient.

The symbols $E$ and $K$ are also found in the literature representing dispersion coefficients.

For mass transport in a single direction in a porous medium, with bulk flow, Equation 2 for rectangular coordinates reduces to

$$\frac{\partial C_A}{\partial t} = - v_x \frac{\partial C_A}{\partial x} + D_{A\ell} \frac{\partial^2 C_A}{\partial x^2} \qquad (6)$$

C. The Capacitance Model

Equations 2-6 imply an "ideal" displacement; i.e. the diffusion term in each equation represents mass transport obeying Fick's Law of Diffusion. Fick's Law assumes that there is no gross bypassing of one fluid by another, and that there are no stagnant pockets of gas in the system under consideration. These assumptions are not always valid for flow through porous media, and it is important to recognize the limitations upon Equations 2-6.

Figure 1, "Capacitance Model," schematically illustrates a capillary tube having a volume which is inaccessible to bulk flow. Flow through a capillary system of this sort would not be expected to obey Fick's Law, although under certain conditions Fick's Law may hold

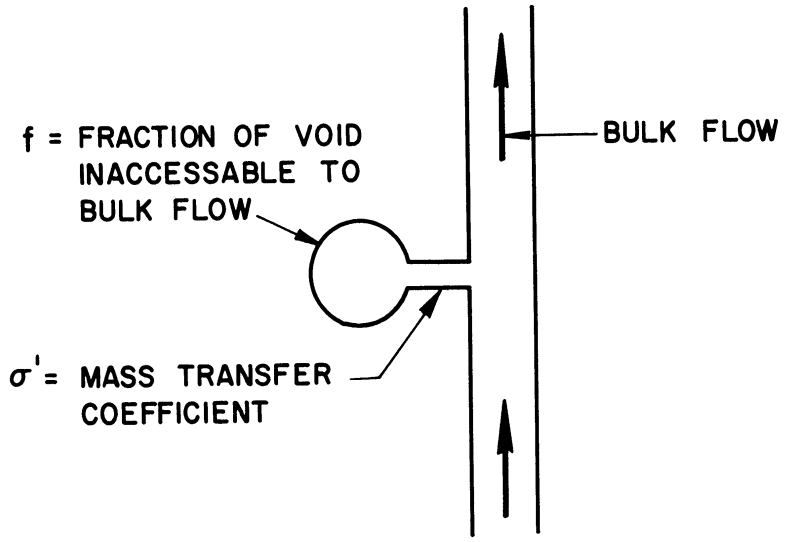


Figure 1. Capacitance Model.

as a valid approximation. The capacitance model has been studied by Coats and Smith[18].

Dispersion in a dead-end capillary system would necessarily be characterized by three parameters. In addition to the dispersion coefficient, $D_\ell$, which characterized mixing in a simple capillary model, the dead-end capillary model would assume that a certain fraction, $f$, of the total void volume of the system was inaccessible to bulk flow, and that a mass transfer coefficient, $\sigma'$, existed to describe molecular transport between the inaccessible portion and the mainstream of flow. Thus the capacitance model would be expected to describe mixing better than a simple linear (Fick's Law) model by virtue of the additional parameters characterizing the system.

We can make two observations which indicate that Fick's Law is a valid approximation for most of the systems studied in this research program. First, we would expect the void fraction inaccessible to bulk flow to be small for sandstones. For limestones and dolomites, however, considerable error might be encountered by neglecting the inaccessible void fraction, $f$.

Second, for gaseous systems we would expect the mass transfer coefficient, $\sigma'$, characterizing molecular transport between the inaccessible volume and the mainstream flow, to be large. Thus, except for liquid systems or gaseous systems at high pressures, we may expect the capacitance model to contribute little to our description of dispersion in a porous medium. For the limiting case of $f = 0$ and $\sigma' \to \infty$, the capacitance model would reduce to a Fick's Law model.

D. Mixing Cell Model and Dispersion Model

A number of authors[6,40,43] have pursued the mixing problem not in terms of the so called "dispersion model" described by Equations 1-6, but in terms of a "mixing cell model." This model supposes that a porous medium is constructed of a large number of small mixing chambers, and that the concentration of the diffusing component within each mixing chamber is given by

For a series of $n$ perfect mixing cells, Aris and Amundson[2] have shown that the concentration of diffusing component in the mixing chamber is given by

$$C_n = 1 - e^{-qt/v''}\left[\sum_{n=1}^{n} \frac{(qt/v'')^n}{n!} + 1\right] \qquad (7)$$

where $q$ = injection rate,

$t$ = time, and

$v''$ = volume of each cell.

This model is discussed further in Section III of this manuscript.

E. Linearity

A second assumption of Equations 2-6 is that the dispersion coefficient, $D_{A\ell}$, is independent of the concentration of $A$, i.e. that the mixing equation is "linear." This has been shown by several authors[17,21] to be an oversimplification, but the concentration dependence of $D_{A\ell}$ is not large enough to contribute significant error to either the present research or the application of Equations 2-6 to field calculations[43].

F. Stability

The most serious limitation upon the assumption of Fick's Law mixing in a porous medium is due to instabilities inherent in some systems because of density and viscosity differences within the fluids and/or inhomogeneities within the porous medium.

A stable displacement is one in which the concentration of a component is uniform in a plane perpendicular to the direction of flow; an unstable displacement is one in which "fingers" of one component advance into the other component. Viscous fingering of immiscible fluids in porous media, such as is illustrated in Figure 2, "Development of Unstable Fingers when Water Displaces Oil from a Porous Medium," is a common phenomenon with which the gas storage industry is acquainted. Miscible components may finger in a like manner, although the finger development is not apt to be as extreme, and there is no readily discernable interface between the fluids. The development of such fingers constitutes "gross bypassing" of one fluid by another, as previously mentioned, and hence is in violation of the assumption of Fick's Law model.

The formation of fingers within a miscible system is known as a conditional instability[45], since these fingers must eventually merge due to transverse dispersion. That is, if two fingers are traveling in a nearly parallel direction, transverse or "sideways" mixing will eventually bring the two fingers together, at which time the displacement will again be stable. We thus consider transverse dispersion to be advantageous and longitudinal dispersion to be detrimental in a gaseous displacement in which a minimum of mixing is desired.

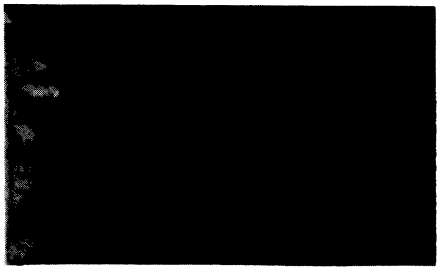

$N_p = W_i = 2.3\%$

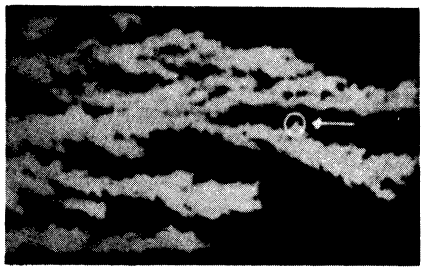

$N_p = 13\%;\ W_i = 23\%$

$N_p = W_i = 6.0\%$

$N_p = 20\%;\ W_i = 34\%$

$N_p = W_i = 9.5\%$

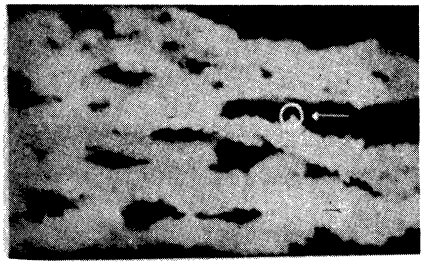

$N_p = 34\%;\ W_i = 180\%$

$N_p = W_i = 12\%$

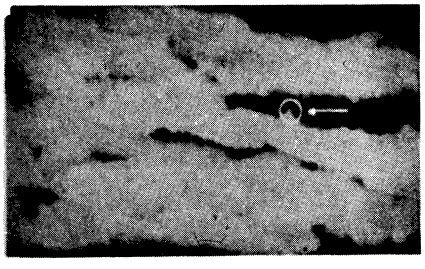

$N_p = 52\%;\ W_i = 650\%$

Figure 2. Development of Unstable Fingers when Water Displaces Oil from a Porous Medium (from van Meurs, Trans. AIME, (Petr.), 213, 103, (1958). $N_p$ = oil production in pore volumes $W_i$ = cumulative water injection in pore volumes.)

There are several factors to be considered in determining whether a gaseous displacement will be stable. The most obvious criterion is reservoir homogeneity; a formation having streaks or layers of varying permeability is very likely to initiate and propagate fingering during displacement.

Both density and viscosity differences are factors affecting stability which can be either favorable or unfavorable. If helium displaces a more dense gas such as nitrogen in a downward direction, for example, a stable displacement is apt to result because buoyancy effects will work to damp out fingers as they are formed. On the other hand, if helium displaces nitrogen in an upward direction, or if nitrogen displaces helium in a downward direction, buoyancy effects will tend to increase fingering.

Similarly, a less viscous fluid will tend to finger into a more viscous fluid during a displacement in any direction. For gases, a decrease in density corresponds to an increase in viscosity. For the example of helium displacing nitrogen in a downward direction in a homogeneous medium, we are insured of stability since both viscous effects and density effects will act to promote this stability. For nitrogen displacing helium in an upward direction, a favorable density difference will encourage stability, but an unfavorable viscosity difference will promote fingering. In this case, we must look more closely at the criteria for stability in order to determine the displacement behavior.

Dumore[24], Schowalter[50], Perrine[45], and Perkins[44] have studied the stability problem for liquids. For liquids, a mathematical analysis may be slightly different than for gases, since a low liquid density corresponds to a low viscosity.

Schowalter[50] uses a perturbation analysis to show that, for liquids, stability can be predicted from several dimensionless parameters, in agreement with Perrine[45]. These authors assume an exponential relationship between viscosity and composition, which is a valid approximation for liquids only.

Stability criteria are mentioned further in Section III of this report. A detailed analysis of stability problems for gaseous systems is, however, beyond the scope of this thesis work; we shall endeavor only to mention qualitatively the variables which must be considered.

## III. THEORY; PREVIOUS RESEARCH

A comprehensive review of diffusion and dispersion in porous media has been presented by Perkins and Johnston[43]. These authors have prepared an extensive list of references on the subject, only part of which is included in the present bibliography.

These authors point out the difficulty in attempting to treat the dispersion and diffusion coefficients as functions of concentration; they also point out that it is usually possible to treat these coefficients as constants by selecting an "effective average," e.g. by using the diffusion coefficient for a 50-50 per cent mixture. Crank[21] has considered the coefficients as functions of concentration.

Perkins and Johnston analyze the capillary model, among others. In this model, a porous medium is represented by a bundle of capillary tubes. This is not a very good representation of a porous rock, so that it does not seem worthwhile to expound upon their results in this manuscript. de Jong[23] and Saffman[49] have also studied a random network of capillary tubes, but their results still do not agree with those for porous rock.

The simplest analysis which provides useful information for the prediction of dispersion coefficients is the electrical resistivity analog, proposed by Brigham, et al.[12], van der Poel[58], and Grane and Gardner[30]. Recognizing that there is an analogy between electrical conductivity and diffusion in porous media, it follows that

$$\frac{D}{D_o} = \frac{1}{F\phi} \tag{8}$$

for either cemented rocks or unconsolidated packs for very low flow rates, since the law governing electrical conductivity is completely analogous to Equation 6. Equation 8 has been substantiated by Kravik and Bissey[34] for gas flow through Berea sandstone, using a variety of gas systems with mobility ratios ranging from 0.5 to 2.0. In the above equation,

$D$ = longitudinal or transverse dispersion coefficient within the porous medium (these are identical for extremely low flow rates), or "apparent diffusion coefficient,"

$D_o$ = molecular diffusion coefficient in the absence of a porous matrix,

$F$ = electrical resistivity factor, and

$\phi$ = fractional porosity of the medium.

Equation 8 implies that mixing is defined in terms of the area open to diffusion; if defined in terms of the total cross-sectional area of the sample, then we would write

$$\frac{D}{D_o} = \frac{1}{F} \tag{8a}$$

For laminar flow it is common practice[10,43] to correlate the ratio of the effective dispersion coefficient to the molecular diffusion coefficient, $De/D_o$, as a function of a Peclet number, $u$(characteristic length)$/D_o$. Perkins and Johnston[43] suggest the relationship

$$\frac{De}{D_o} = \frac{1}{F\phi} + 0.5\left(\frac{u\,d_p\,\sigma}{D_o}\right) \tag{9}$$

which is shown in Figure 3, "Typical Dispersion Characteristics for Porous Media." In Equation 9, $\sigma$ represents a packing or inhomogeneity factor.

Other authors prefer a more general expression of the type

$$\frac{D_e}{D_o} = \frac{1}{F\phi} + \alpha\left(\frac{\bar{r}\,u}{D_o}\right)^m \qquad (9a)$$

in which $\bar{r}$ = a characteristic length such as pore diameter or grain diameter,

$\alpha$ = a proportionality constant, and

$m$ = the power dependence of dispersion upon velocity.

Brigham, et.al.[12] states that the proportionality constant, $\alpha$, of Equation 9a is a function of the mobility ratio of the flowing fluids, as well as the physical properties of the porous medium.

The practice followed in this manuscript is to assume dispersion characteristics of the type

$$\frac{D_e}{D_o} = \frac{1}{F\phi} + 0.5\left(\frac{u\,d_p\sigma}{D_o}\right)^m . \qquad (9b)$$

Determination of the parameters $d_p\sigma$ and $m$ then completely characterizes the mixing properties of a porous medium for a given binary system.

## A. Dispersion Mechanisms

We refer in particular to Figures 4 and 5 in attempting to analyze the regions of different flow behavior. As the flow rate is increased for any two miscible fluids flowing in a given porous medium,

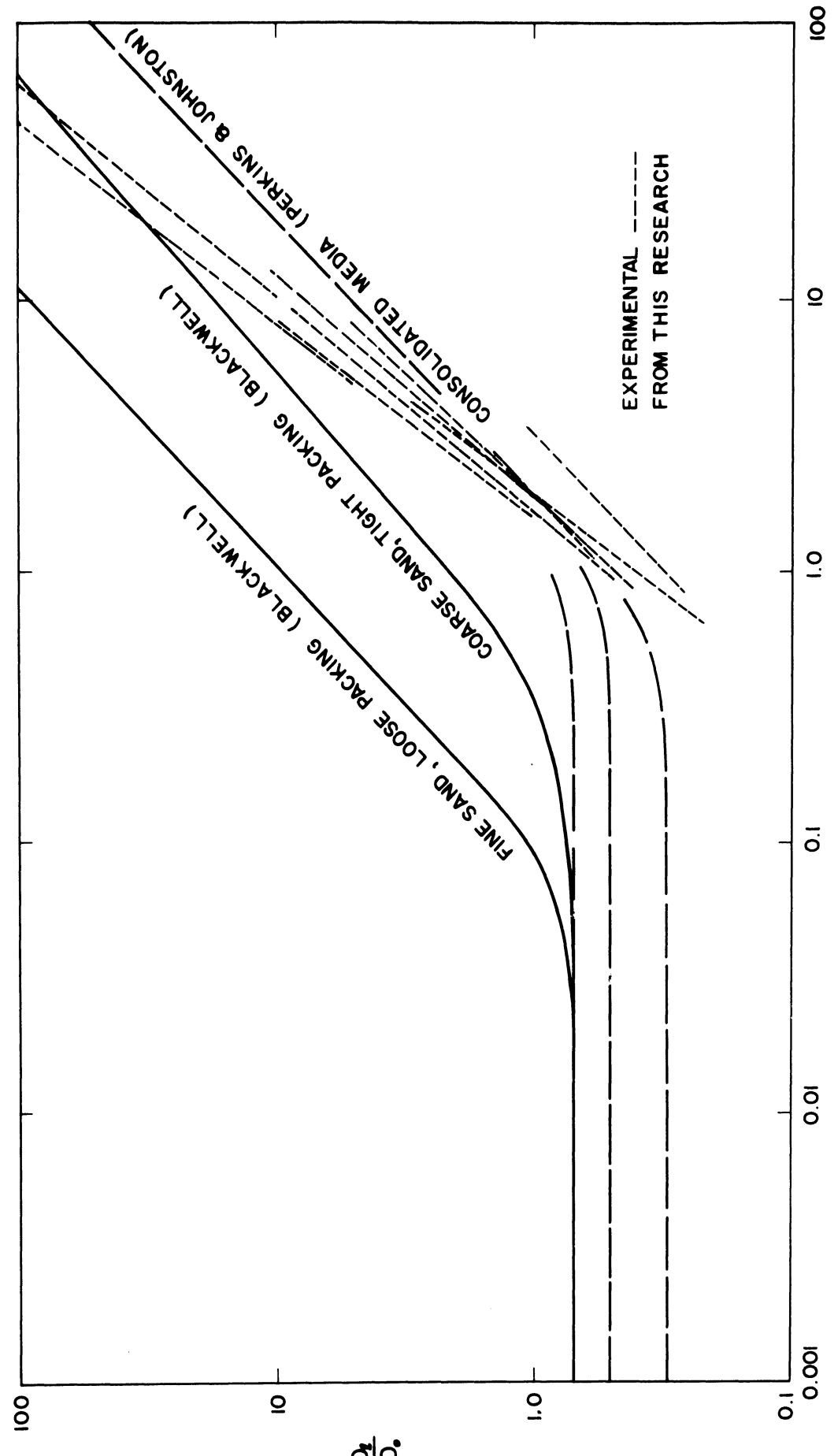


Figure 3. Typical Dispersion Characteristics for Porous Media.(10,43)

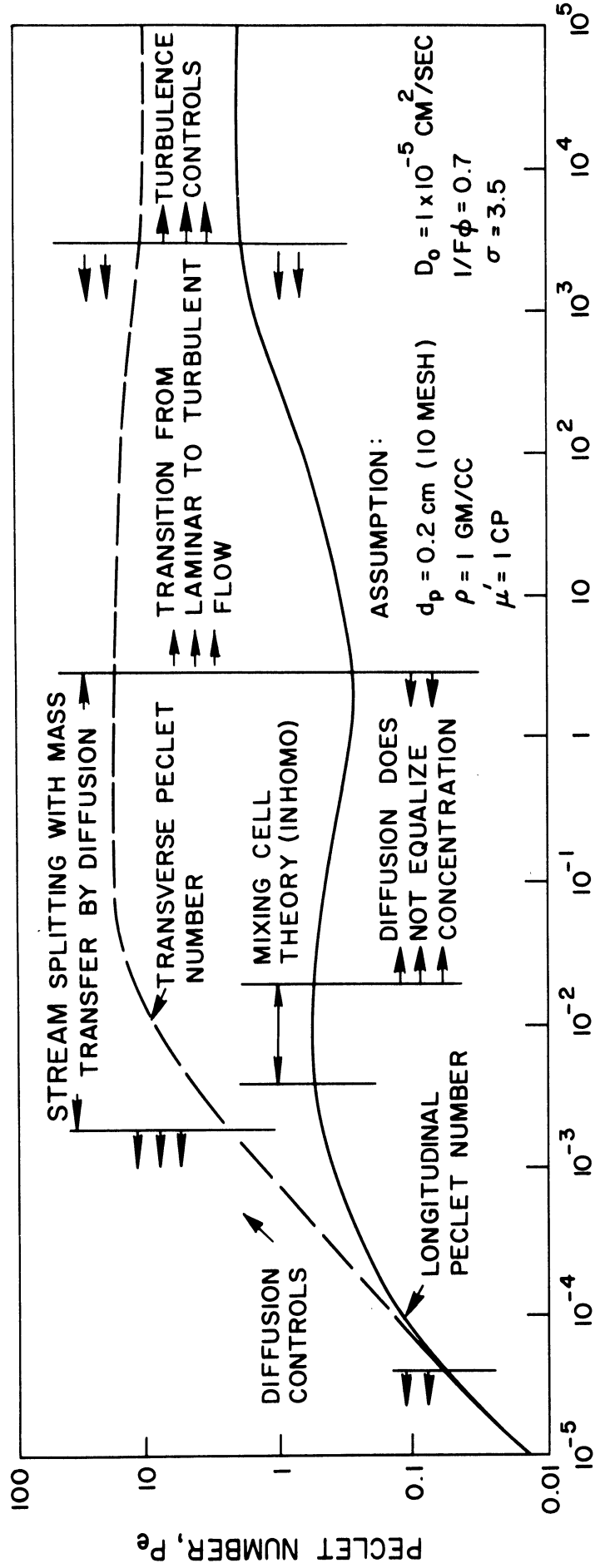


Figure 4. Peclet Numbers for an Aqueous System (after Perkins and Johnston).

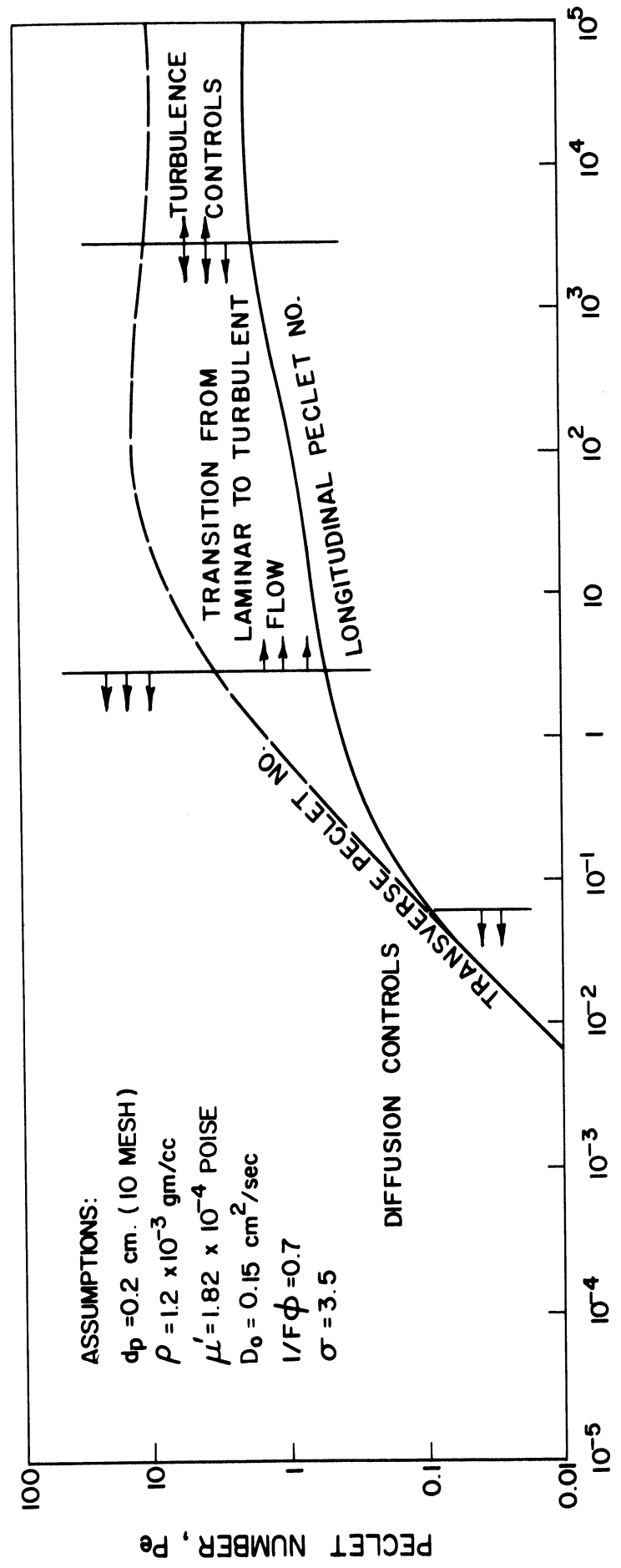


Figure 5. Peclet Numbers for a Gaseous System (air) (after Perkins and Johnston).

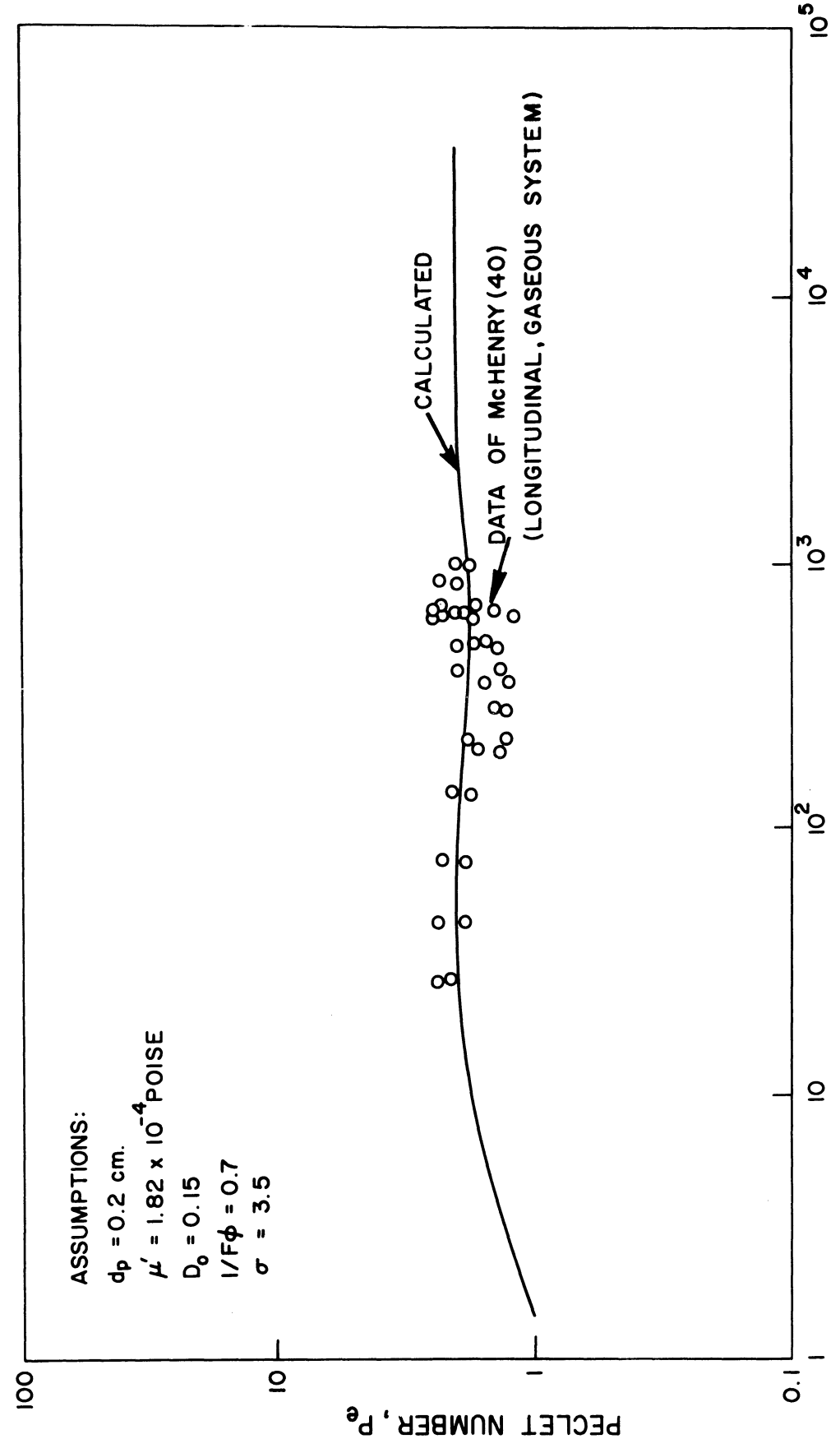


Figure 6. Comparison of Calculated and Experimental Data (longitudinal dispersion: gaseous system)(after Perkins and Johnston).

the flow undergoes a transition from laminar to turbulent, and there is a concomitant increase in the effect of convective mixing. In the following paragraphs we shall assume that the flow rate is gradually increased from a zero value to a high value and attempt to describe the various mixing regimes encountered.

1. Zero Velocity; Pure Molecular Diffusion

If, at time $t = 0$, a sharp interface exists between two miscible fluids at rest ( $Re = 0$ ), then molecular diffusion alone will cause the two fluids to mix. The concentration, $C$, of either fluid at time $t$ will be given by

$$C = \frac{1}{2}\left[1 \pm \operatorname{erf}\left(\frac{|x|}{2\sqrt{D_e t}}\right)\right] \tag{10}$$

where $X$ = distance measured from the initial position of the interface, and

$\operatorname{erf}$ = error function.

For unconsolidated porous media, it may be stated as an approximation[16] that the apparent diffusion coefficient is given by

$$\frac{D}{D_o} = \frac{1}{\sqrt{2}} \tag{11}$$

Equation 11 is based on the approximation that a randomly chosen fluid particle moving through a porous bed is statistically probable to be moving at 45° with respect to the direction of bulk flow.

2. Low Velocities; Molecular Diffusion Dominating

If, as before, a sharp interface exists between the two fluids at time $t = 0$, but there is bulk flow of the fluids at a low velocity

in a direction normal to the interface, then molecular diffusion will still control the mixing. Until a Reynolds number of about $4 \times 10^{-5}$ is reached for liquids, or $Re = 6 \times 10^{-2}$ for gases, mixing will still occur by molecular diffusion alone(43). As long as convective effects do not begin to appear, the longitudinal and transverse dispersion coefficients will be identical, as indicated in Figures 4 and 5. The Peclet number will be proportional to the Reynolds number up to this point, since the velocity term is expressed in the numerator of each dimensionless variable.

As the above Reynolds numbers ($Re = 4 \times 10^{-5}$ for liquids, or $Re = 6 \times 10^{-2}$ for gases) are slightly exceeded, mixing is best described by a combination of diffusion and mixing cell theory. When diffusion alone controlled the mixing, we could assume that the concentration of diffusing material was uniform within each pore space; as the velocity increases, there will be insufficient residence time within each pore space for the concentration to become uniform. This will at first ($Re < 2 \times 10^{-3}$ for liquids or $Re < 3$ for gases) not affect the transverse dispersion, since there is still very little flow perpendicular to the direction of bulk flow.

As these Reynolds numbers are surpassed, however, "stream splitting" will occur; i.e. there will be significant mixing effects in the transverse direction.

3. Transition Zone; Molecular and Convective Mixing

Above Reynolds numbers of about 4, and up to Reynolds numbers of about 4,000, the flow will undergo a transition from the laminar

to the turbulent regime. Inertial effects will begin to appear, and turbulent eddies will occur within the larger pore spaces, resulting in complete mixing. Laminar flow may still exist within the smaller pore spaces. As the flow rate is increased to the upper limit of the transition zone, the Peclet number will approach a limiting value for turbulent flow.

4. Turbulent Flow; Convective Dispersion

Above a Reynolds number of 1,000-4,000, the flow may be considered completely turbulent. The limiting value of the Peclet number will be about 2 for longitudinal dispersion, and about 11 for transverse dispersion. The molecular diffusion will play no part in the mixing; inertial effects, or convection, will control the mixing.

B. Parameters Affecting Experimental Results

Perkins and Johnston[43] identify the following factors as relevant in obtaining consistent measurements of dispersion coefficients in the laboratory:

(1) edge effects in packed tubes

(2) particle size distribution

(3) particle shape

(4) packing or permeability heterogeneities

(5) viscosity ratios

(6) gravity forces

(7) amount of turbulence

(8) effect of an immobile phase

Although several of these factors apply only to unconsolidated packs, it seems appropriate to review their implications upon our current research.

1. Edge Effects

For random packs of spherical particles Schwartz and Smith[53] show that there is a zone of high porosity extending two to three particle diameters from the cylinder walls. Data of Singer and Wilhelm[51], Fahien and Smith[26], and Latinen[35] indicate that error due to wall effects is less than 10% for a particle diameter to tube diameter ratio of less than 0.04; for a particle diameter to tube diameter ratio of 0.1, the error may be as high as 50%.

In this research, particle diameter to core diameter ratios of less than 0.01 were encountered. Since all samples were mounted in a rubber sleeve which conformed to the sample boundaries, we feel safe in neglecting edge effects.

2. Particle Size Distribution

In a solid pack of particles having a wide distribution of sizes, small particles may be contained in the interstices between the larger particles. The median particle size, in this case, does not adequately characterize the size of the average pore space. Perkins and Johnston[43] used the data of Raimondi, et. al.[48] to conclude that the "effective particle size" for a packed bed (i.e. the particle size used to correlate dispersion data) should be that size corresponding to a 10% cumulative fraction, assuming that the particle size distribution of naturally occuring sands follows a log-normal distribution.

Raimondi, et. al.[48] and Orlob and Radhakrishna[42] show that increased dispersion will result from a wide particle size distribution.

3. Particle Shape

Various investigators[6,14,25] have studied mixing phenomena in packs of cubes, spheres, rings, saddles, etc., and have found that packs of non-spherical particles produce greater dispersion than packs of spherical particles.

The sphericity of a particle is defined as

$$\psi = \frac{\text{surface area of a sphere having the same volume as the particle}}{\text{surface area of the particle}} \qquad (12)$$

No good correlation is evident for the dependence of dispersion on sphericity.

4. Packing and Permeability Heterogeneities

Heterogeneities may be present in either random packs or in cemented formations. Increases in heterogeneity will result in increased dispersion.

Very little can be said to clarify the effect of heterogeneity upon dispersion, since there is no obvious method of characterizing heterogeneity or homogeneity. Perkins and Johnston[43] have compiled data from the literature in an attempt to characterize a medium by an inhomogeneity factor, $\sigma$, but these data show a wide scatter over a 10-fold range of values. It can be said roughly that packings of smaller particles will have a higher inhomogeneity factor and show a corresponding increase in dispersion. The packing, or inhomogeneity factor, is discussed further in section V of this manuscript.

The effect of viscosity ratio upon dispersion was mentioned earlier. For ratios greater than unity (i.e. when the viscosity of the displaced fluid is greater than the viscosity of the displacing fluid), unstable fingering may result. The treatment of these instabilities is beyond the scope of this thesis, although we do consider it essential that the criteria for stability are understood.

6. Gravity Forces

Gravity forces, or density differences between displaced and displacing fluids, also fall into the category of instabilities which is beyond the scope of this work. We recognize only that if a dense fluid is above a less dense fluid in a vertical displacement, then gravity may cause redistribution quite separate and distinct from redistribution by dispersion.

7. Turbulence

From the standpoint of an engineer designing a packed reactor column for maximum efficiency, turbulence may be desirable. Laminar flow is more often desirable in a petroleum or gas storage reservoir, since turbulence increases dispersion or mixing.

We define the laminar flow region as that region in which Darcy's Law is valid, i.e. for Reynolds numbers ( $d_p u \rho / \mu'$ ) of less than about 10. Fully developed turbulent flow occurs at Reynolds numbers greater than about 1000.

Dispersion coefficients in the turbulent region are normally reported in terms of the Peclet number defined by Equation 13.

$$Pe = \frac{d_p u}{D} \tag{13}$$

where $d_p$ = particle diameter

$u$ = interstitial velocity

$D$ = dispersion coefficient, longitudinal or transverse.

(When $D = D_L$, then $Pe = Pe_L$ ; when $D = D_t$, then $Pe = Pe_t$ .) The Peclet number is commonly expressed as a function of the Reynolds number, as indicated in Figures 4 and 5. There is some ambiguity in the literature in that some authors[10] have defined the Peclet number in terms of particle radius or bed length, and the symbol $K$ or $E$ is often used to represent the convective dispersion coefficient. The Peclet number may also use the molecular diffusion coefficient, $D_o$ , instead of $D_L$ , in other applications, e.g. in the laminar flow range.

The amount of turbulence in a porous medium is dependent not only upon the Reynolds number, but also upon the particle shape and packing. These properties of the porous material may be correlated by defining the turbulence factor, $\beta$ , which modifies Darcy's Law as shown in Equation 14.

$$-\frac{dP}{dL} = \frac{\mu' v}{K} + \beta \rho v^2 \tag{14}$$

We consider that the turbulence factor, like the resistivity factor, should provide a measure of the "mixing properties" of a rock.

Prausnitz[47], Aris and Amundson[2] and Carberry[14,15] use the mixing-cell to theoretically predict a longitudinal Peclet number of about 2.0 for fully developed turbulence. Figure 7, "Peclet Numbers for Longitudinal Dispersion in Turbulent Flow," shows literature data verifying the theoretical value for longitudinal mixing. Data for transverse mixing tend to give values slightly lower then the theoretically predicted value of 11 for gaseous systems.

By combining theories of laminar and turbulent mixing, we can estimate Peclet numbers for any Reynolds number. Figure 4, "Peclet Numbers for an Aqueous System," and Figure 5, "Peclet Numbers for a Gaseous System," illustrate Peclet numbers for a wide range of Reynolds numbers. Figure 6, "Comparison of Calculated and Experimental Data," includes the data of McHenry[40] for longitudinal dispersion in a gaseous system. Figures 4 and 5 for liquid and gaseous systems, respectively, show the regions where the various mixing theories seem to apply.

8. Effect of an Immobile Phase

Orlob and Radhakrishna[42] studied the effect of an immobile gas phase upon dispersion in a liquid displacement, and found that an increased "capacitance effect" resulted; i.e. several per cent of the total pore volume was inaccessible to flow because of blocked passages in the interstices of the medium. They also found that dispersion was decreased by gas entrapment. A significant amount of gas entrapment (more than 5% of the total pore volume) is necessary to affect the dispersion, however.

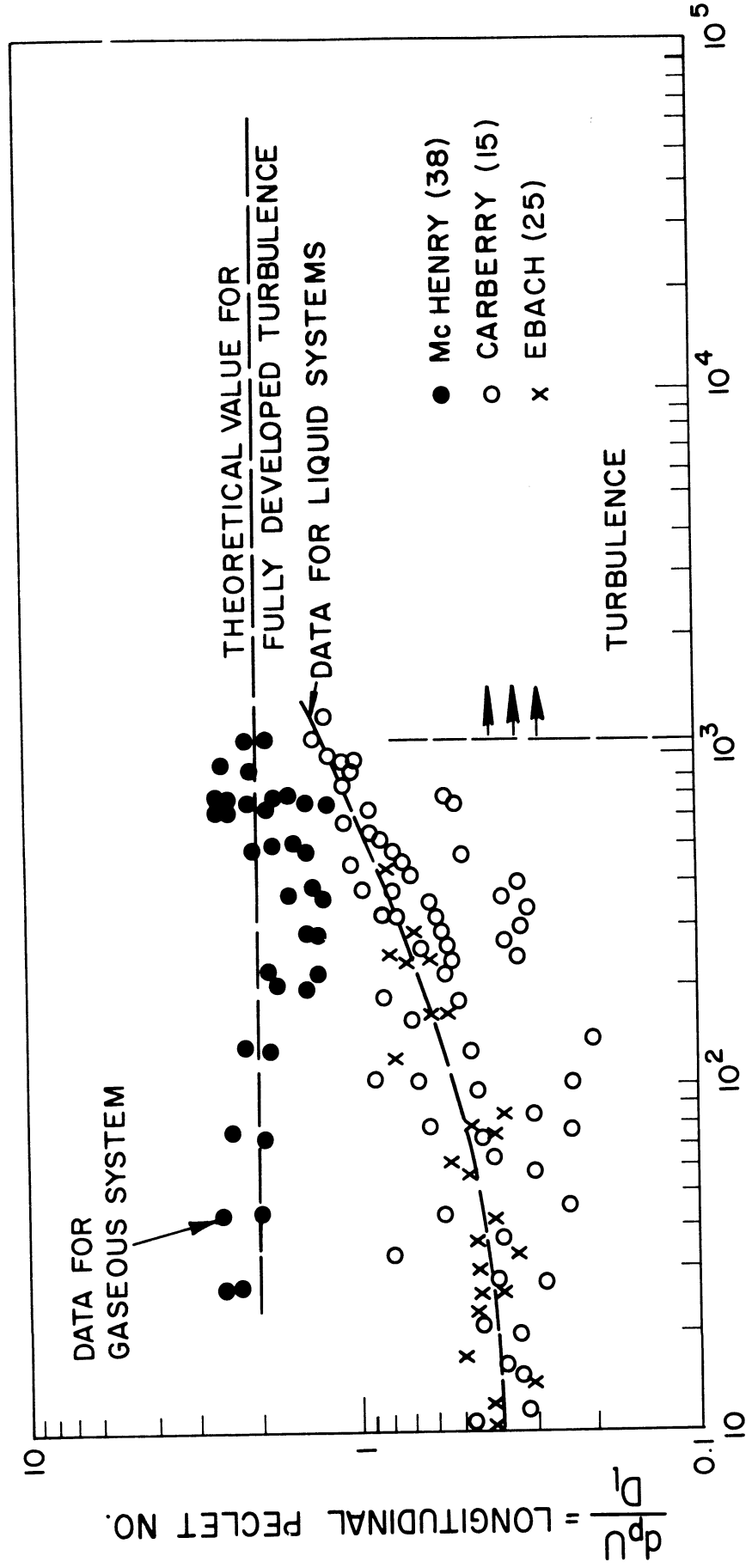


Figure 7. Peclet Numbers for Longitudinal Dispersion in Turbulent Flow (after Perkins and Johnston).

## IV. EXPERIMENTAL PROGRAM

A Fick's Law model was chosen to represent mixing for flow through a porous medium, since this model permitted a convenient analytical technique for determining dispersion coefficients for a variety of short core samples. We must recognize that a Fick's Law model is not the most sophisticated model that can be used to describe such mixing, and that it is valid only for a stable displacement, without capacitance effects, and for a dispersion coefficient which is independent of concentration.

Figure 8, "Dispersion Model," illustrates Fick's Law mixing in a porous bed. Dispersion coefficients for this system may be determined by the stimulus-response technique described by Levenspiel[9,36,37,57].

Prior to describing Levenspiel's method, however, it will be well to define the following symbols and terms, Equations 15-21;

$v'$ = volumetric flow rate

$u$ = interstitial velocity

$V$ = bed volume (void)

$L$ = core or bed length

$$\bar{t} = \mu = V/v' = \text{mean residence time} \tag{15}$$

$\mathcal{M}_k$ = $k^{th}$ moment integral of $f(t)$ about the mean, $\mu$

$$= \frac{\int_0^\infty (t-\mu)^k f(t)\,dt}{\int_0^\infty f(t)\,dt} \tag{16}$$

If we define the integral

$$M_k' = \int_0^\infty t^k f(t)\,dt \tag{17}$$

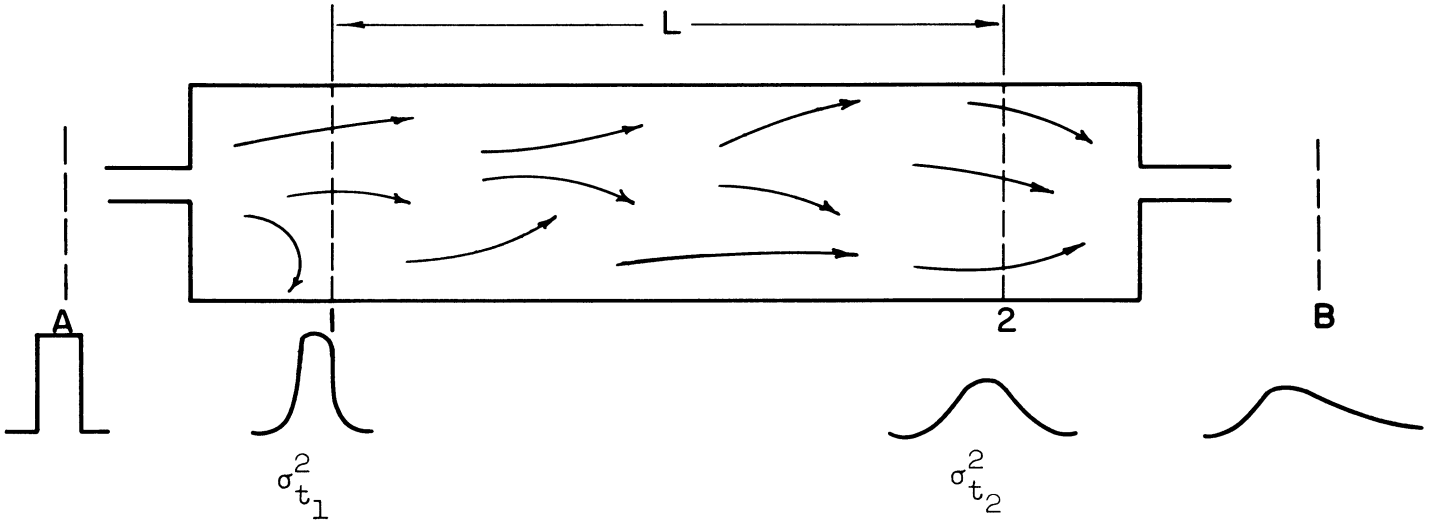


$$\Delta\sigma^2 = \Delta\sigma_t^2 \left(\frac{v'}{V}\right)^2 = \Delta\sigma_t^2 \left(\frac{u}{L}\right)^2$$

$$= \frac{2D_\ell}{uL}$$

or

$$D_\ell = \frac{uL}{2} \Delta\sigma^2$$

$$= \frac{uL}{2} \left(\frac{u}{L}\right)^2 \Delta \left[\frac{\int_o^\infty t^2 C(t)dt}{\int_o^\infty C(t)dt} - \left(\frac{\int_o^\infty tC(t)dt}{\int_o^\infty C(t)dt}\right)^2\right]$$

Figure 8. Dispersion Model.

then the following relationships may be expressed conveniently in terms of the above definitions.

$$M_0' = \int_0^\infty f(t)\,dt$$

$$\bar{t} = \mu = \frac{M_1'}{M_0'} = \frac{\int_0^\infty t\,f(t)\,dt}{\int_0^\infty f(t)\,dt} \tag{18}$$

= mean residence time (19)

$$M_2' = \int_0^\infty t^2 f(t)\,dt \tag{20}$$

$\sigma_t^2 = m_2$ = variance of $f(t)$ about mean, $\mu$

$$= \int_0^\infty (t-\mu)^2 f(t)\,dt \Big/ \int_0^\infty f(t)\,dt$$

$$= \int_0^\infty t^2 f(t)\,dt \Big/ \int_0^\infty f(t)\,dt - \mu^2$$

$$= \frac{M_2'}{M_0'} - \left(\frac{M_1'}{M_0'}\right)^2 \tag{21}$$

We can now state the results of Levenspiel's analysis:

If $f(t)$ represents the concentration profile at a point in a core or packed bed (see Figure 8, "Dispersion Model"), then the dispersion coefficient, $D_e$, which characterizes Fick's Law mixing between any two points, 1 and 2, in the bed may be found from Equation 22:

$$\Delta\sigma_{12}^2 = \Delta\sigma_t^2 (v'/v)^2 = \Delta\sigma_t^2 (u/L)^2$$

$$= \left(\frac{u}{L}\right)^2 \Delta\left[\left(\frac{M_2'}{M_0'}\right) - \left(\frac{M_1'}{M_0'}\right)^2\right]_{1-2}$$

$$= \frac{2D_e}{uL} \tag{22}$$

The dimensionless group $uL/D_e$ is known as the axial Peclet number, and the reciprocal $D_e/uL$ is often called the dispersion number.

We must note that the points 1 and 2 indicated in Figure 8 are defined to exclude entrance and exit zones, so that the mixing zone under consideration is "open-ended." If concentration profiles were to be determined at points A and B, so that end effects were included in the mixing zone under consideration, then higher order terms would appear in Equation 22. Analysis of such a model was attempted in this research program, and found to be unsatisfactory for short core samples.

## A. Measurement of Physical Properties

From the above analysis we see that in order to calculate a dispersion coefficient to characterize mixing for flow through a porous medium, we must measure or calculate:

(1) the interstitial velocity, $u$ , of gas through the medium,

(2) the specimen length, $L$ , and

(3) the inlet and outlet concentration profiles, $C(t)$ , and their corresponding moment integrals $M_0'$ , $M_1'$ , and $M_2'$ .

Porosity, permeability, electrical resistivity factors, and turbulence factors were also determined for each core specimen in order to completely characterize the sample.

Core lengths were easily determined, and the porosities of all consolidated samples used were furnished by the suppliers or measured experimentally. Permeabilities, turbulence factors, and electrical

resistivity factors of all samples were determined experimentally by the method of Katz and Cornell[20,32]. The turbulence factor is defined in terms of a quadratic modification of Darcy's Law,

$$-\frac{dP}{dL} = \frac{\mu' v}{K} + \beta \rho v^2 \tag{14}$$

where $P$ = pressure, atm.,

$L$ = length, cm.,

$\mu'$ = viscosity, cp.,

$K$ = permeability, Darcys,

$\rho$ = density, gm/cc, and

$\beta$ = turbulence factor, atm-sec$^2$/gm. or ft.$^{-1}$

For gases, it is convenient to express Equation 14 in terms of mass velocity $W/A = \rho v$ since the mass velocity is constant while the linear velocity may vary.

$$\rho\left(-\frac{dP}{dL}\right) = \rho \frac{v\mu'}{K} + \beta \rho^2 v^2 = \frac{\mu' W}{KA} + \beta \left(\frac{W}{A}\right)^2 \tag{23}$$

Using $$\rho = MP/\mathcal{Z}RT \tag{24}$$

and integrating between points 1 and 2,

$$-\frac{M}{\mathcal{Z}RT}\int_1^2 dP = \left[\frac{\mu' W}{KA} + \beta\left(\frac{W}{A}\right)^2\right]\int_1^2 dL \tag{25}$$

where $W$ = mass flow rate, gm/sec,

$A$ = cross sectional area, sq. cm.,

$M$ = molecular weight,

$\mathcal{Z}$ = compressibility factor,

$R$ = gas constant, and

$T$ = absolute temperature,

one obtains

$$\frac{M(P_1^2-P_2^2)}{2\mathcal{R}RT\mu' L}\frac{A}{W} = \frac{W}{A}\frac{\beta}{\mu'} + \frac{1}{K} \qquad (26)$$

When one plots the parameter $\frac{M(P_1^2-P_2^2)A}{2\mathcal{R}RT\mu' LW}$ vs. $\frac{W}{A\mu'}$, the resulting graphs have straight lines with the turbulence factor, $\beta$, as their slope and 1/K, reciprocal permeability, as intercept.

Turbulence factors and permeabilities were obtained by flowing nitrogen through each specimen while it was mounted in the Hassler high pressure sleeve. Upstream pressures and downstream flow rates were recorded for a number of different flow rates and the results were correlated with varying degrees of success. Experimental values were found to be slightly higher than predicted by the correlation of Cornell and Katz[32]. Sample calculations are included in Appendix I.

Porosities were determined by gravimetric measurements. Dry weights and bulk volumes were first determined for each sample. The core was then evacuated in a bell jar, flooded with water, and returned to atmospheric pressure. The weight of the wet sample then indicated the mass, and therefore the volume, of water contained in the void fraction of the sample.

Electrical resistivity factors were determined using a 0.1 normal solution of potassium chloride. Each core was first evacuated and saturated with the KCl solution by the same method used for porosity determinations. The electrical resistance, and thus the electrical resistivity, were measured by mounting the sample between

two platinum foil electrodes and then balancing against an AC bridge. The electrical resistivity factor is the ratio of the resistivity of the saturated core sample to the resistivity of pure 0.1 N KCl solution at the given temperature.

Sample calculations of porosity and electrical resistivity factors are also included in Appendix I.

B. Equipment

Figure 9, "Experimental Apparatus," shows schematically the equipment used to determine dispersion coefficients for the nitrogen-argon system. The system includes components for pressure and flow rate regulation, a core holder, a thermal conductivity cell, an amplifier-recorder, an analog computer, and an instrument panel for switching and data monitoring.

1. Pressure and Flow Rate Regulation of Gas Supply

Since pulses are injected into the system using solenoid valves, sensitive pressure and flow controls are required. In order to minimize pressure pulses upon switching, a system using two pressure regulators, four needle valves, a mano-stat rotameter, and a high pressure manometer was constructed. For a given downstream pressure, usually atmospheric, all of the needle valves must be simultaneously adjusted to obtain the desired flow rate, as read on the downstream rotameter.

Upstream flowing pressures are dependent upon the permeability and length of the sample being studied, i.e. the pressure drop through the sample, and are therefore determined by the flow rate.

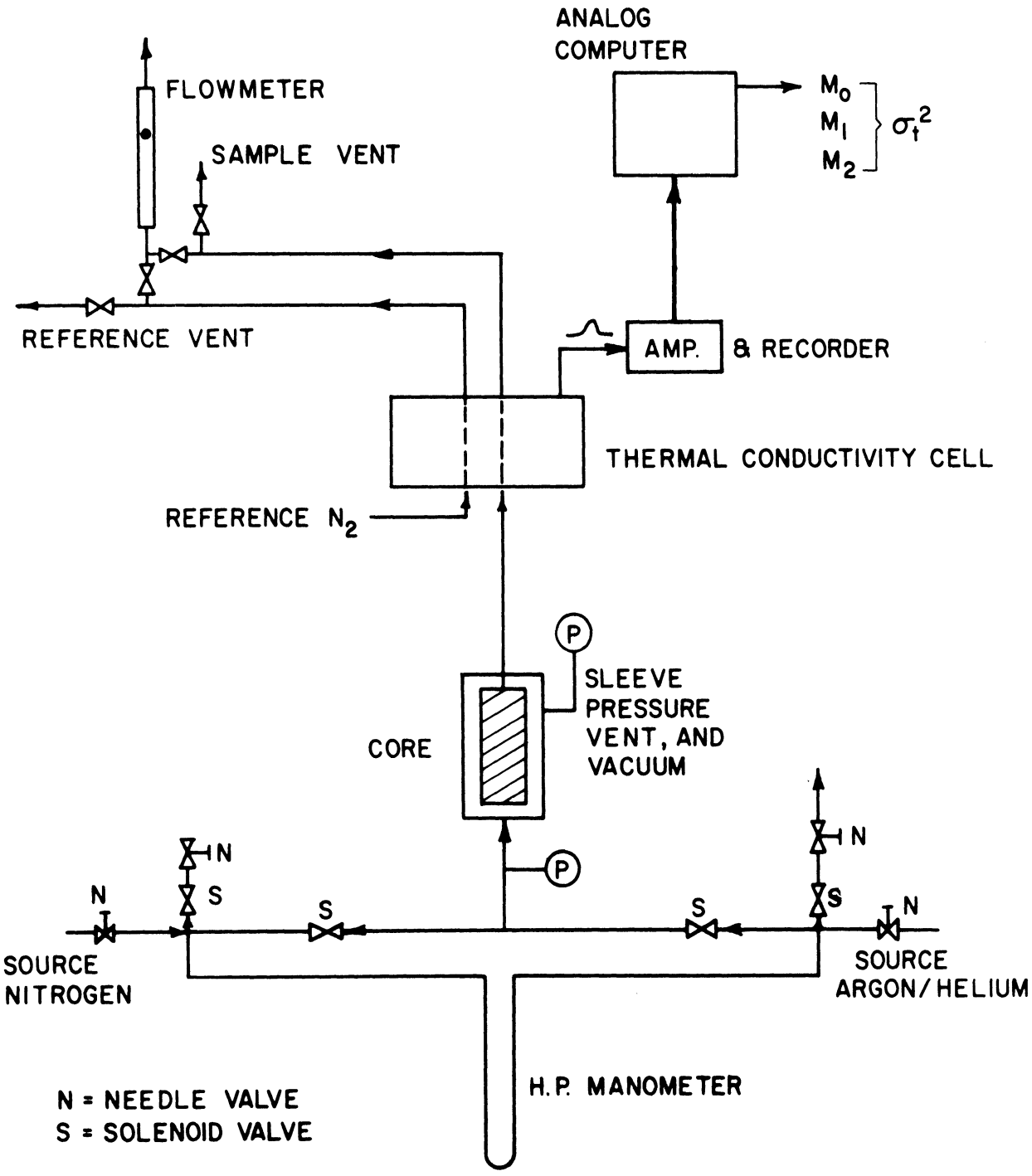


Figure 9. Experimental Apparatus.

These pressures ranged from essentially zero to 60 psig for the range of permeabilities studied.

Needle valves, which are used to control the flow rates during each run, are mounted immediately downstream of the pressure regulators on the gas cylinders. Each pressure regulator and needle valve is adjusted so that sonic flow is maintained through the valve. In this manner, disturbances downstream of the needle valves, such as switching of the solenoid valves, cannot affect the delivery pressure of the regulators.

The valves are arranged so that both pressure regulators are always delivering at equal pressure, no matter which stream is flowing through the core sample. That is, when flow through the core by, say, nitrogen is terminated by closing a solenoid valve, another solenoid valve is simultaneously opened to vent the nitrogen through another needle valve; the needle valve is set to provide the same resistance to flow as the core sample.

Although it is somewhat tedious to adjust the four needle valves simultaneously, accurate pressure balancing is obtained by this method. For permeable samples and/or low flow rates, the upstream pressure is essentially atmospheric, so that both vent valves can be left fully open, thereby simplifying the adjustments considerably. We may also note that the blow-over pots of the high pressure manometer (see Figure 10) act as surge tanks, which helps to damp out any pressure pulses which result from switching the solenoid valves.

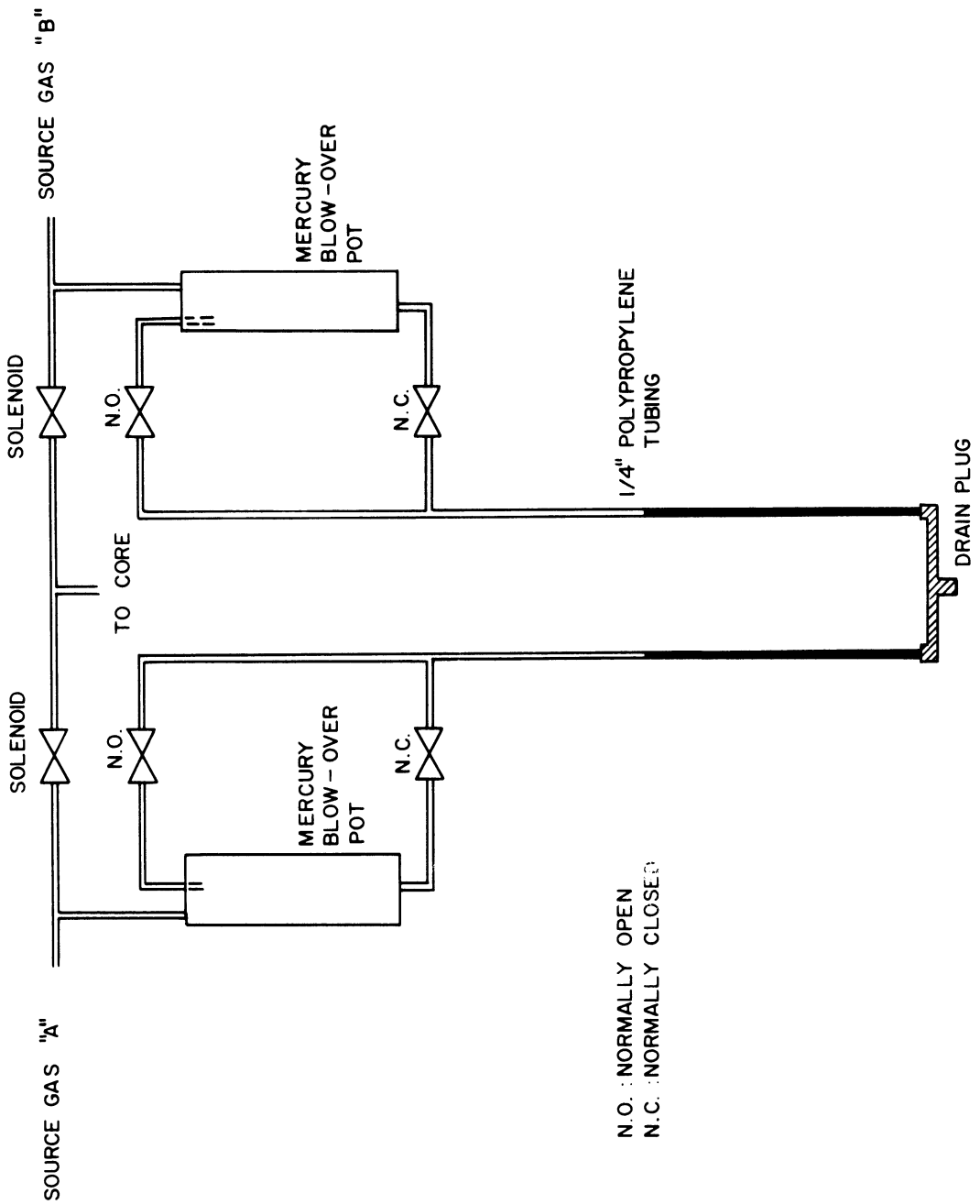


Figure 10. High Pressure Manometer.

2. Core Holder

From the pressure balancing apparatus a line runs to the Hassler sleeve which holds the porous sample. The Hassler sleeve is designed for pressures to 1,000 psi, but auxilliary lines are designed for a limiting pressure of 600 psi. The upstream pressure may be measured at the inflow face of the porous medium mounted in the holder. The core holder is of our own construction, and will hold a $1\frac{1}{2}$ inch diameter core of lengths from $3/4$ inch to 6 inches.

3. Thermal Conductivity Cell

After leaving the sample at atmospheric pressure, the gas flows to a Gow-Mac Model TR2-B thermal conductivity cell. This cell features a fast response time, but is sensitive to flow rate fluctuations, so that it is necessary to balance the bridge of the cell and/or adjust the reference gas (nitrogen) flow rate for each data point taken.

4. Amplifier and Recorder

Since output signals from the thermal conductivity cell are only a few millivolts, it is necessary to amplify this signal for further processing on the analog computer.

The output signal from the cell was fed to a Beckman-Offner Type RS Dynograph recorder. The amplified output from the recorder (normally used to operate the pen arm), which ranged to 10 volts, was used as input to the analog computer. Use of the recorder amplifier allowed variable amplification and permitted a strip-chart record of the thermal conductivity cell output when desired.

5. Analog Computations

The advantage of obtaining the concentration profile as a voltage output is to facilitate calculation of the moment integrals $M_0', M_1', M_2'$ using an analog computer. An Applied Dynamics Model 2401 computer (shown in Figure 11) is used for this purpose.

Figure 12, "Schematic Computer Flow Diagram," illustrates the basic calculations performed by the computer. Essentially two multiplications and four integrating amplifiers are required for the calculation, but sign changes and gain reductions increase the complexity of the circuitry somewhat. Figure 13, "Analog Computer Program," presents the detailed circuitry which is shown schematically in Figure 12. Figure 14, "Analog Computer Symbols," clarifies this flow diagram.

Since the computer performs all calculations in real time, and the equipment does not perform linearly at voltages above 140 volts, it is necessary to introduce several "scale factors" to prevent saturation (overloading) of the integrating amplifiers. Although we first attempted to accomplish this scaling by the use of external resistors and capacitors, it later proved advantageous to use internal components only. Complete flexibility was maintained, since input voltage ranges could be changed by varying the gain of the recorder-amplifier. The circuit illustrated was found to operate satisfactorily as long as the signal was adjusted to have a "peak" value of 2 to 10 volts.

The multipliers operate in a fashion to produce 100 volts as output when voltage inputs of 100 volts are multiplied. Thus, a scale factor of 100 is introduced by each multiplication operation. Since

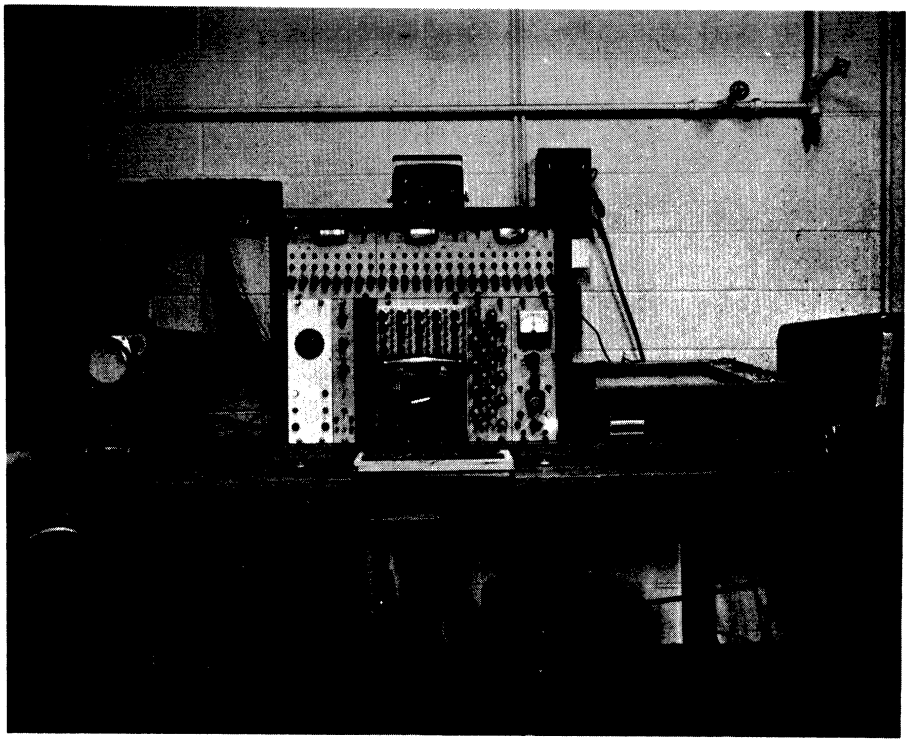

Figure 11. Analog Computer.

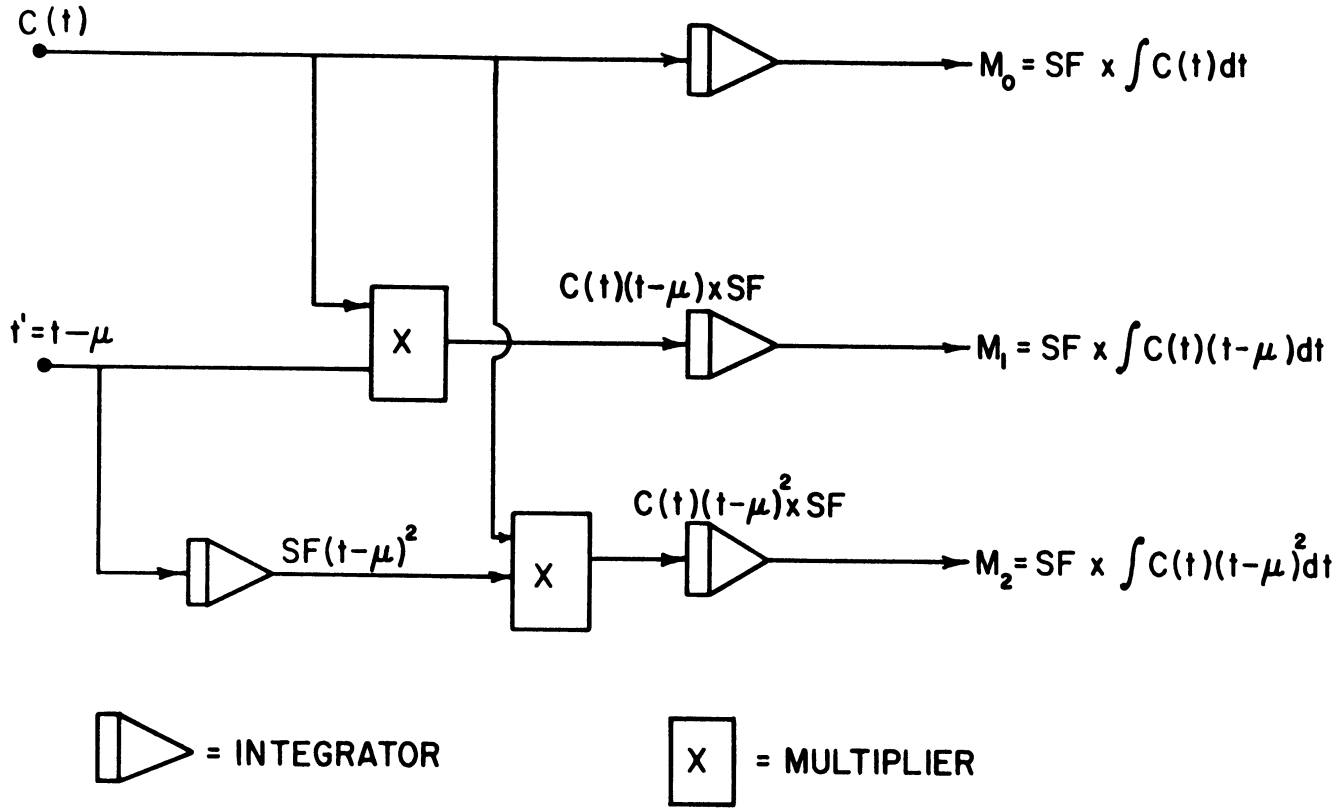


Variance of C(t) about mean, $\mu$ =

$$\sigma_t^2 = \frac{M_2'}{M_0'} - \left(\frac{M_1'}{M_0'}\right)^2$$

$$D_\ell = \frac{\Delta\sigma_t^2}{2} \times \text{interstitial velocity} \times \text{length (Equation 22)}$$

= longitudinal dispersion coefficient.

Figure 12. Schematic Analog Computer Flow Diagram.

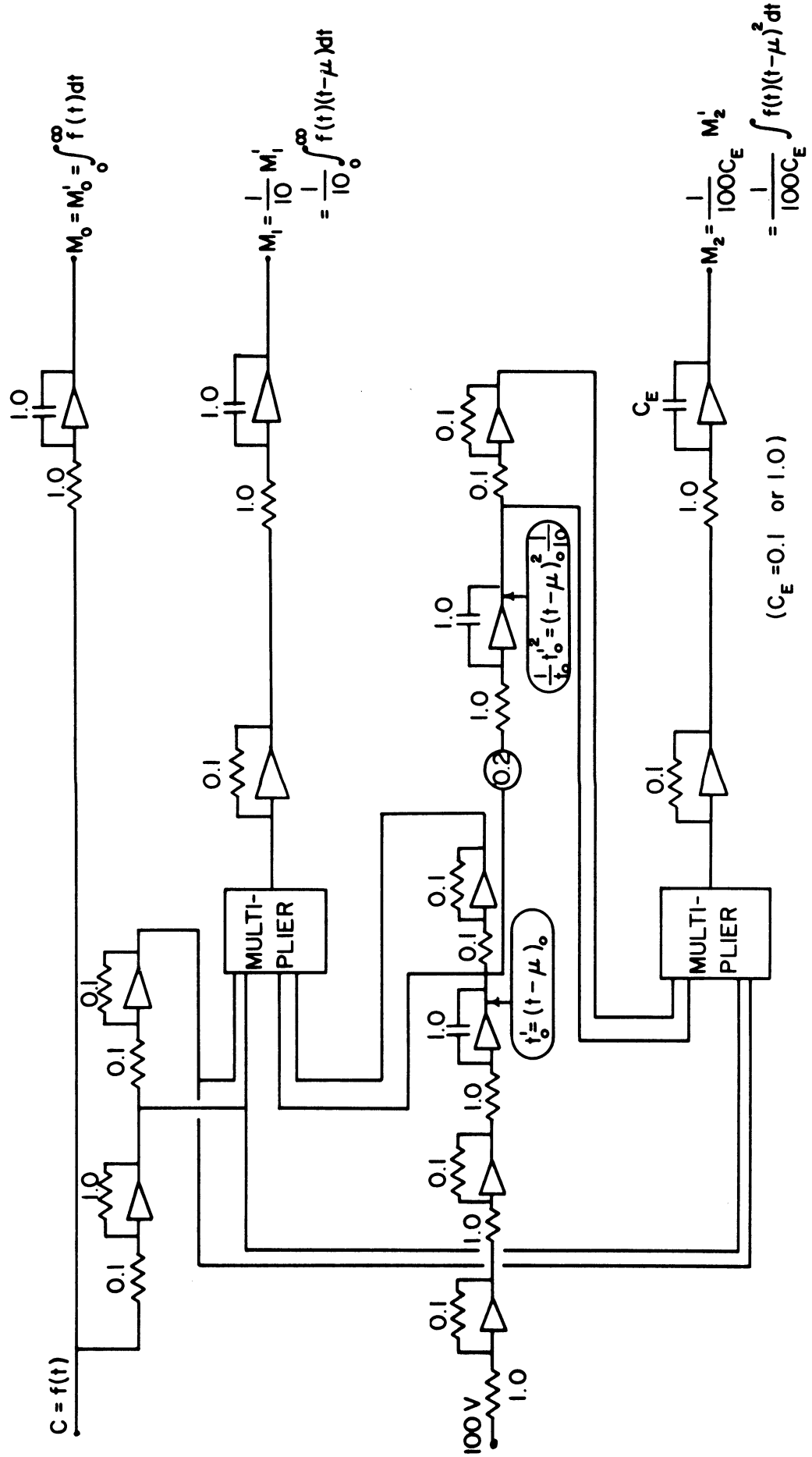


Figure 13. Analog Computer Program.

1) INVERTER

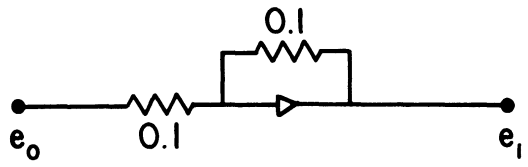


$$e_1 = -e_o$$

2) AMPLIFIER-MULTIPLIER

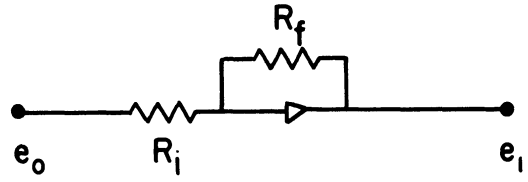


$$e_1 = -\frac{R_f}{R_i} e_o$$

3) INTEGRATOR

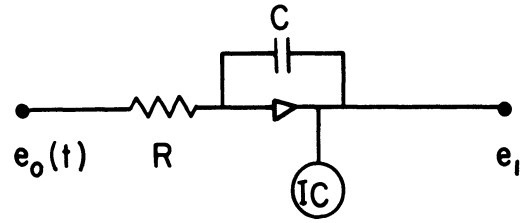


$$e_1 = -\frac{1}{RC} \int e_o \, dt$$

IC = INITIAL CONDITION
(IF IC NOT SHOWN, THEN IC=0)

4) MULTIPLIER

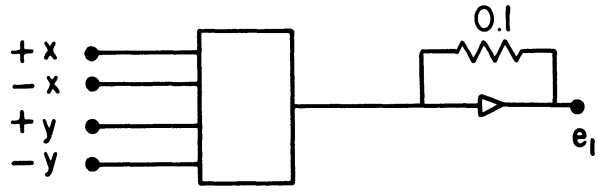


$$e_1 = -x.y$$

5) POTENTIOMETER

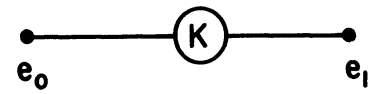


$$e_1 = Ke_o$$

$$0 < K < 1.0$$

Figure 14. Analog Computer Symbols.

the multipliers are guaranteed only within 70 millivolts, a 7% error can arise from the multiplication of two numbers of 1 volt order of magnitude. For this reason, the input voltage is multiplied by 10 (using an amplifier with gain $R_f/R_i = 10$) prior to the multiplication operations.

The capacitor $C_\epsilon$, used in computing the second moment integral, $M_2$, is allowed a value of either $0.1\mu f$ or $1.0\mu f$ to increase flexibility. The value used must of course be considered in the analysis of results.

One other modification is necessary for special cases, i.e. for runs in which the response signal was detectable for a period greater than about 80 seconds. Since the computer program described here generates a signal $0.1t'^2$, a limitation is placed on the duration of the run; if $0.1t'^2$ reaches 140 volts, then the amplifier which produces this signal will overload. It may be observed from the flow diagram, however, that $0.1t'^2$ is generated by the integrating $t'$, which in turn is obtained by integrating a one volt constant signal. If, instead, 1/2 volt or 1/3 volt is integrated to produce $t'$, then an additional scale factor of 1/2 or 1/3 is introduced into the calculated values of $M_1$ and $M_2$. This manipulation will allow the analysis of runs at lower flow rates.

Since these various scale factors are introduced into the computation, the moment integrals produced by the computer are not identical to the integrals $M_0'$, $M_1'$, $M_2'$ previously defined (Equation 17). The following relationships may be deduced from the flow diagram shown in

Figure 13. $M_0$, $M_1$, and $M_2$ represent the integrals produced by the computer.

$$M_0' = M_0 \tag{27}$$

$$M_1' = 10 \times M_1 \tag{28}$$

$$M_2' = 100 \times C_E \times M_2 \tag{29}$$

Figure 15, "Typical Voltage Profiles," illustrates parameters as they might be computed for a typical experimental run. The parameters $t_0'$ and $t_0'^2$ are estimated prior to the run to correspond as closely as possible to the time from the initial appearance of the response signal to the mean of the response signal, and are set (by potentiometers) as initial conditions on the integrating amplifiers which generate the $t'$ and $t'^2$ signals. The computer is held in the "reset" mode until the response signal is first detected, and is in "operate" mode only while the response signal is actually being monitored. When the output signal (from the thermal conductivity cell) returns to zero, the computer is switched to "hold" mode, and the results are read on a "Digitek" digital voltmeter (DVM) having an accuracy of better than 0.1%.

It will be observed that, if the computation had been started at the beginning of the pulse injection, it would be unnecessary to estimate the initial conditions $t_0'$ and $t_0'^2$; also, one integrating amplifier could be eliminated, since the quantity $t^2 \times C(t)$ could be generated by multiplying $t$ times $t \times C(t)$, instead of $t^2$ times

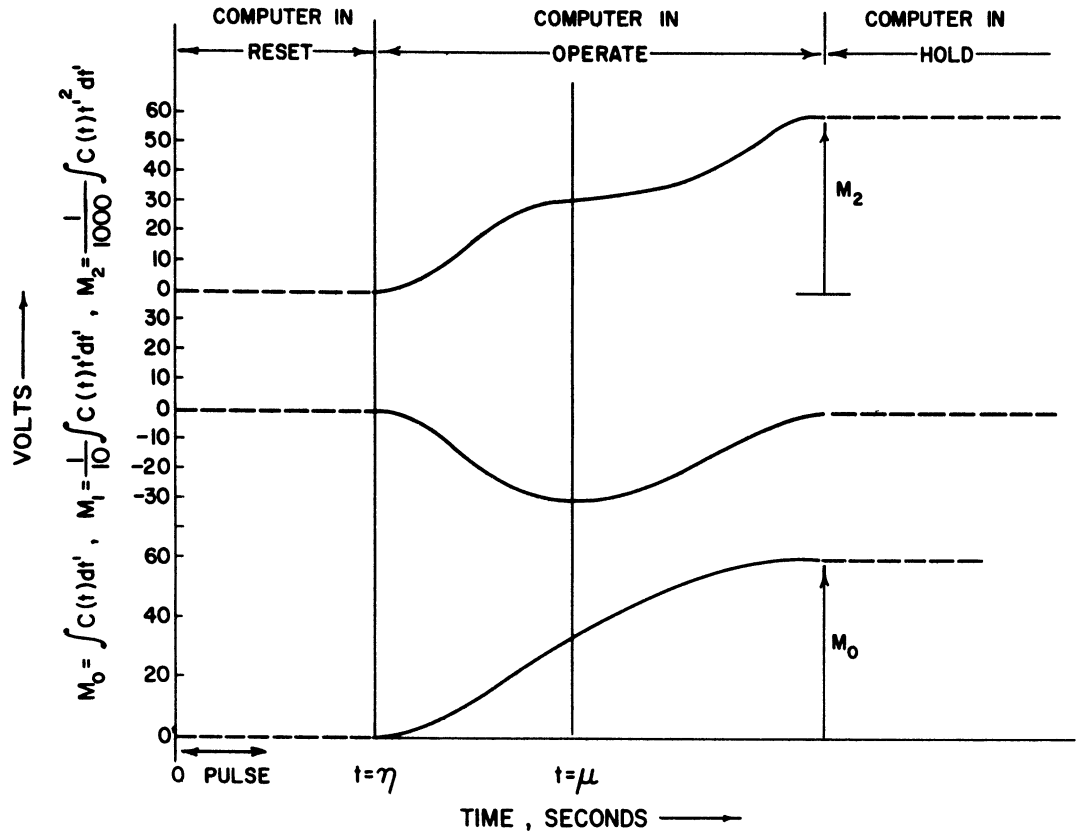


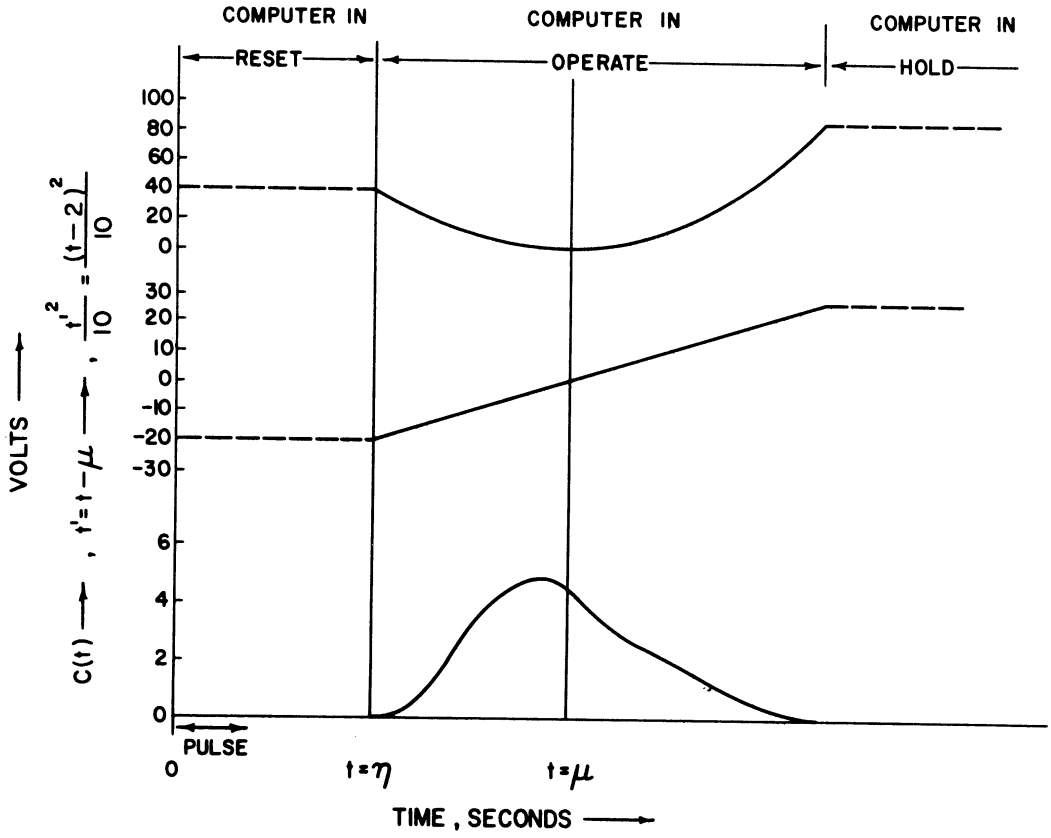


Figure 15. Typical Voltage Profiles.

$C(t)$. This method was attempted and found unsatisfactory for several reasons. First, the variance, $\sigma_t^2$, was obtained as the result of subtracting one large number from another, yielding very poor accuracy. Second, it is possible for the thermal conductivity cell output, and the output of the computer amplifiers, to drift several millivolts during the course of the run. When multiplied by $t^2$ and integrated over the duration of the run, considerable error could result. This error is not eliminated, but is minimized, by avoiding computation when the response signal is not being detected.

It is shown in Appendix II that Equation 22 is still valid when the moment integrals are computed in this manner, even if the estimated values of $t_0'$ and $t_0'^2$ are not accurate.

The computation scheme outlined in this section has sufficient flexibility to compute $M_0$, $M_1$, and $M_2$, and hence a dispersion coefficient, for all of the nitrogen-argon runs attempted. Analysis is simplified by the fact that the thermal conductivity of nitrogen-argon mixtures, relative to pure nitrogen, is linearly proportional to argon concentration; thus, the voltage profile produced by the thermal conductivity cell is the same as the concentration profile of the gas passing through the cell.

This is not true for helium-nitrogen mixtures, as evidenced by Figure 16, "Thermal Conductivity of Helium-Nitrogen Mixtures." For these runs, a diode circuit was programmed into the computer to correct the voltage profile to a concentration profile. If the cell is adjusted so that pure helium produces a signal which is amplified by the

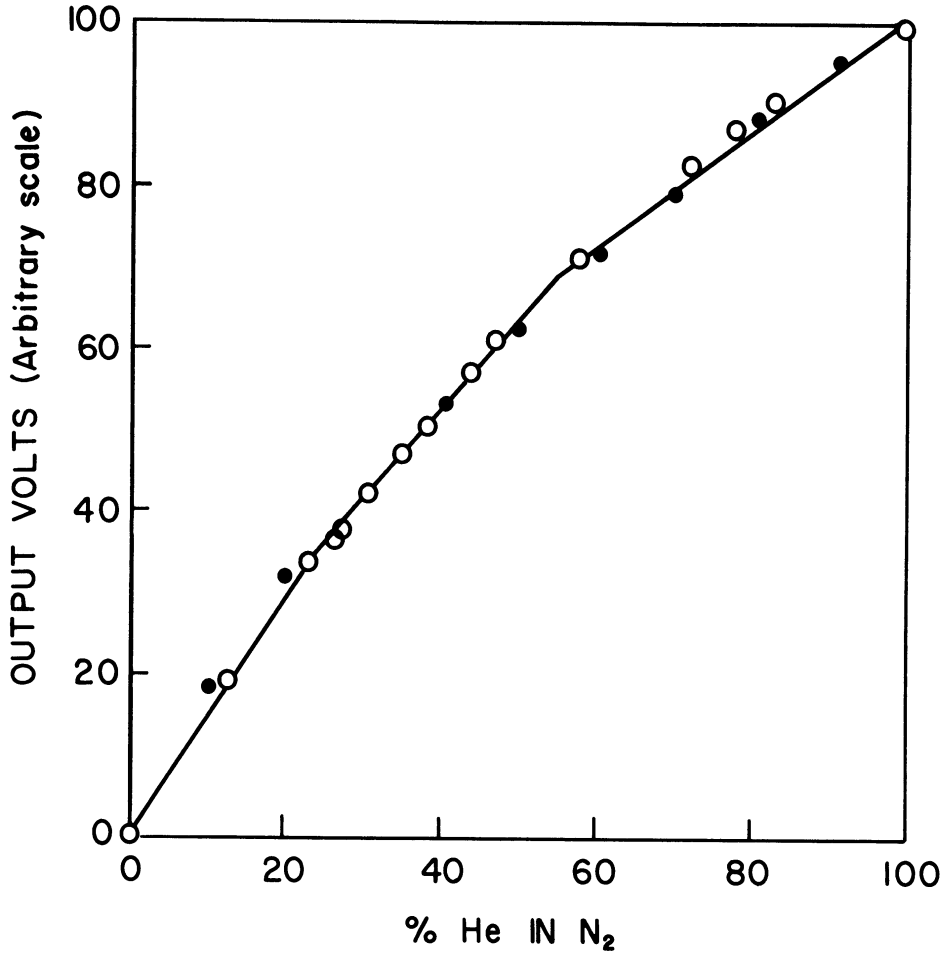


Figure 16. Thermal Conductivity of Helium-Nitrogen Mixtures.

recorder-amplifier to 10.0 volts, and if we denote the amplified cell output by $V(t)$ and the concentration of helium by $C(t)$, then examination of Figure 16 reveals that the concentration profile may be closely approximated by three straight line segments as follows.

$$C(t) = 0.6\,V(t),$$

$$0 < V(t) < 2.44 \text{ v.} \tag{30}$$

$$C(t) = 0.6\,V(t) + 0.4[V(t) - 2.44],$$

$$2.44 < V(t) < 5.875 \text{ v.} \tag{30a}$$

$$C(t) = 0.6\,V(t) + 0.4[V(t) - 2.44] + 0.26[V(t) - 5.875],$$

$$5.875 < V(t) < 10.0 \text{ v.} \tag{30b}$$

The diode circuit shown in Figure 17, "Correction for Helium Concentration Profile," was designed to accomplish this correction...

6. Instrumentation

The instrument panel constructed for the operation of all electrical equipment is shown in Figure 18, "Experimental Apparatus." An automatic timer was installed for the accurate control of short pulse injections; a semi-manual switch is also available to simultaneously switch the solenoid valves controlling both flowing and diffusing gas streams. Manual switches are provided for completely autonomous control of the solenoid valves, so that they can be simultaneously on or off when desired.

All of the computer outputs are connected to audio-connectors on the instrument panel via a jack panel, so that they can be

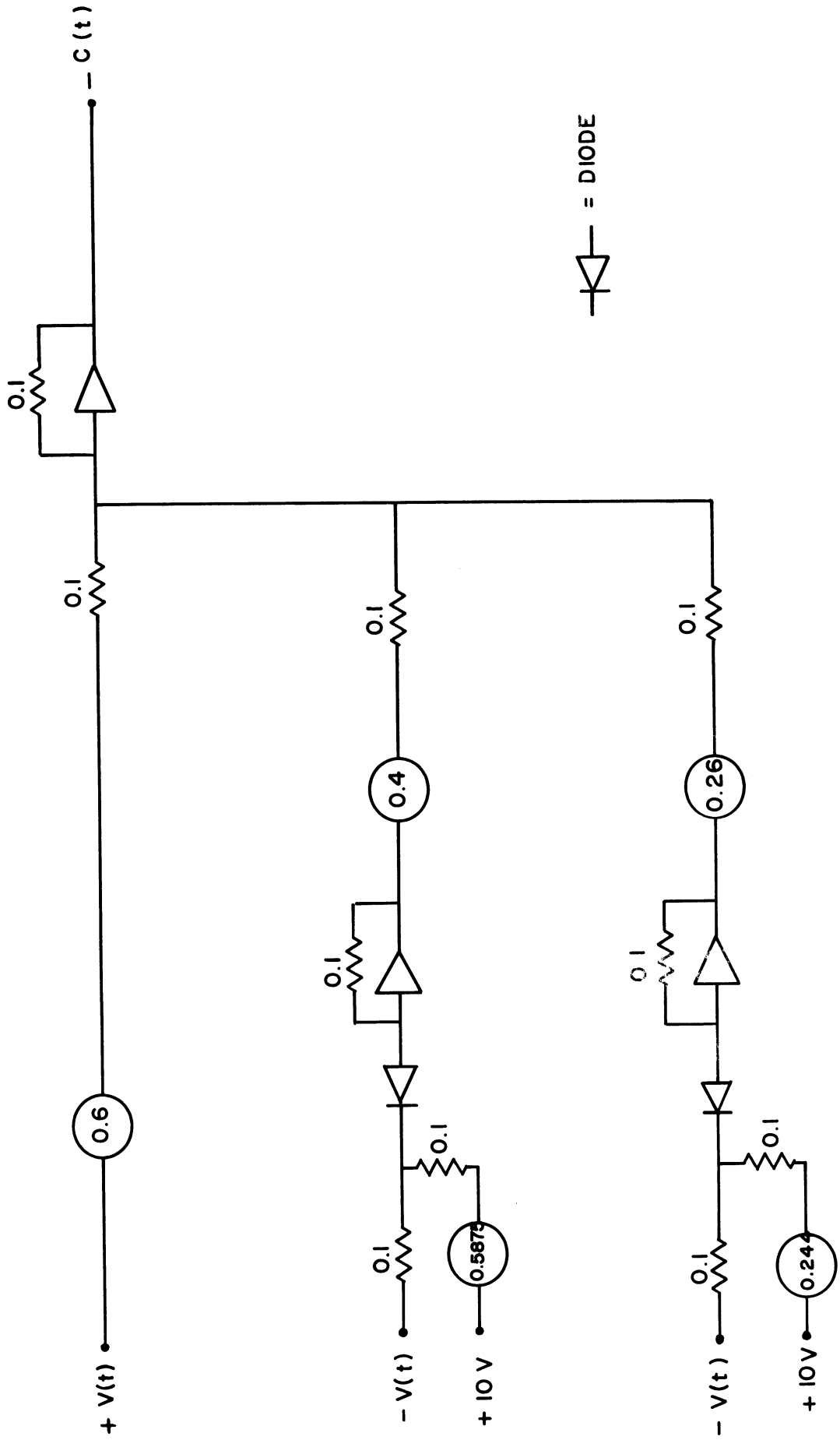


Figure 17. Correction for Helium Concentration Profile.

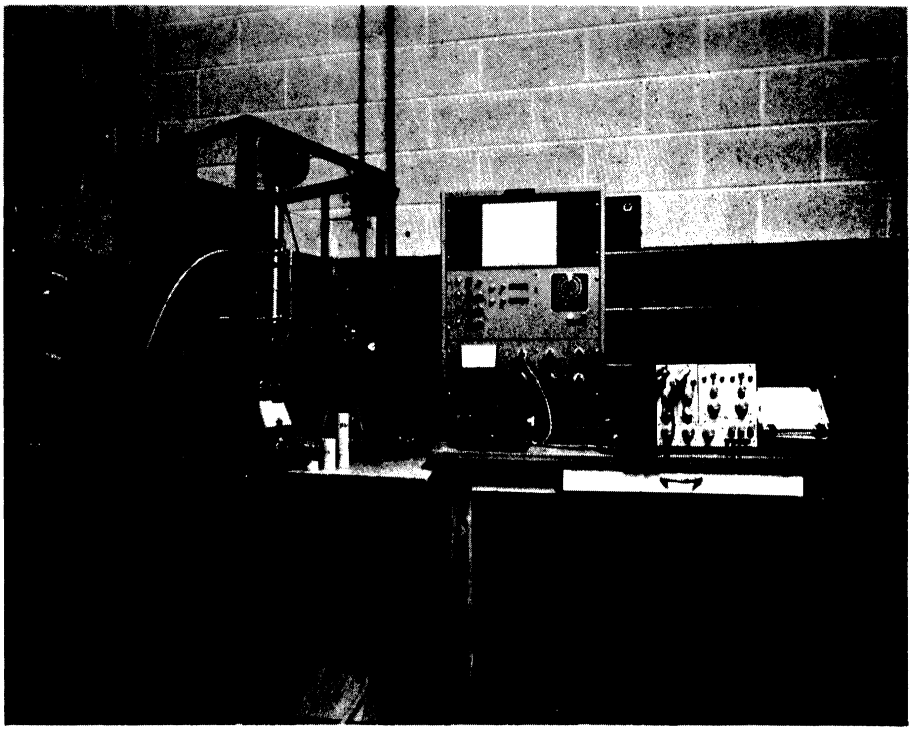

Figure 18. Experimental Apparatus.

read on an ammeter or connected conveniently to chart recorders or the digital voltmeter.

C. Calibration Procedures

The pressure gauges recording the sleeve and core pressure within the Hassler holder were calibrated using a dead-weight tester. All pressures read from the gauges were corrected using these calibration curves.

The Mano-stat rotameter indicating the flow rate through the core holder was calibrated (see Appendix II) using a wet test meter built by Precision Instruments Company.

The Hassler sleeve and other pieces of pressure equipment were hydrostatically tested to 900 psi.

The analog computer program was analyzed by processing a square wave voltage input of 2.00 volts amplitude. Computer results were found to agree with hand calculated values within 1%.

Thermal conductivity as a function of composition was determined experimentally for the helium-nitrogen system by passing samples of known concentration through the thermal conductivity cell. Experimental results were in agreement with published values, as shown in Figure 16. Published values were used for the thermal conductivity of argon-nitrogen mixtures.

The diode circuit used to correct voltage output signals from the thermal conductivity cell for helium-nitrogen mixtures was checked by recording the response to a "ramp" input signal generated by the computer.

To test thermal conductivity cell response time, step concentrations of argon were injected into a nitrogen stream close to the entrance of the cell. At flow rates up to about 0.01 cubic feet per minute, a

half-second delay time between zero output and full scale output was considered insignificant.

An approximate method was used to check each system for instability, i.e. miscible "fingering." Since stability is controlled by the density and viscosity differences between gases, we reason that if, say, the downward displacement of nitrogen by argon is unstable, then the downward displacement of argon by nitrogen is apt to be stable at the same flow rate. By recording the concentration profile responses to step inputs of nitrogen on argon and argon on nitrogen, we are able to determine visually whether the two displacements are similar. When the two responses are identical, we can conclude that both displacements are stable, but if one response profile is more "smeared" than the other, we can conclude that that displacement is unstable.

This method indicated stable displacements for the argon-nitrogen system at all flow rates studied, but the displacement of helium by nitrogen (in the downward direction) appeared to be unstable even at low flow rates for the short cores studied. We should observe that some minimum core length to diameter ratio is required in order to observe these instabilities, since a finger will in effect be obliterated by transverse dispersion if it travels a sufficient distance, in which case the response would appear to be stable.

D. Operating Procedures

From 50 to 150 raw data points were taken to constitute of set of data. A set of data is that which is required to describe the dependence of the dispersion coefficient upon flow rate for a range of flow rates.

Flow rates ranged from approximately 0.002 to 0.015 cubic feet per minute (measured at 14.7 psia, 70°F.). An upper limitation is set by the response time of the thermal conductivity cell used, and the lower limitation is effectively set by drift characteristics of the thermal conductivity cell and the analog computer.

It is first necessary to obtain a measure of the mixing which occurs in the peripheral plumbing and ends of the flow system, for the entire range of velocities under consideration. This is done by inserting one or two small (1 to 2 inches in total length) core plugs in the holder and measuring responses (i.e. variances, $\sigma_t^2$) to a square wave input, normally of five second duration. Each data point is taken three times in order to obtain a check of the effect of thermal conductivity cell drift, etc.

The sample being studied is then inserted in the holder, in addition to the core plug(s) used in determining the end effects. If two end plugs were used, the sample is positioned between them; in this case, the "end plugs" may or may not be of the same material as the sample being studied. If only one small plug is used in obtaining the end effects, then it must be of the same material as the sample. Responses (variances) are then determined for the new system, using the same square wave input, for the same range of flow rates.

The resulting set of data points expresses variance as a function of flow rate for (1) the core plus ends and plumbing, and (2) the ends and plumbing. By subtracting the second from the first we obtain the change in variance due to mixing in the core itself, which may be used with Equation (22) to determine a dispersion coefficient for a given velocity.

The subtraction of variances in this manner is dependent upon the linearity of Equation 6. The superposition principle permits the subtraction of variances if it is assumed that Equation 6 may be quasi-linearized by evaluating the velocity and dispersion coefficient at an average flowing pressure.

Analysis of the raw data is discussed further in Part E of this section, and sample calculations are included in Appendix I. With the understanding that a number of data points are necessary to characterize the mixing properties of a porous medium, this section will attempt to describe the operational procedures involved in obtaining each data point.

(1) The analog computer and thermal conductivity cell are turned on in advance to allow sufficient warm-up time. After warm-up (30 minutes or so) all amplifiers are balanced. The Dynograph amplifier-recorder and the digital voltmeter are turned on and balanced, and the switch is thrown to allow power to the solenoid valves and timer.

(2) The core and/or "end" plug is mounted in the Hassler core holder and the sleeve is pressurized to at least 50 psi in excess of the maximum anticipated flowing pressure for the run. All electrical connections must be checked between runs, since others also use the computer and occasionally find it necessary to break connections associated with this apparatus.

(3) The gas cylinders are opened, and nitrogen is allowed to bleed slowly through the reference side of the thermal conductivity cell. Argon (or helium) and nitrogen flow rates are adjusted to yield equal pressure drops through the core sample. Vent needle valves must also be adjusted so that the switching of solenoid valves does not

cause a pressure perterbation at the core inlet. The inlet pressure and the outlet flow rate are then noted. Ambient temperatures need not be recorded, since the temperature is regulated at 70°F for all runs.

(4) The time, in seconds, between the initial appearance of the response signal and the mean, $\mu$, of the response signal, must be estimated. The parameters $t_0'$ and $t_0'^2$ are set as initial conditions on the computer's integrating amplifiers which generate the $t'$ and $t'^2$ signals. This is accomplished by setting two potentiometers. An accurate estimate of $t_0'$ is not necessary, but will result in better accuracy.

(5) A pulse time is selected and set on the timer switch. A five second pulse is used for all runs with short cores, since calculations are simplified by using a standard pulse length. All electrical connections are checked, and the digital voltmeter is connected to read the computer input signal, i.e. the amplified thermal conductivity cell output.

(6) With nitrogen flowing through the system ("ends," or "ends plus core sample"), the timer switch is tripped to allow a square concentration wave of argon (or helium) to enter the system. That is, argon flow is started and nitrogen flow is simultaneously stopped, and then five seconds later the solenoid valves are reversed to their original position, with nitrogen again flowing.

(7) As soon as argon begins to appear at the system exit, as monitored by the thermal conductivity cell, the computer is switched from "reset" to "operate" mode. When the response signal has "peaked"

and returned to zero, the computer is switched to "hold" mode. The parameters $M_0$, $M_1$, and $M_2$ are then read on the digital voltmeter.

(8) Steps 6 and 7 are repeated twice in order to check the reproducibility of the results. The initial conditions $t_0'$ and $t_0'^2$ may also be re-estimated if necessary. A new flow rate is then chosen, and steps 3, 4, and 5 are repeated.

E. Calculation Procedures

Having obtained the computer outputs $M_0$, $M_1$, and $M_2$ for both the "ends" and "ends plus core," over a range of velocities, with inlet pressures, core dimensions and core properties known, a dispersion coefficient may be calculated for each velocity using Equation 22. It is the purpose of this section to summarily describe the calculation procedures used, although more detail may be found in the sample calculations in Appendix I.

The variance of the response signal is first determined for each run using Equations 22 and 31.

$$\sigma_t^2 = \frac{M_2'}{M_0'} - \left(\frac{M_1'}{M_0'}\right)^2 = \frac{100 \times C_E \times M_2}{M_0} - \left(\frac{10 M_1}{M_0}\right)^2 \qquad (31)$$

These variances are then plotted as a function of flow rate. Two "bands" of data points result; one describes the change of variance due to mixing in the core plus ends and lines, and the other characterizes the change of variance due to mixing in the ends and lines. Each set of points is "banded" by two curves, rather than attempting a fit by a single curve. In this manner both a maximum and a minimum

value of $\Delta\sigma_t^2$ is obtained for each velocity. Figure 19, "Evaluation of Mixing Within a Porous Medium, schematically represents the model by which the change in variance due to mixing within the core sample is determined.

A modification to this method is required when a significant pressure drop exists across the core sample, i.e. for high flow rates and/or low permeabilities. The "end effects" or mixing in ends and plumbing, were found to depend upon volumetric flow rate, rather than mass flow rate; hence, if the inlet pressure is significantly above atmospheric, then the "end effects" determined in the absence of a core sample will not apply in the presence of the sample. In order to modify the calculation procedure for such cases, it is necessary to make the approximation that the volume of the plumbing upstream of the core is equal to the volume of the plumbing downstream of the core, and then estimate an "average" volumetric flow rate in terms of the measured mass flow rate (i.e. the measured volumetric flow rate at ambient conditions); the "end effects" curve ( $\sigma_t^2$ vs. flow rate) is then modified to describe $\Delta\sigma_t^2$ as a function of this average volumetric flow rate, as follows.

Let $\mu_u$ = upstream residence time

$$= \frac{V_u}{v'_u} = \frac{P_u V_u}{v'_{14.7}} = \frac{P_u V}{2 v'_{14.7}}$$

$\mu_d$ = downstream residence time

$$= \frac{V_d}{v'_d} = \frac{P_d V_d}{v'_{14.7}} = \frac{P_d V}{2 v'_{14.7}}$$

I SYSTEM = "ENDS"

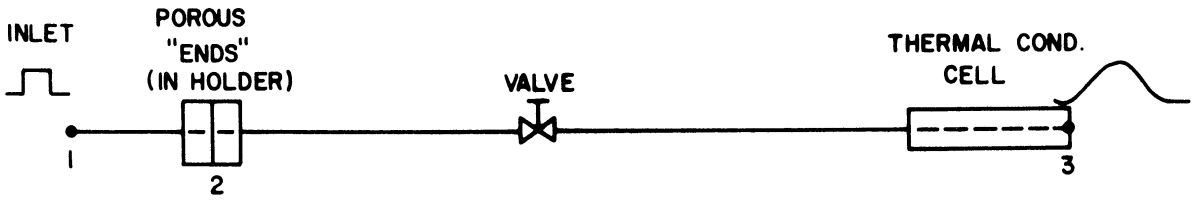


Mixing Occurs in Lines, End Plugs, Valve, and Thermal Conductivity Cell.

II SYSTEM = "ENDS" PLUS CORE

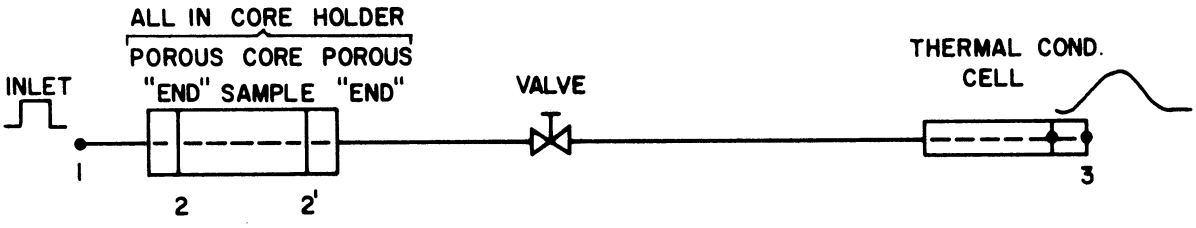


Mixing Occurs in Lines, Porous Ends, Core Sample, Valve, and Thermal Conductivity Cell.

$$\Delta\sigma^2_{t_{2-2'}} = \Delta\sigma^2_{t_{12}} + \Delta\sigma^2_{t_{2-2'}} + \Delta\sigma^2_{t_{2'-3}} - (\Delta\sigma^2_{t_{1-2}} + \Delta\sigma^2_{t_{2-3}})$$

$$= \Delta\sigma^2_{t_{II}} - \Delta\sigma^2_{t_I} = \sigma^2_{t_{3_{II}}} - \sigma^2_{t_{3_I}}$$

= change in variance due to mixing in core.

Figure 19. Evaluation of Mixing Within Porous Medium.

$\mu$ = total residence time $= \mu_u + \mu_d$

$$= \frac{V}{v'_{14.7}}(P_u + P_d) = \frac{V}{v'_{14.7}}(P_u + 1)$$

Then the ratio of the average volumetric flow rates is equal to the reciprocal of the ratio of residence times, or

$$v'_{\text{corrected}} = \left(\frac{P_2 + 1}{P_1 + 1}\right) v'_{\text{measured}} \qquad (32)$$

where $P_1$ = upstream pressure when the core is not in place, atm. abs.,

$P_2$ = upstream pressure when the core sample is in place, atm. abs.,

$v'_{\text{measured}}$ = the flow rate (cubic feet per minute) as measured on the rotameter, when the core is not in place, and

$v'_{\text{corrected}}$ = the flow rate against which $\sigma_t^2$ for the end effects should properly be correlated.

Having obtained maximum and minimum values of $\Delta\sigma_t^2$ as a function of flow rate for a sample, it is necessary to convert this value to a "relative change in variance," $\Delta\sigma^2$, by dividing by the square of the residence time, $(L/u)^2$. The relative change of variance simply de-dimensionalizes the variance change, since $\Delta\sigma_t^2$ has units of time$^2$.

In order to make this conversion, it is necessary to determine the average interstitial velocity, $u$, i.e. the interstitial velocity at the average flowing pressure. The average flowing pressure may be found in terms of the inlet pressure (assuming atmospheric pressure at the outlet) by the application of Darcy's Law for gas flow

(see Appendix II).

$$P_{avg} = \frac{2}{3} \frac{P_{inlet}^3 - 1}{P_{inlet}^2 - 1} \qquad (33)$$

In Equation 33, pressures are expressed in atmospheres absolute.

The relative variance change is then used to calculate the dispersion coefficient by Equation 22:

$$D_e = \frac{\Delta\sigma^2}{2} \text{(avg. interstitial velocity)(core length)} \qquad (22)$$

Appropriate units for the dispersion coefficient are $cm^2/sec$.

Following the practice established in the literature, data are correlated by describing the ratio of the dispersion coefficient to the molecular diffusion coefficient, $D_e/D_o$, as a function of a Peclet number, $u d_p \sigma / D_o$. Here, $\sigma$ is an "inhomogeneity factor" which is conveniently combined with the particle diameter, $d_p$, to form a parameter ($d_p\sigma$) which may be used to characterize the mixing properties of the porous medium. Since the interstitial velocity, $u$, and the molecular diffusion coefficient, $D_o$, are both inversely proportional to the flowing pressure, it follows that $D_e/D_o$ may be plotted vs. the volumetric flow rate measured at atmospheric pressure, and the parameter ($d_p\sigma$) may be determined as that number which makes the data fit the model of Equation 9b.

$$\frac{D_e}{D_o} = \frac{1}{F\phi} + 0.5\left(\frac{u d_p \sigma}{D_o}\right)^m \qquad (9b)$$

The molecular diffusion coefficient, $D_o$, may be computed using the Chapman-Enskog or Lennard-Jones collision integral theory[7,8,17]. For a given binary system at constant temperature, it is shown in Appendix I that $D_o$ depends only upon pressure.

# V. EXPERIMENTAL RESULTS

The results of this experimental program may be considered conveniently in three parts. First, dispersion coefficients were obtained for the nitrogen-argon system using samples 2 to 5 inches in length; unsatisfactory data were obtained for the helium-nitrogen data using these short cores. Second, two of these short cores were treated with a pentane-paraffin solution to provide various degrees of blocking by an immobile phase, and dispersion coefficients were again determined. Third, a longer sample was mounted in epoxy, and dispersion coefficients were obtained in order to check the effect of core length upon results. Dispersion characteristics were also determined for the helium-nitrogen system using the long core, but the interpretation of the results is open to some question.

## A. Short, Dry Samples

Experimental results obtained using short, dry core samples are shown in Figures 20 a-i. Approximate error limits are indicated in these illustrations. Experimental accuracy is considered good, since conservative means were used to obtain the indicated error limits. Better data were obtained, as expected, for longer cores, since the analysis of end effects was not as critical in this case. The physical properties of the core specimens are shown in Tables I and II.

All data in Figures 20 a-i were obtained for the nitrogen-argon system. Attempts to obtain similar data for the helium-nitrogen system

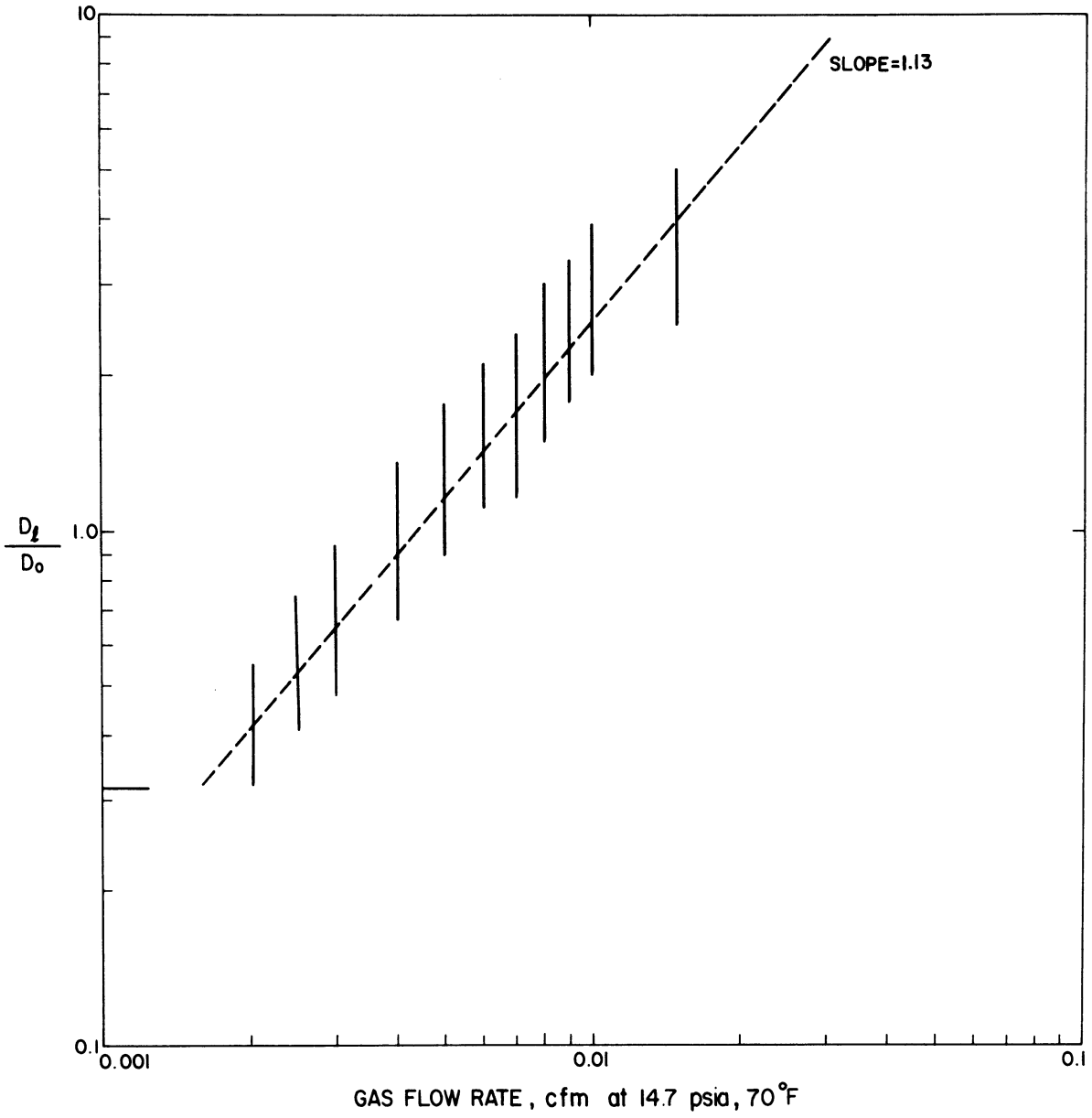


Figure 20a. Dispersion Characteristics as a Function of Flow Rate. Core BA-2, Bandera Sandstone.

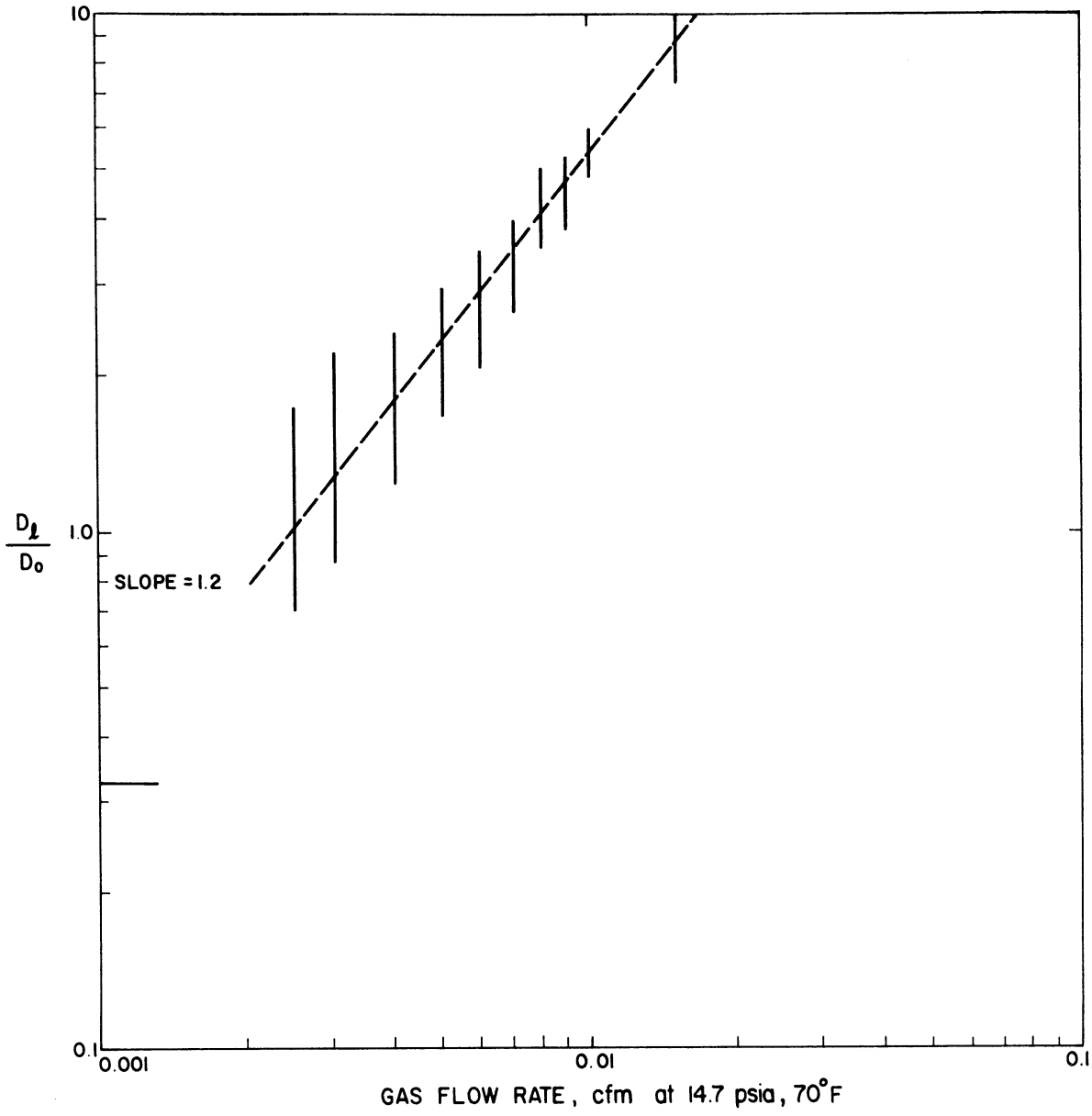


Figure 20b. Dispersion Characteristics as a Function of Flow Rate. Core BA-3, Bandera Sandstone.

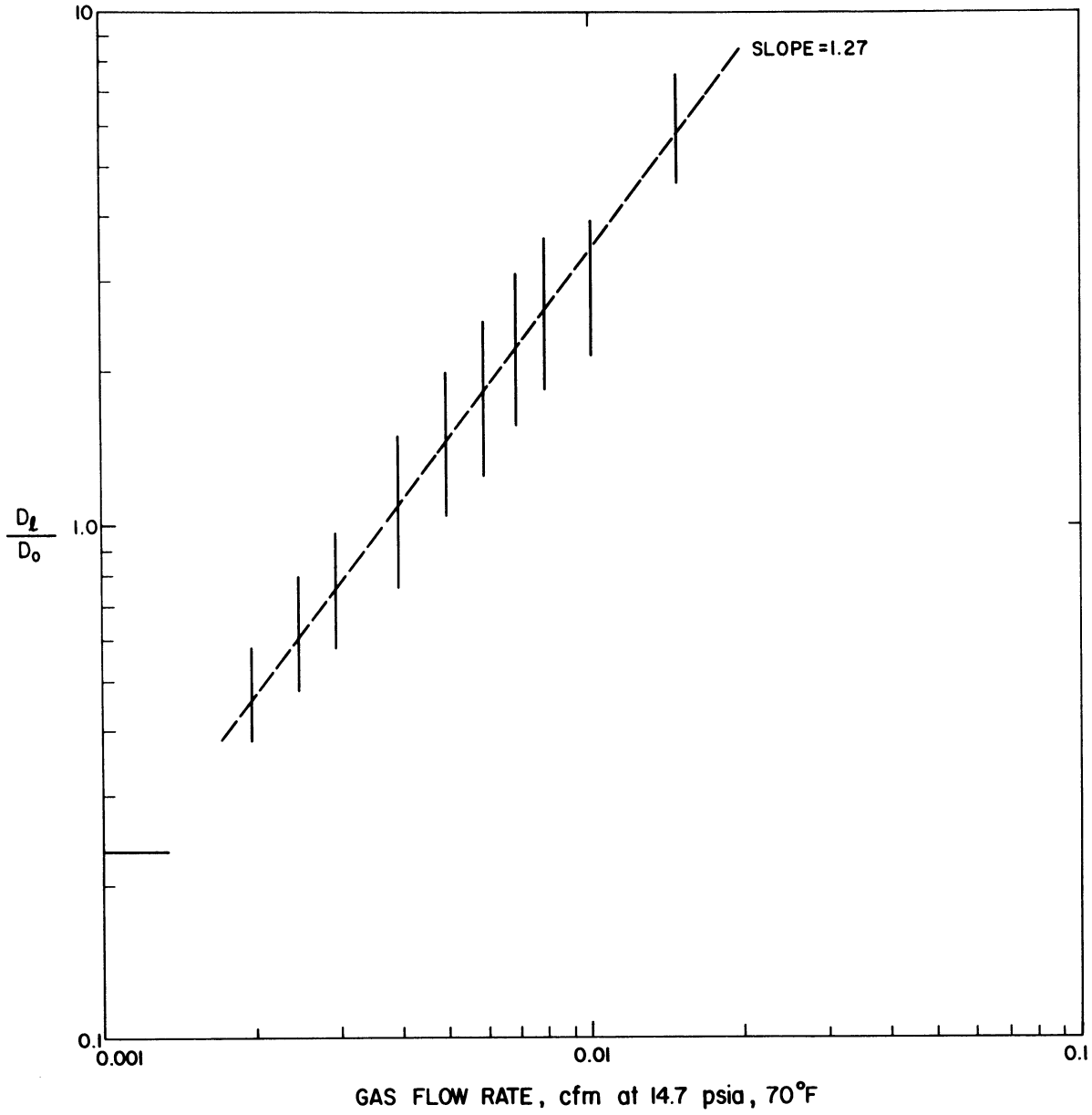


Figure 20c. Dispersion Characteristics as a Function of Flow Rate. Core BO-1, Boise Sandstone.

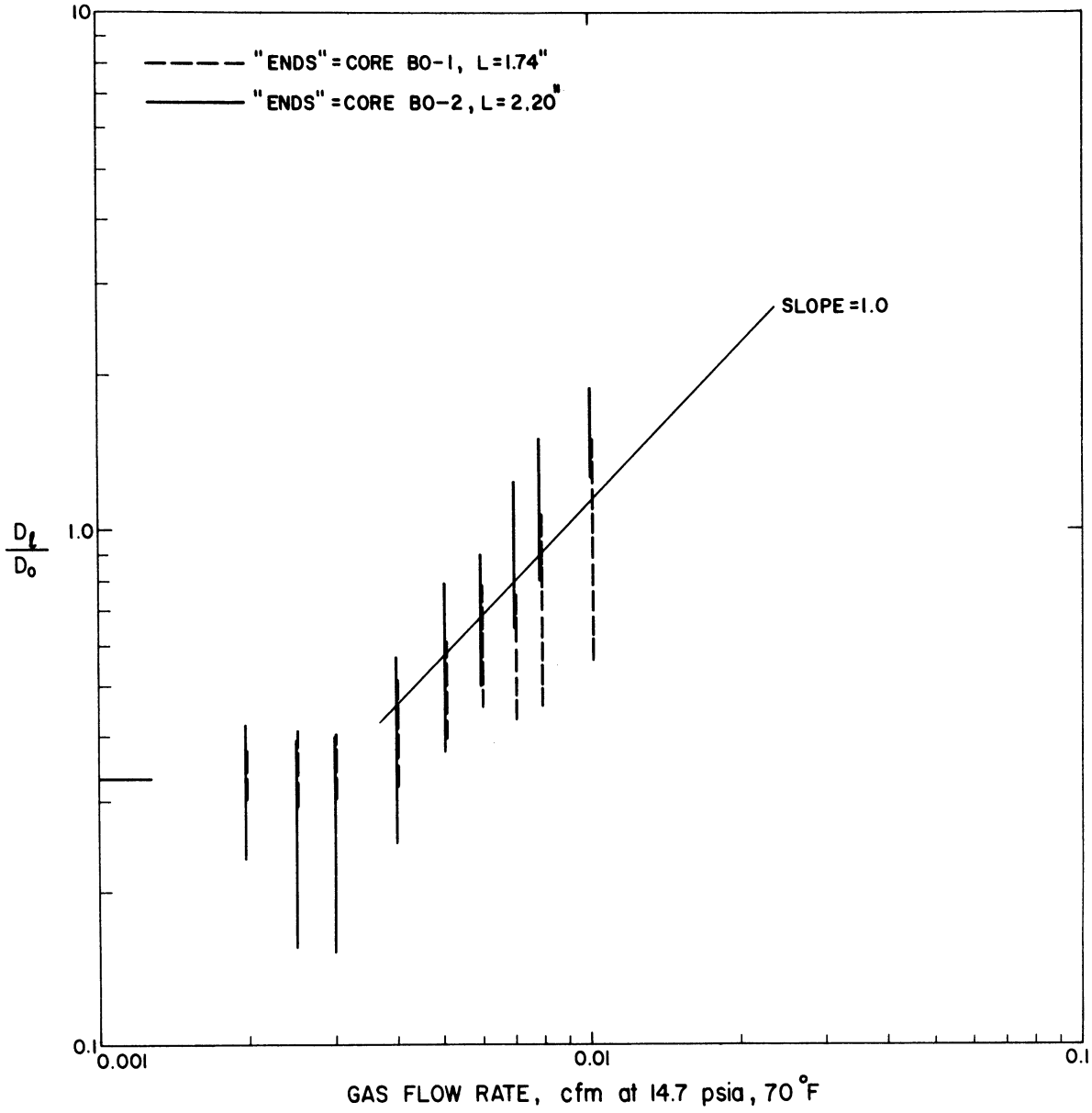


Figure 20d. Dispersion Characteristics as a Function of Flow Rate. Core BO-2, Boise Sandstone.

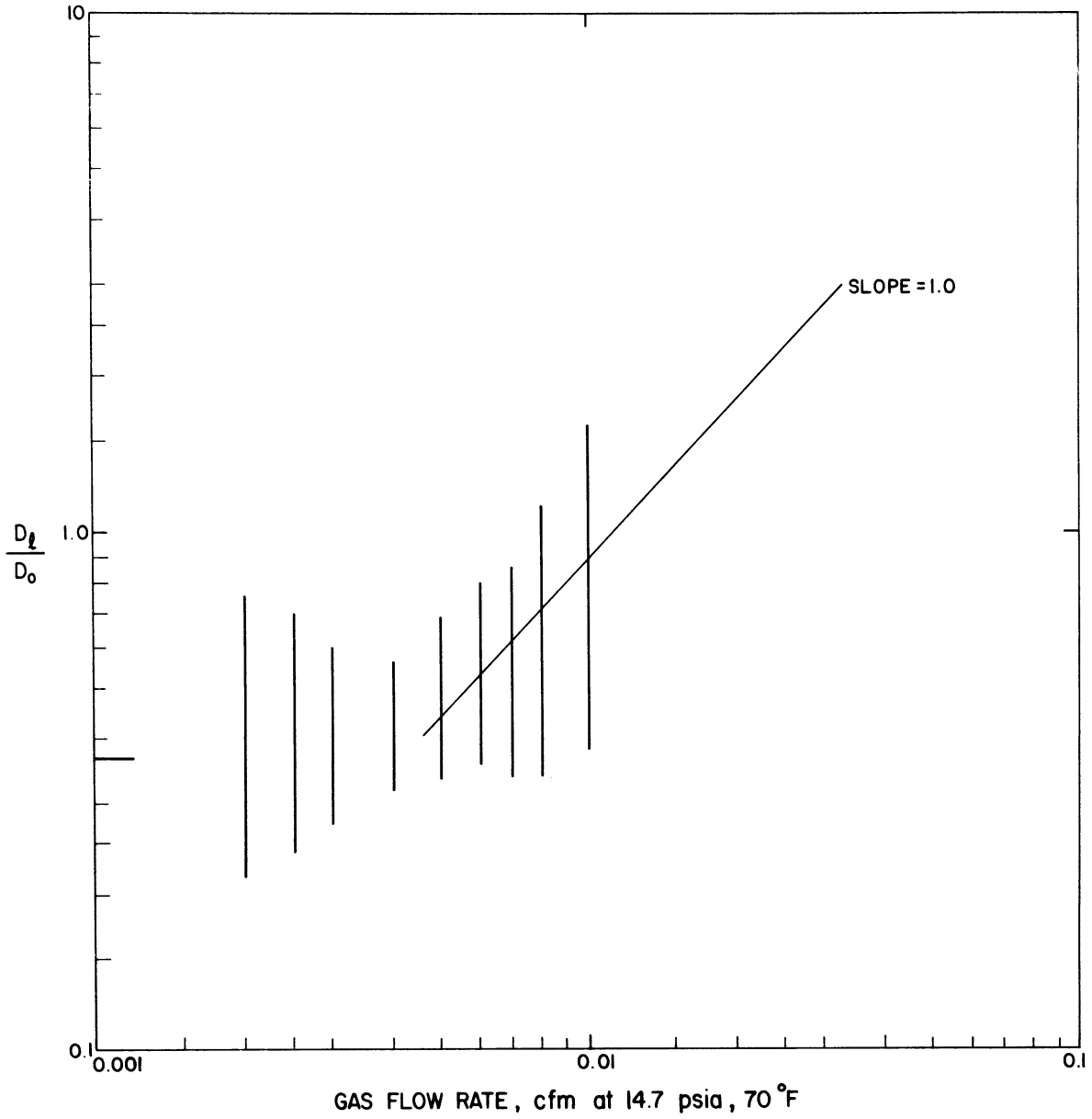


Figure 20e. Dispersion Characteristics as a Function of Flow Rate. Core BO-3, Boise Sandstone.

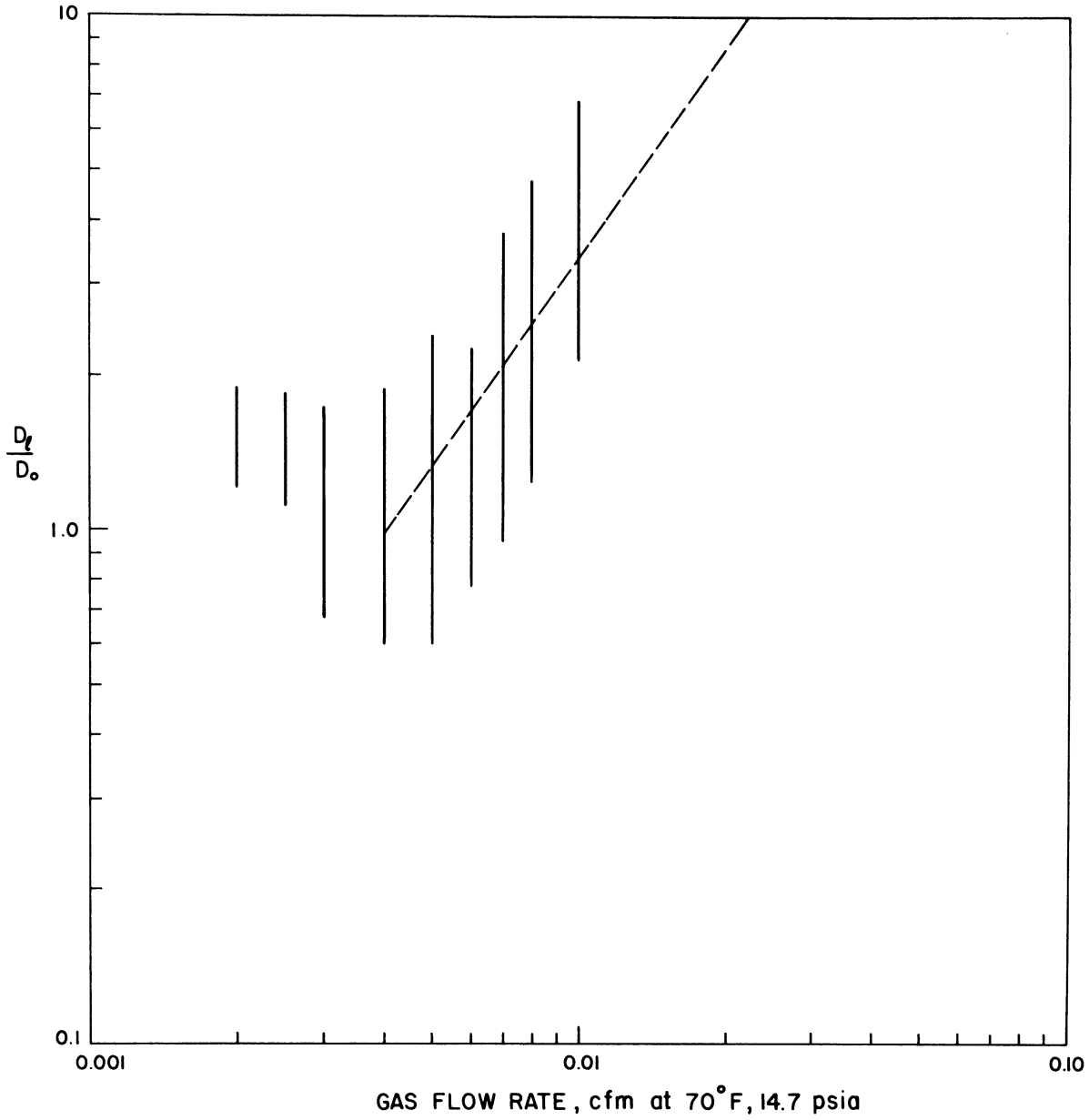


Figure 20f. Dispersion Characteristics as a Function of Flow Rate. Core FYX-A, Nodosaria Sandstone.

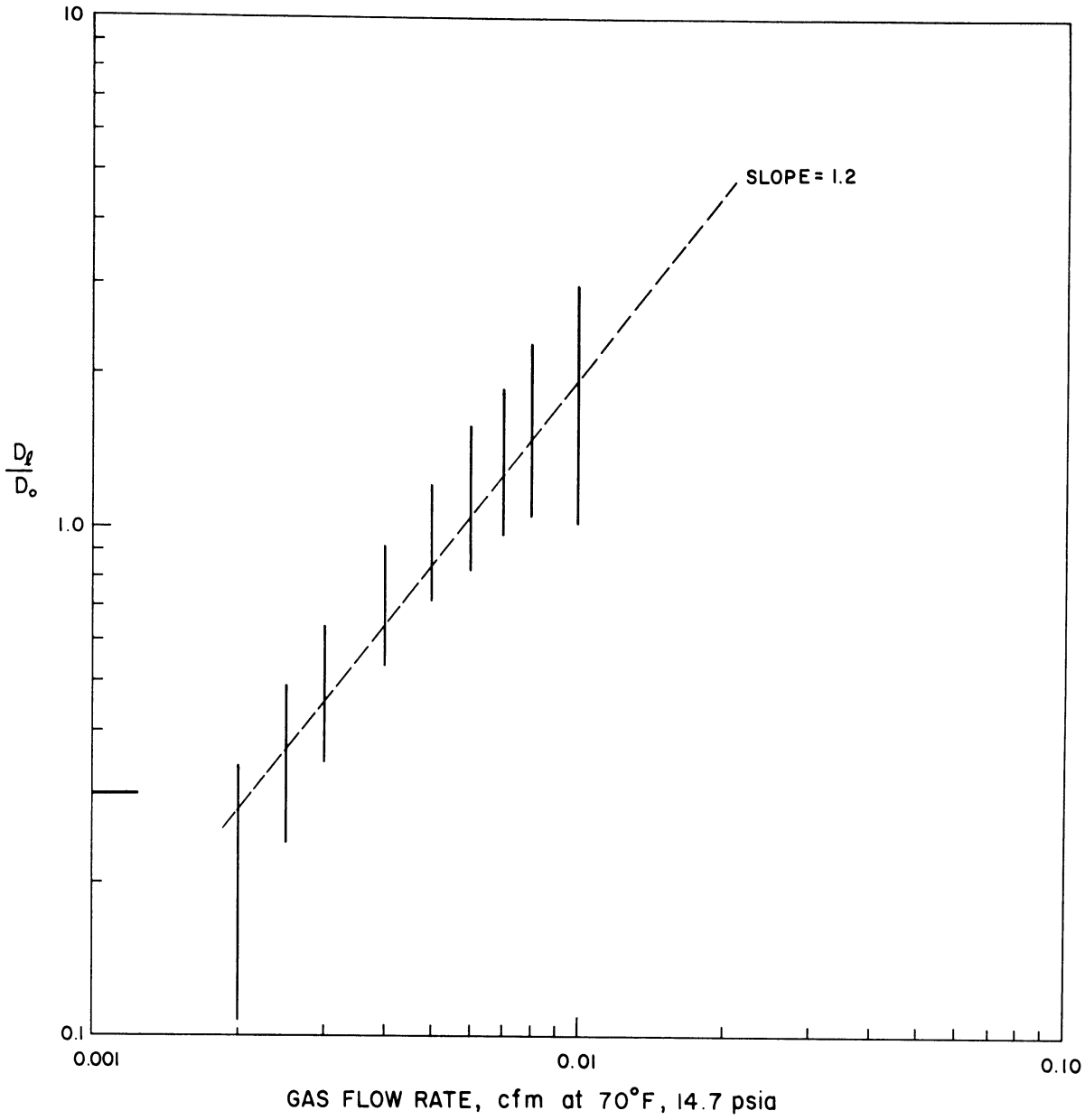


Figure 20g. Dispersion Characteristics as a Function of Flow Rate.
Core FYX-B, Nodosaria Sandstone.

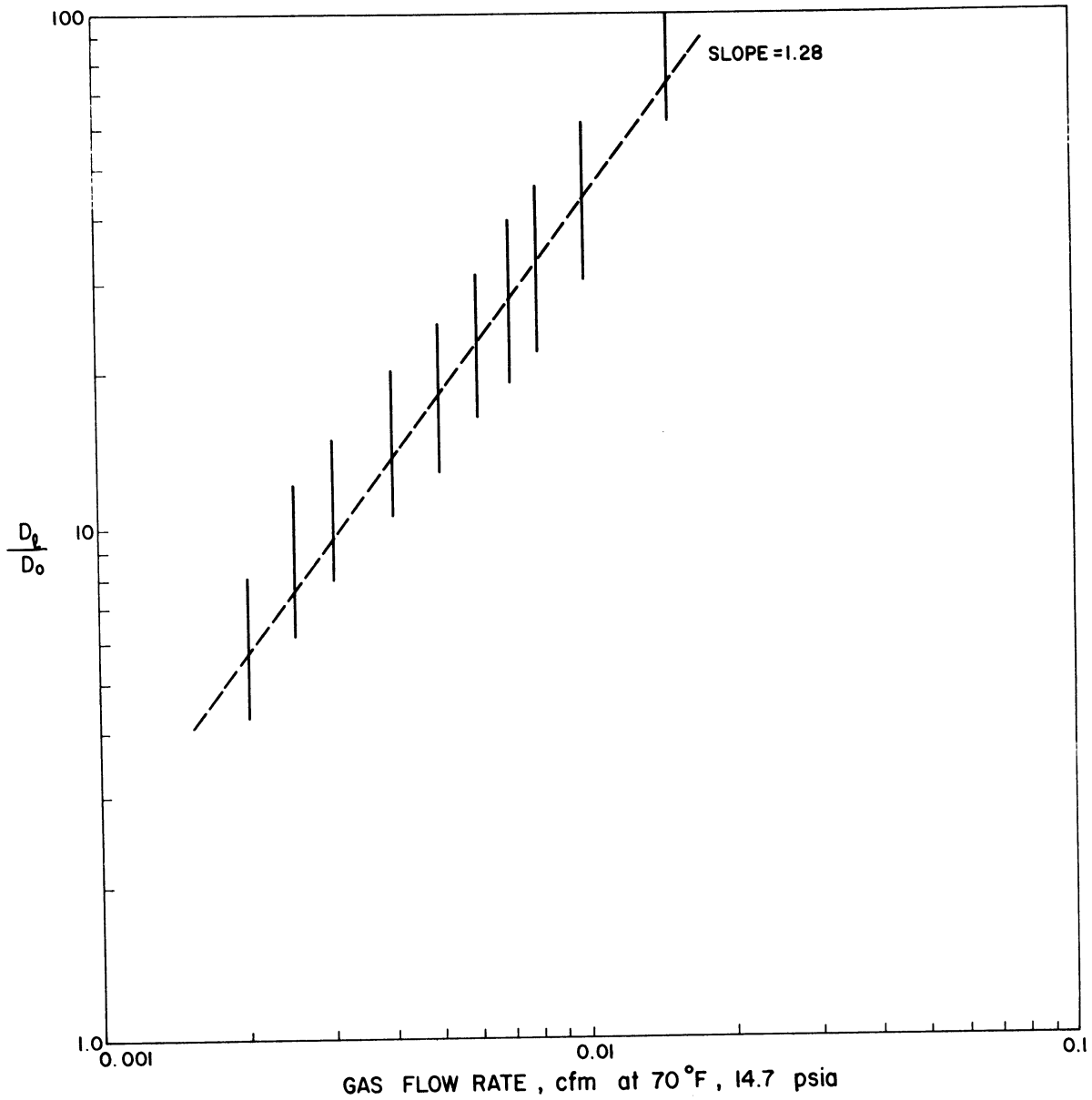


Figure 20h. Dispersion Characteristics as a Function of Flow Rate. Core 3501, Dolomite.

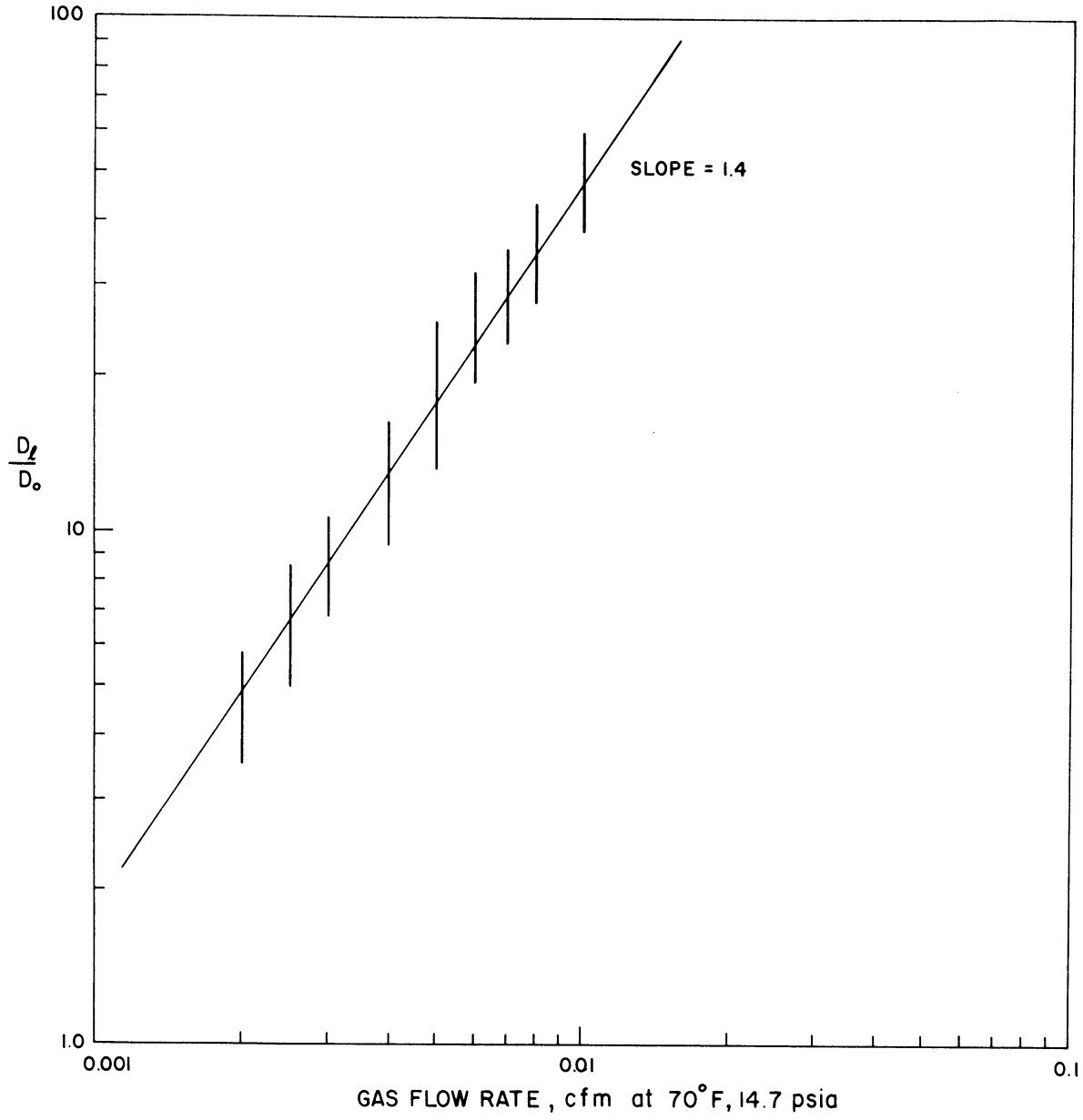


Figure 20i. Dispersion Characteristics as a Function of Flow Rate. Core 3514, Dolomite.

were unsuccessful, since the mixing in these short cores was dominated by instabilities. That is, experimental results were not reproducible within a tolerable range of error; the variance-responses to square wave stimuli showed particular scatter at higher flow rates.

The "characteristic length," $d_p\sigma$, and power dependence, or slope, $m$, were determined from experimental data for each specimen (see sample calculations in Appendix I) in order to fit the results to the equation

$$\frac{D_c}{D_i} = \frac{1}{F\phi} + 0.5\left(\frac{u\, d_p\sigma}{D_c}\right)^m \qquad (9b)$$

The calculated values of these parameters are included in Table II, "Specimen Properties." The characteristic lengths, ($d_p\sigma$) vary from 0.23 cm to 1.87 cm, in fair agreement with the average value of 0.36 cm reported by Perkins and Johnston[43]. The sandstones used here have an average characteristic length of $d_p\sigma = 0.423$ cm, but the dolomite samples show abnormally high values.

Comparison of Equation 14 with a friction factor equation of the type (32)

$$\frac{\Delta P}{L} = \left[\frac{150(1-\phi)^2\mu'}{\phi^3 g_c d_p^2}\right]v + \left[\frac{1.75\,\rho(1-\phi)}{g_c d_p \phi^3}\right]v^2 \qquad (34)$$

shows that the particle diameter for a porous medium should be inversely related to the turbulence factor. If a constant value of the packing factor, $\sigma$, is assumed for each rock type, then this observation is verified by the data of Table II, in further support of the validity of these experimental results.

TABLE I

SPECIMEN TYPES
(See also Table II)

| Core Label | Length, Inches | Type | Source |
|---|---|---|---|
| (1) BA-2 | 4.73 | Bandera sandstone | Continental Oil Company |
| $BA-2_A$ | 0.96 | | |
| $BA-2_B$ | 1.14 | | |
| (2) BA-3 | 4.97 | " " | " |
| $BA-3_A$ | 0.83 | | |
| $BA-3_B$ | 0.96 | | |
| (3) BO-1 | 4.88 | Boise sandstone | " |
| $BO-1_A$ | 0.86 | | |
| $BO-1_B$ | 0.88 | | |
| (4) BO-2 | 3.92 | " " | " |
| $BO-2_A$ | 2.20 | | |
| (5) BO-3 | 3.20 | " " | " |
| $BO-3_A$ | 2.02 | | |
| $BO-3_B$ | 1.00 | | |
| (6) FYX-A | 2.32 | Nodosaria sandstone | " |
| (7) FYX-B | 2.61 | " " | " |
| (8) BE-1 | 4.20 | Berea sandstone | Cleveland Quarries |
| BE-2 | 5.22 | | |
| BE-3 | 23.90 | | |
| (9) 3501 | 2.66 | Dolomite | U. S. Bureau of Mines |
| (10) 3514 | 3.44 | " | " |

All diameters = 1.50 inches

TABLE II

SPECIMEN PROPERTIES
(See also Table I)

| Core Label | Porosity, Percent | Perm., Md. | Turbulence Factor, $Ft.^{-1}$ | Resistivity Factor, F | $d_p\sigma$, cm. | Exponent m, (Eq. 9b) |
|---|---|---|---|---|---|---|
| (1) BA-2 | 23.4 | 40. | $1.25 \times 10^{9}$ | 13.3 | 0.475 | 1.13 |
| (2) BA-3 | 21.8 | 41.6 | $6.4 \times 10^{8}$ | 14.2 | 0.75 | 1.20 |
| (3) BO-1 | 31.0 | 1030 | $4.6 \times 10^{6}$ | 13.9 | 0.67 | 1.27 |
| (4) BO-2 | 32.0 | 258 | $1.4 \times 10^{7}$ | 9.5 | 0.346 | -- |
| (5) BO-3 | 32.0 | 1430 | $1.72 \times 10^{8}$ | 8.3 | 0.25 | -- |
| (6) FYX-A | 21.8 | 1008 | not determined | 13.6 | 0.41 | 1.36 |
| (7) FYX-B | 25.2 | 227 | " | 13.3 | 0.366 | 1.20 |
| (8) BE-1 | 19.0 | 300 | " | 15.2 | 0.316 | 1.24 |
| BE-2 | " | 267 | " | " | -- | -- |
| BE-3 | " | 228 | " | " | 0.232 | 1.24 |
| (9) 3501 | 12.5 | 61.4 | $5.2 \times 10^{8}$ | 27.6 | 1.87 | 1.28 |
| (10) 3514 | 12.1 | 4.45 | $3.2 \times 10^{10}$ | 41.6 | 1.44 | 1.40 |

A study of a Berea sandstone is also discussed in Part C of this section; the results are shown in Table II.

The power dependence, $m$ , of the dispersion coefficient upon velocity, is seen to range from approximately 1.0 to 1.40, which is in good agreement with data obtained by Brigham, et. al.[12] and Blackwell, et. al.[11]; these authors obtained values of $m = 1.17$ to 1.24 for Berea sandstone cores using liquid systems. Brigham, et. al. also found that $m = 1.2$ for unconsolidated bead packs.

Figures 20 a-i also indicate the values of $\frac{1}{F\phi}$ which the data should approach at low flow rates. Reasonable results were obtained. Kravik and Bissey[34] obtained data for gaseous systems at low flow rates, and found that for mobility ratios between 0.5 and 2.0, Equation 8 is valid, i.e. that there is no effect of instability at very low flow rates.

## B. Short Cores, Immobile Phase in Interstices

Two cores (BA-2 and BO-2) were treated with a paraffin and pentane solution to provide varying degrees of pore "blocking" ranging from 4% to 20% of the pore volume. Water was not used as the immobile phase, since thermal conductivity measurements would have become too complicated.

Paraffin wax was first dissolved in commercial grade n-pentane, and the specimens were then soaked in the solution for several hours. After air drying, the cores were subjected to a vacuum for 30 minutes to an hour to evaporate the pentane, leaving the paraffin deposited

in the interstices. The volume of the paraffin deposited was determined by gravimetric measurements, which agreed within 5% with volumes determined by soaking a dry core in a pentane-paraffin solution of precisely measured composition.

Dispersion characteristics for the nitrogen-argon system were determined for each saturation by the established procedure. Results are shown in Figures 21 and 22. Permeabilities were estimated for each saturation using the inlet pressure data and Darcy's Law for gas flow. After obtaining data at the highest paraffin saturations (18.7% and 21.5%), the samples were heated to 140°F and blown down with warm nitrogen in an attempt to redistribute the paraffin in the interstices without substantially altering the fraction of the pore space which was blocked. Electrical resistivity factors were determined both before and after this operation, but, as an oversight, were not measured for intermediate runs.

It was concluded from this series of runs that the dispersion characteristics of the porous medium were affected by the distribution (microscopic and/or macroscopic) of the immobile phase as well as the amount of the immobile phase.

For the Boise sandstone sample, which had a rather large grain size (as determined by mere visual observation), dispersion was in all cases increased by the presence of the immobile phase. The power dependence of dispersion upon flow rate is seen to vary from approximately 1.0 to 1.5, but not as a monotonic function of the volume of immobile phase present.

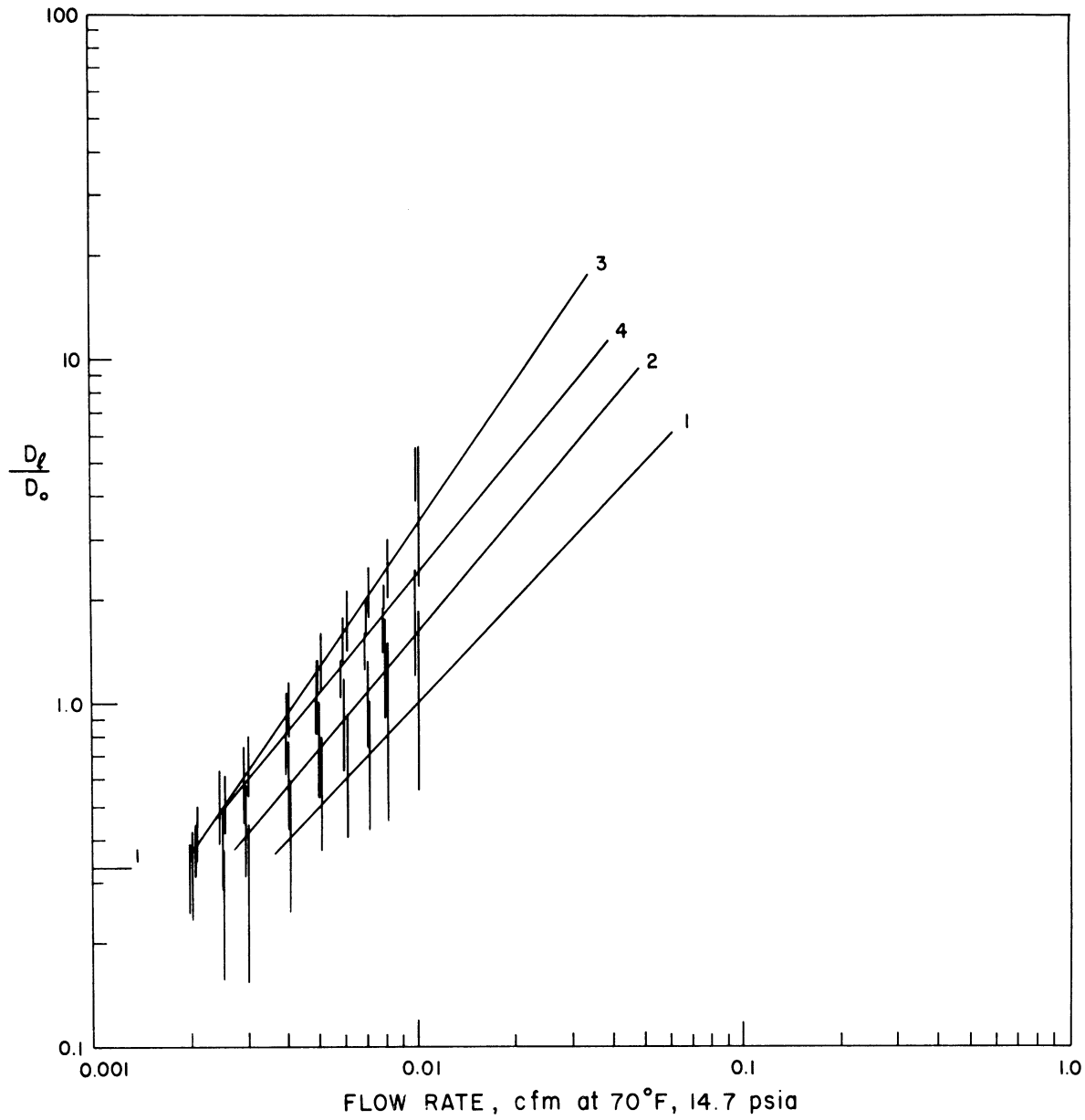


Figure 21a. Dispersion Characteristics as a Function of Flow Rate, Immobile Phase in Interstices (Boise Sandstone).

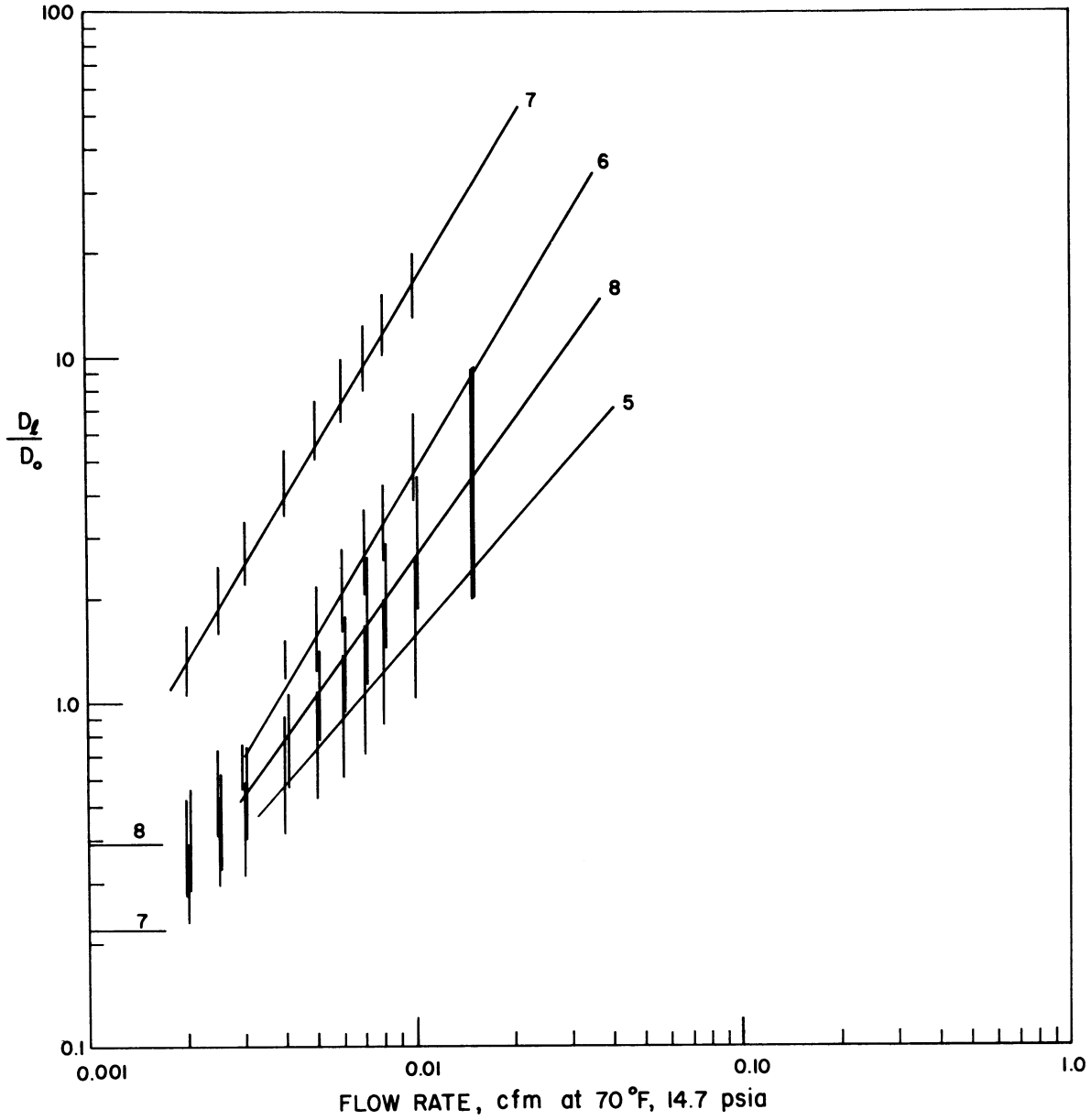


Figure 21b. Dispersion Characteristics as a Function of Flow Rate, Immobile Phase in Interstices (Boise Sandstone).

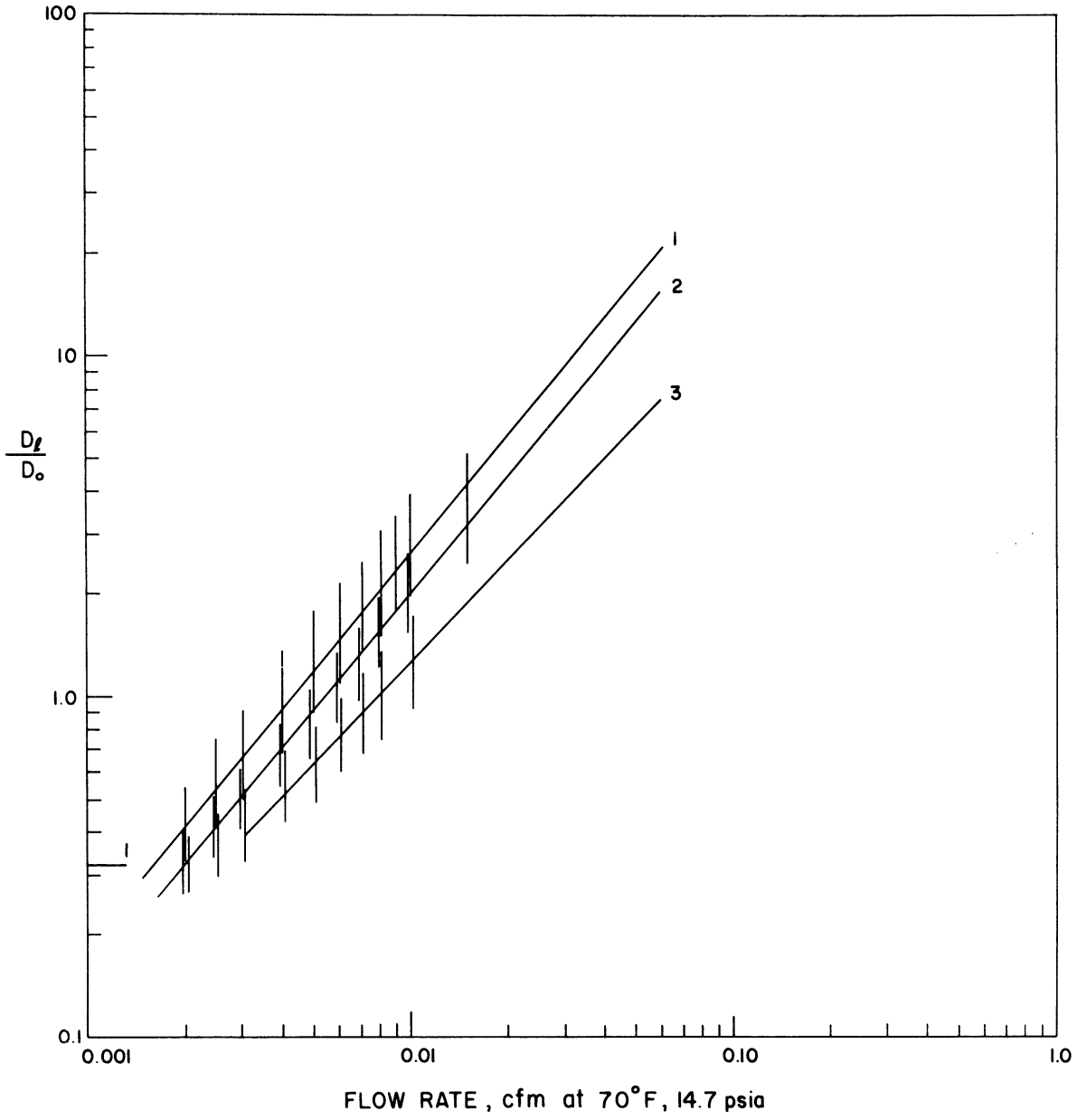


Figure 22a. Dispersion Characteristics as a Function of Flow Rate, Immobile Phase in Interstices (Bandera Sandstone).

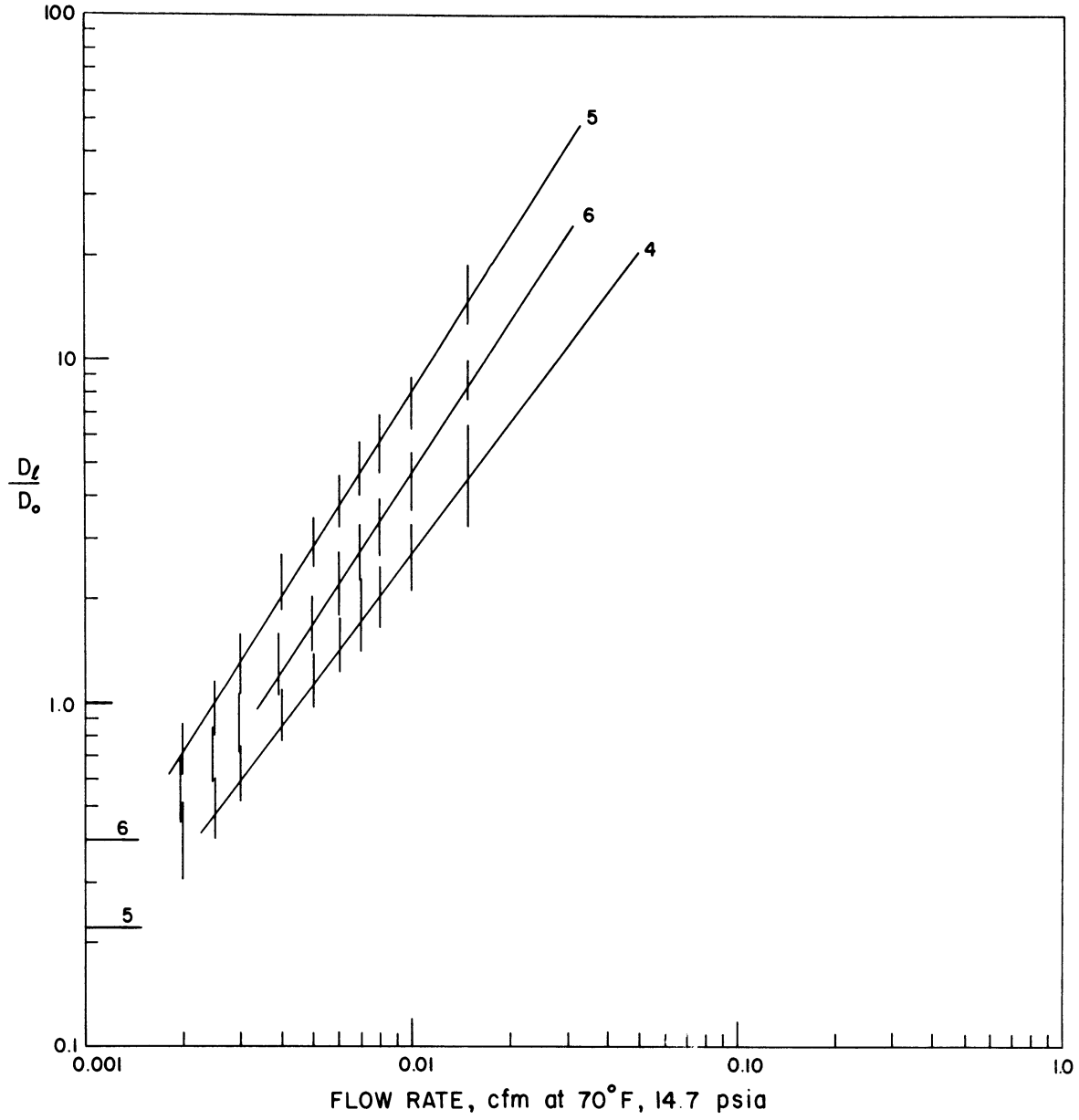


Figure 22b. Dispersion Characteristics as a Function of Flow Rate, Immobile Phase in Interstices (Bandera Sandstone).

TABLE III

EFFECT OF AN IMMOBILE PHASE UPON DISPERSION CHARACTERISTICS

A. Core BA-2, Figure 21.

| Percent of Interstices Blocked | Porosity, $\phi$, Per Cent | Permeability, K, Millidarcies | Resistivity Factor, F | Power Dependence, m | Characteristic length, $d_p\sigma$, cm |
|---|---|---|---|---|---|
| 1. 0 | 23.4 | 40 | 13.3 | 1.13 | .475 |
| 2. 4.6 | 22.3 | 34.9 | - | 1.13 | .365 |
| 3. 7.86 | 21.6 | 32.2 | - | 1.0 | .272 |
| 4. 12.9 | 20.4 | 19.1 | - | 1.25 | .495 |
| 5. 18.7 | 19.0 | 26. | 23.7 | 1.50 | .685 |
| 6. 18.2 | 19.1 | 20.9 | 13.2 | 1.45 | .605 |

B. Core BO-2, Figure 22.

| | | | | | |
|---|---|---|---|---|---|
| 1. 0 | 32.0 | 258 | 9.5 | 1.0 | .346 |
| 2. 4.45 | 30.6 | 263 | - | 1.13 | .475 |
| 3. 6.7 | 29.8 | 171 | - | 1.38 | .675 |
| 4. 10.4 | 28.7 | 222 | - | 1.13 | .62 |
| 5. 10.45 | 28.7 | 230 | -- | 1.07 | .535 |
| 6. 14.2 | 27.4 | 230 | - | 1.50 | .675 |
| 7. 21.5 | 25.2 | 135 | 17.9 | 1.58 | 1.55 |
| 8. 20.4 | 25.5 | 338 | 10.1 | 1.31 | .65 |

We were forced to conclude that the method of depositing the immobile phase in the interstices did not provide uniform deposition. We can nevertheless conclude that the effect of an immobile interstitial phase should be considered in any practical approach to reservoir problems.

C. Long, Dry Cores

In order to ascertain that experimental results were valid for the short cores used, the experimental technique described earlier was also used to determine dispersion characteristics for a Berea sandstone 23.9 inches in length by 1 1/2 inches in diameter.

Three segments of the sandstone were used in the investigation. First, a 4.20 inch specimen was cut, and dispersion characteristics were determined as a function of flow rate with the core mounted in the Hassler sleeve as before. Samples 5.22 inches and 23.90 inches in length were mounted in epoxy, and detachable end plates were made from lucite plastic. Response characteristics (i.e. variances of the output concentration profiles) were obtained for each segment using a 10 second pulse injection of argon or helium; the short segment (5.22 inches) represented the "ends" of the core, and the longer (23.9 inches) segment represented the "ends plus sample." The difference between the two responses was a measure of the mixing in the core itself (18.68 inches), as before.

The results of this study are shown in Figure 23, "Effect of Core Length upon Computed Dispersion Characteristics." Physical

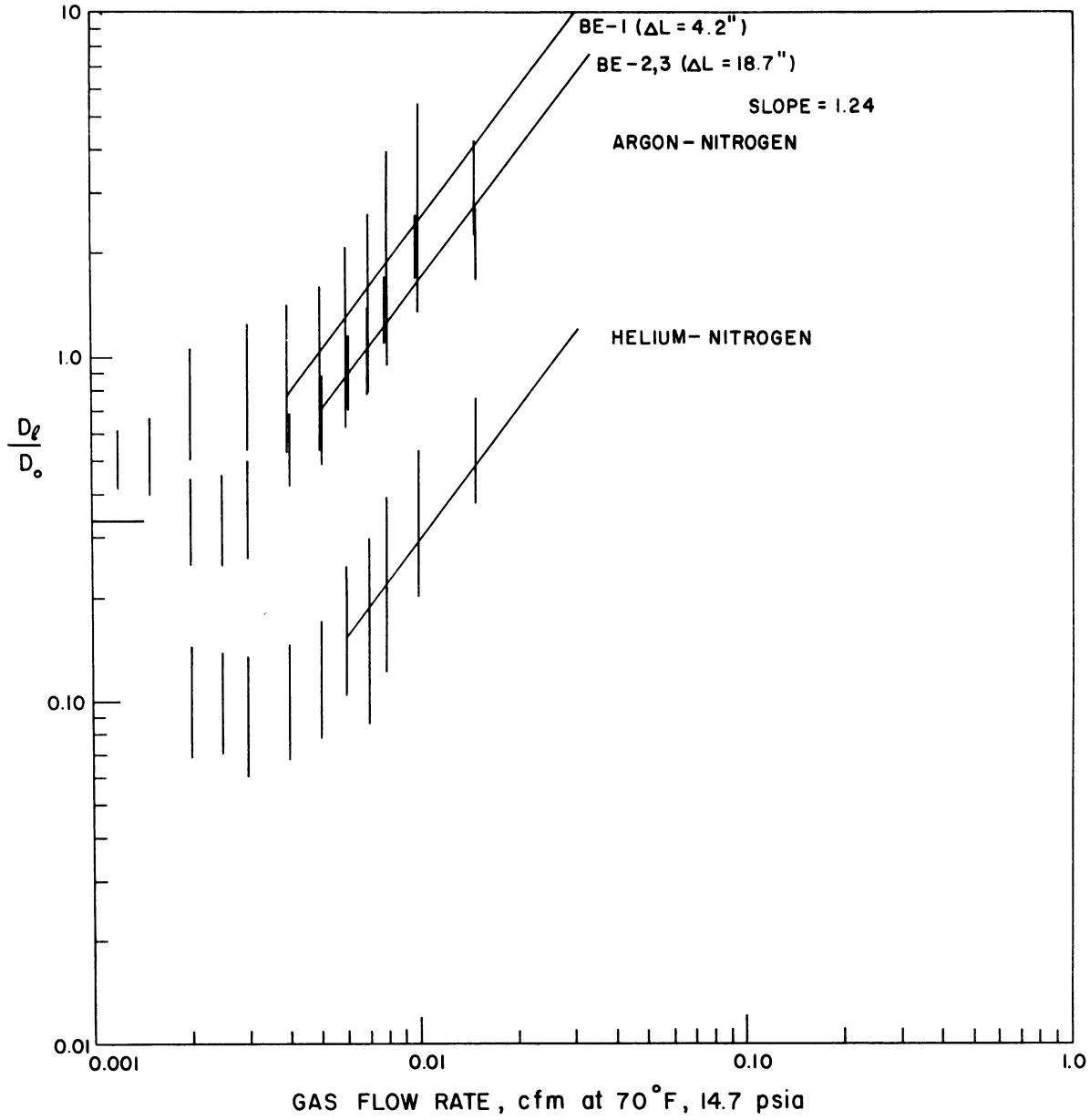


Figure 23. Dispersion Characteristics as a Function of Flow Rate - Effect of Core Length, Berea Sandstone.

properties of the core (BE) are included in Table II. The characteristic length, $d_p\sigma$, is seen to be between 0.23 cm and 0.32 cm, and the power dependence is approximately 1.24, in fair agreement with Brigham, et. al.[12], who determined values of $d_p\sigma = 0.39$ cm and $m = 1.2$ for a Berea core of similar porosity and permeability.

It will be noted from Table II that the longer cores seem to have a lower permeability than the short (4.2 inch) core. This may be due to a slight amount of epoxy imbibed into the core, although precautions were taken to minimize this possibility.

We were able to conclude from this phase of the experimental investigation that reasonable results had been obtained using short core samples.

Data obtained for the helium-nitrogen system, using the long Berea core, are also shown in Figure 23. These data are seen to be displaced by a factor of about three from the results anticipated from the argon-nitrogen data. Our only explanation for this anomaly is to hypothesize that the computed value of the molecular diffusion coefficient, $D_o$, was too large. The Chapman-Enskog equation predicted a diffusion coefficient of $D_o = 0.684$ cm$^2$/sec at one atmosphere; a value of $D_o \simeq 0.2$ cm$^2$/sec would be required to yield the expected dispersion characteristics.

In the absence of published experimental values for the diffusion coefficient, we are forced to conclude that our investigation of the helium-nitrogen system was inconclusive.

# VI. SUMMARY AND CONCLUSIONS

The objectives of this thesis were to review the state of our knowledge of longitudinal mixing for flow through porous media, to develop a new experimental technique for the rapid determination of dispersion coefficients in core samples of convenient size, to ascertain the validity of this technique, to observe the effects of an immobile interstitial phase upon gaseous dispersion, and to correlate the mixing properties of naturally occurring porous media with other physical properties of the media. All of these goals were attained, except that anomalous results were obtained for gases of extreme density difference, and correlations of questionable value were determined for dispersion coefficients as a function of rock properties.

The longitudinal mixing properties of a porous medium may be characterized by an equation of the form

$$\frac{D_e}{D_o} = \frac{1}{F\phi} + 0.5\left(\frac{u d_p \sigma}{D_o}\right)^m \qquad (9b)$$

If the parameters $d_p\sigma$ and $m$ are determined for a porous medium of known porosity and electrical resistivity factor, then a dispersion coefficient may be estimated for a given flow rate and a given gas pair.

A new method was developed and used to determine these mixing parameters for eight naturally occurring sandstones and two

dolomite samples. The method features "on-line" gas analysis by thermal conductivity and "on-line" data reduction by analog computation, providing a rapid means of determining longitudinal dispersion properties for core samples only 3 or 4 inches in length by 1-1/2 inches in diameter. By injecting pulses of argon into nitrogen flowing through core samples of various lengths, the relative change in variance of the argon concentration profile may be found for a segment of core sample, exclusive of end effects. The variance, which is determined by processing the output signal of a thermal conductivity cell on an analog computer, is related to the longitudinal dispersion coefficient by the equation

$$\Delta\sigma^2 = \Delta\sigma_t^2\left(\frac{u}{L}\right)^2 = \frac{2D_\ell}{uL} \qquad (22)$$

It was found that the dispersion ratio , $D_\ell/D_o$ , has a power dependence of greater than 1.0 upon flow rate. The power dependence, i.e. the exponent "m" of Equation (9b), can vary between 1.0 and 1.5, and should be considered a property of a porous medium. Poor correlations were found between the dispersion characteristics and rock properties beyond the low velocity range where dispersion consists of molecular effects only, i.e. beyond the range where Equation (8) is applicable.

The parameters $d_p\sigma$ and m (Equation (9b)) are plotted as functions of permeability and the electrical resistivity factor in Figures 24 to 27. The other correlations attempted were of similar questionable value.

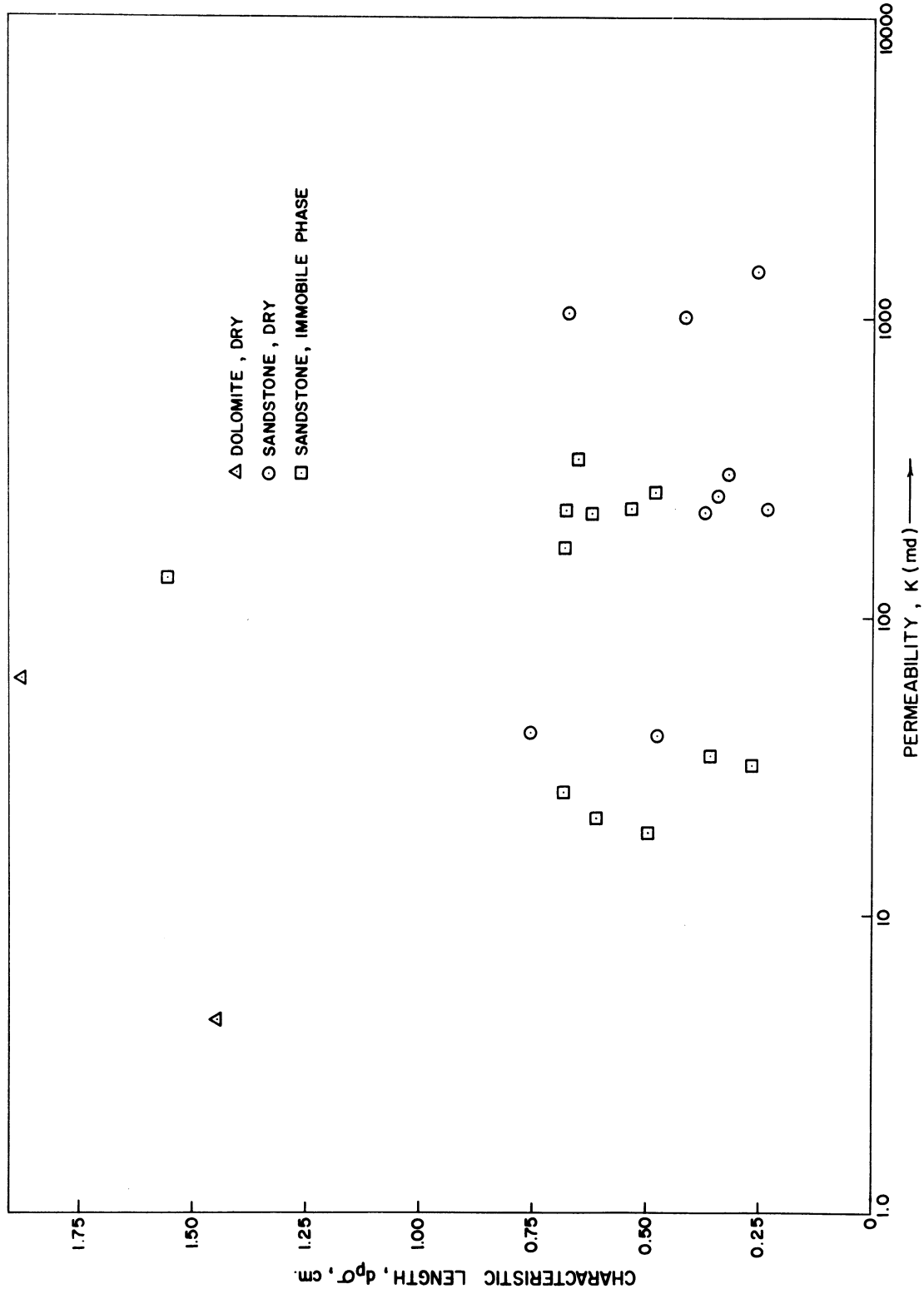


Figure 24. Characteristic Length, $d_{p\sigma}$ (cm) vs. Permeability, K (md.)

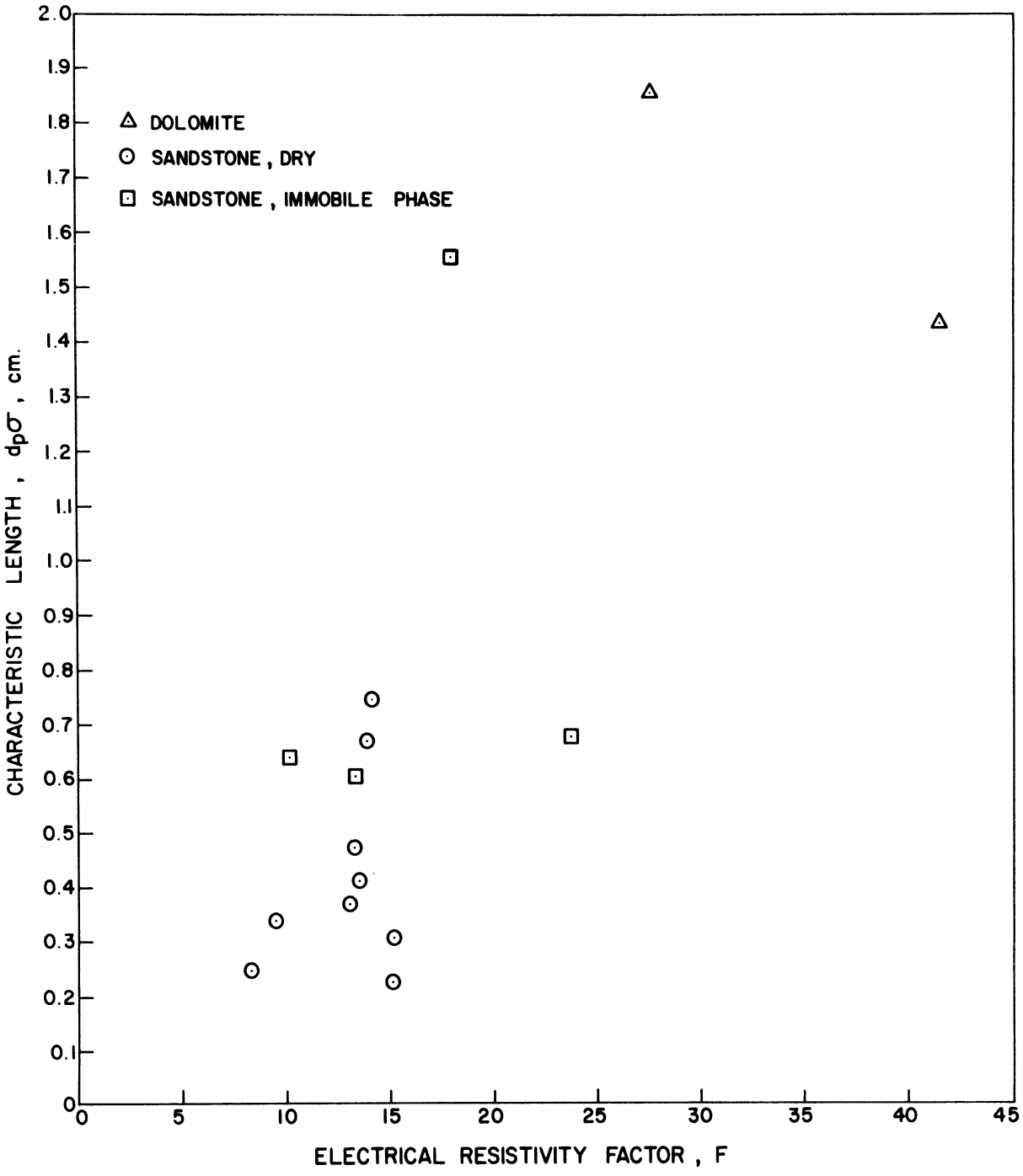


Figure 25. Characteristics Length, $d_p\sigma$ (cm) . vs. Electrical Resistivity Factor.

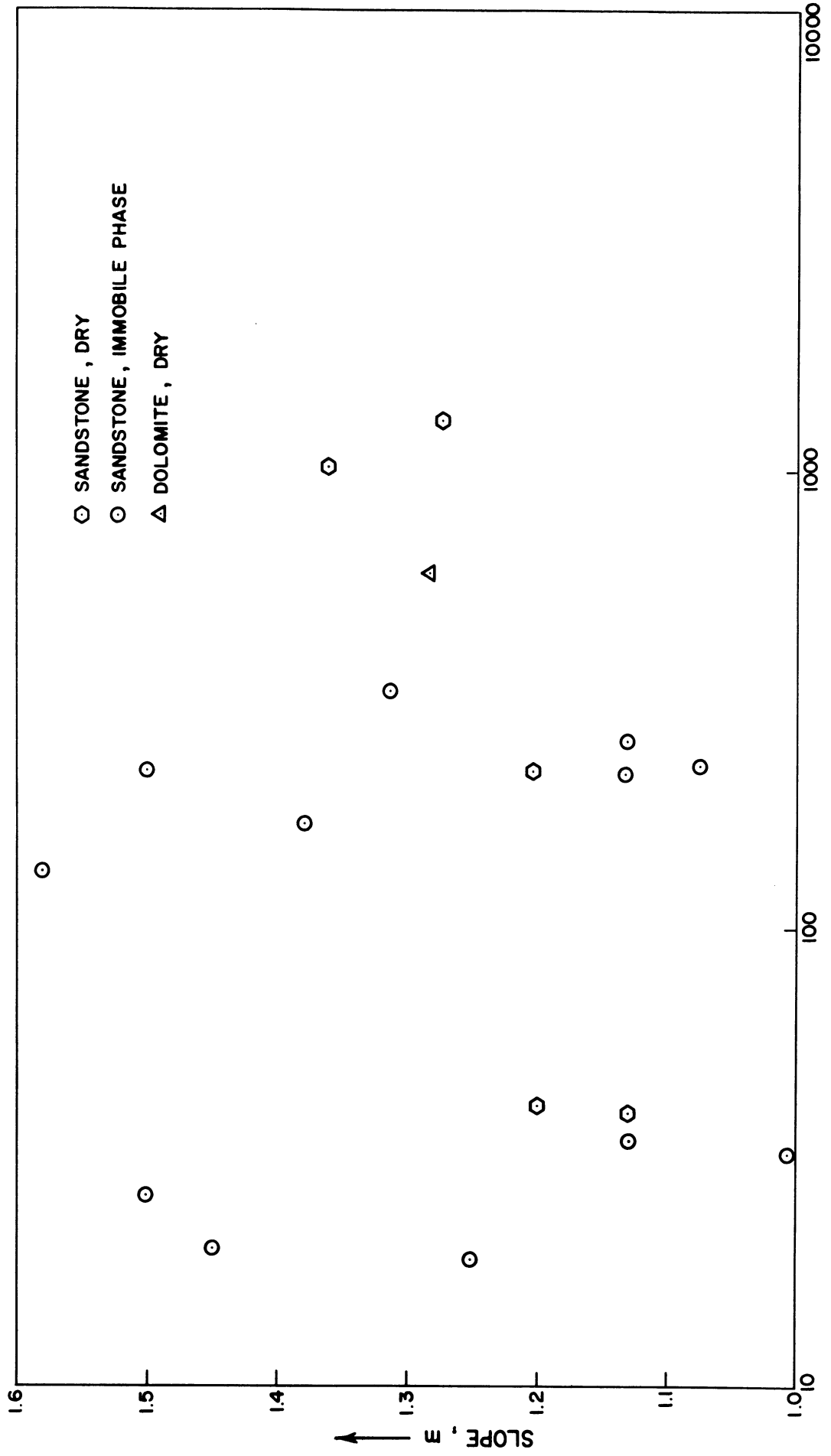


Figure 26. Exponent, m , vs. Permeability, K (md.)

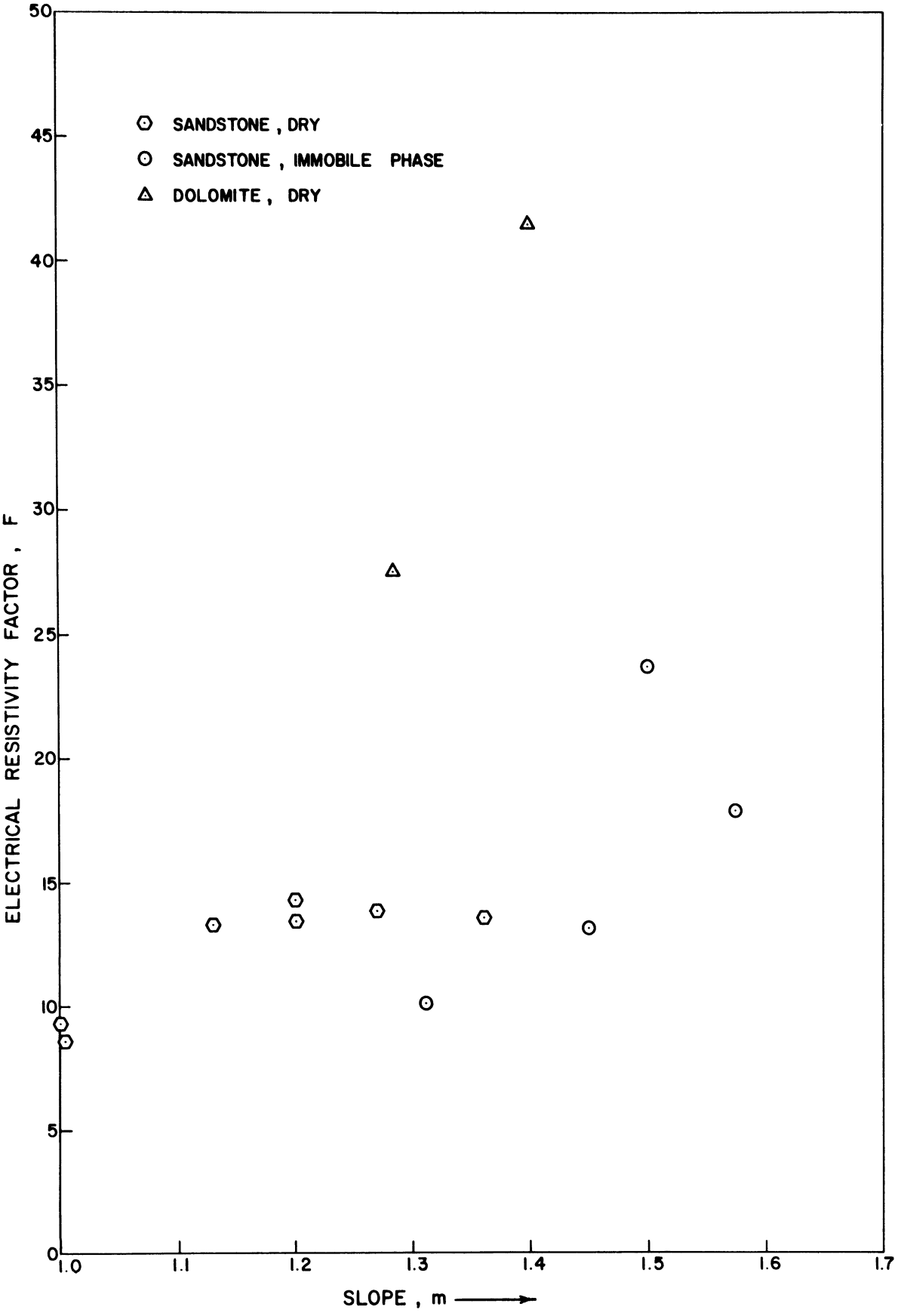


Figure 27. Exponent, m , vs. Resistivity Factor, F .

Longitudinal dispersion characteristics were determined to be substantially the same for Berea sandstone cores 4 inches in length and 18 inches in length, indicating that the technique yielded reliable results for the shorter samples.

Two of the samples studied were saturated with a pentane-paraffin solution of varying proportions and allowed to dry, leaving the paraffin deposited as an immobile phase in the interstices of the rocks. Paraffin saturations ranged from 5 per cent to 20 per cent of the pore volume. It was shown that the longitudinal dispersion characteristics were significantly affected by the presence of the immobile phase, but several anomalous data sets led to the conclusion that the method used to deposit the interstitial paraffin was not reliable, i.e. did not result in uniform deposition. This prevented a positive conclusion which would relate the dispersion characteristics uniquely to the amount of the immobile phase present in the interstices, but we were able to conclude, as a generalization, that the effect of the immobile phase is to increase the exponent, $m$, and the characteristic length, $d_p\sigma$, of Equation (9b). The presence of an immobile phase should, therefore, be considered in the analysis of any real reservoir problem.

Experimental results for the helium-nitrogen system were inconclusive. Poor results were obtained for the short samples due to instability problems. For the longer Berea core, the lack of agreement between experimental and predicted results could only be explained by hypothesizing that an incorrect value of the molecular diffusion coefficient was computed by the Chapman-Enskog and Gilliland equations.

No attempt was made to analyze stability problems for gaseous systems. Further research in this area is essential in obtaining the ultimate goal of predicting reservoir behavior.

Further research should also include attempts to extend the velocity range which can be studied by the proposed method. A logical approach to this problem would be to verify that similar dispersion characteristics are obtained for gaseous and liquid systems, and then to study liquid dispersion, substituting an electrical conductivity cell for the thermal conductivity cell used in this research.

# BIBLIOGRAPHY


1. Aris, R., "Notes on the Diffusion Type Model for Longitudinal Mixing in Flow," Letter to Editor, Chem. Eng. Sci. 9, 4 (1959)

2. Aris, R., and Amundson, N. R., "Some Remarks on Longitudinal Mixing or Diffusion in Fixed Beds," AIChE Jour, 3, 2, 280 (1957)

3. Babcock, R. E., Green, D. W., and Perry, R. H., "Longitudinal Dispersion Mechanisms in Packed Beds," Preprint 43a, AIChE Feb. 7-11, 1965, Houston, Texas

4. Baldwin, D. E. Jr., "Prediction of Mixing During Miscible Displacement in a Five-Spot Pattern," SPE Preprint 1230, Denver, Colorado, Oct. 3-6, 1965

5. Bentson, R. G., and Nielson, R. F., "A Study of Plane Radial Miscible Displacement in a Consolidated Porous Medium," SPE Jour, 5, 1, 1 (1965)

6. Bernard, R. A., and Wilhelm, R. H., "Turbulent Diffusion in Fixed Beds of Packed Solids," Chem. Eng. Prog. 46, 233 (1950)

7. Berry, V. J., and Koeller, R. C., "Diffusion in Compressed Binary Gaseous Systems," Preprint 45, SPE-AIChE Joint Symposium on Non-Equilibrium Fluid Mechanics, Kansas City, May 17-20, 1959

8. Bird, R. B., Stewart, W. E., and Lightfoot, E. N., Transport Phenomena, Wiley and Sons, New York, 1960

9. Bischoff, K. B., "Notes on the Diffusion-Type Model for Longitudinal Mixing in Flow," Comm. to Editor, Chem. Eng. Sci. 12, 69, (1960)

10. Blackwell, R. J., "Laboratory Studies of Microscopic Dispersion Phenomena," SPE Jour 1, (March, 1962)

11. Blackwell, R. J., Terry, W. M., and Rayne, J. R., "Factors Influencing the Efficiency of Miscible Displacement," Trans. AIME 217, 1 (1959)

12. Brigham, W. E., Reed, P. W., and Dew, J. N., "Experiments on Mixing by Fluid Flow in Porous Media," SPE Jour, 1 (March, 1961)

13. Cairns, E. J., and Prausnitz, J. M.; "Longitudinal Mixing in Packed Beds," Chem. Eng. Sci. 12, 20 (1960)

14. Carberry, James J., "Axial Dispersion and Void-Cell Mixing Efficiency in Fluid Flow in Fixed Beds," Comm. to the Editor, AIChE Jour, 4, 1 (1958)

15. Carberry, J. J., and Bretton, R. H., "Axial Dispersion of Mass in Flow Through Fixed Beds," AIChE Jour 4, 3 (1958)

16. Carman, P. C., "Permeability of Saturated Sands, Soils, and Clays," Jour. Agri. Sci. 29, 262 (1939)

17. Chapman and Cowling, Mathematical Theory of Non-Uniform Gases, Second Edition, Cambridge Univ. Press, (1951)

18. Coats, K. H., and Smith, B. D., "Dead-End Pore Volume and Dispersion in Porous Media," SPE Preprint 647, New Orleans, La., Oct 6-9, 1963

19. Cornell, D., "Flow of Gases Through Consolidated Porous Media," Ph.D. Thesis, Univ. Michigan (1952)

20. Cornell, D., and Katz, D. L., "Flow of Gases Through Consolidated Porous Media," Ind. Eng. Chem. 45, 2145 (1953)

21. Crank, J., The Mathematics of Diffusion, Oxford-Clarendon Press, New York (1957)

22. Davis, B. R., and Scott, D. S., "Measurement of Effective Diffusivities in Porous Particles," Preprint 48d, 58th Meeting AIChE, Philadelphia, Pa., Dec. 9, 1965

23. de Jong, G. de Josselin, "Longitudinal and Transverse Diffusion in Granular Deposits," Trans. AGU, 39, 67 (1958)

24. Dumore, J. M., "Stability Considerations in Downward Miscible Displacement," SPE Preprint 961, Houston, Oct. 11-14, 1964

25. Ebach, E. A., and White, R. R., "Mixing of Fluids Flowing Through Beds of Packed Solids," AIChE Jour, 4, 2, (1958)

26. Fahien, R. W., and Smith, J. M., "Mass Transfer in Packed Beds," AIChE Jour, 1, 28, (1955)

27. Gorring, R. L., "Multiphase Flow of Immiscible Fluids in Porous Media," Ph.D. Thesis, Univ. Michigan, 1962

28. Goddard, R. R., "Fluid Dispersion and Distribution in Porous Media Using the Frequency Response Method with a Radioactive Tracer," SPE Preprint 1228, Denver, Colo., Oct. 3-6, 1965

29. Gow-Mac Instrument Co., Instructions for Operation of Thermal Conductivity Cell

30. Grane, F. E., and Gardner, G. H. F., "Measurements of Transverse Dispersion in Granular Media," Jour Chem. Eng. Data 6, 283, (1961)

31. Helander, D. P., "The Effect of Pore Configuration, Pressure, and Temperature on Rock Resistivity," Ph.D. Thesis, Univ. Oklahoma (1965)

32. Katz, et. al., Handbook of Natural Gas Engineering, McGraw-Hill, New York 1959

33. Klinkenberg, R. R., "Residence Time Distributions and Axial Spreading in Flow Systems (With Their Application in Chemical Engineering and Other Fields)," Trans. Instn. Chem. Engrs., 43, T141 (1965)

34. Kravik, G. D., and Bissey, L. T., "A Study of Mixing During Gaseous Displacement at Low Flow Rates in a Consolidated Porous Medium," Proceedings 24th Tech. Conference of Petroleum Production, Oct. 23-25, Penn State University, University Park Pa.

35. Latinen, G. A., "Mechanism of Fluid Phase Mixing of Fixed and Fluidized Beds of Uniformly Sized Particles," Ph.D. Thesis Princeton Univ., 1951

36. Levenspiel, O., Chemical Reaction Engineering, Wiley and Sons, New York 1962 (ch. 9)

37. Levenspiel, O., and Smith, W. K., "Notes on the Diffusion-Type Model for the Longitudinal Mixing of Fluids in Flow," Chem. Eng. Sci. 6, 4 and 5 (1956)

38. Longwell, P. A., and Sage, B. H., "Some Molecular Transport Characteristics in Binary Homogeneous Systems," AIChE Jour, 5, 1 (1965)

39. Mathur, G. P., and Thodos, G., "The Thermal Conductivity and Diffusivity of Gases for Temperatures to 10,000°K," AIChE Jour, 11, 1, 164 (1965)

40. McHenry, K. W., and Wilhelm, R. H., "Axial Mixing of Binary Gas Mixtures Flowing a Random Bed of Packed Spheres," AIChE Jour, 3, 83 (1957)

41. Munnerlyn, R. D. (Division of Helium Resources, U. S. Bureau of Mines), Personal Communication, Oct. 12, 1964

42. Orlob, G. T., and Radhakrishna, G. N., "The Effects of Entrapped Gases on the Hydraulic Characteristics of Porous Media," Trans. AGU, 39, 648 (1958)

43. Perkins, T. K., and Johnston, O. C., "A Review of Diffusion and Dispersion in Porous Media," SPE Jour, March, 1963

44. Perkins, T. K., and Johnston, O. C., "Mechanics of Viscous Fingering in Mixcible Systems," SPE Preprint 1229, Denver, Colo., Oct. 3-6 1965

45. Perrine, R. L., "The Development of Stability Theory for Miscible Liquid-Liquid Displacement," Trans. AIME 222, II-17 (1961)

46. Peterson, E. E., "Diffusion in a Pore of Varying Cross Section," AIChE Jour, 4, 3, (1958)

47. Prausnitz, J. M., "Longitudinal Dispersion in a Packed Bed," Comm. to the Editor, AIChE Jour, 4, 1 (1958)

48. Raimondi, P., Gardner, G. H. F., and Petrick, C. B., "Effect of Pore Structure and Molecular Diffusion on the Mixing of Miscible Liquids Flowing in Porous Media," Preprint 43, AIChE-SPE Joint Symposium on Fundamental Concepts of Miscible Fluid Displacement, Part II, San Francisco, Dec. 6-9, 1959

49. Saffman, P. G., "Dispersion in Flow Through a Network of Capillaries," Chem. Eng. Sci. 11, 125 (1959)

50. Schowalter, W. R., "Stability Criteria for Miscible Displacement of Fluids from a Porous Medium," AIChE Jour, 11, 1 (1959)

51. Singer, E., and Wilhelm, R. H., "Heat Transfer in Packed Beds; Analytical Solution and Design Method; Fluid Flow, Solids Flow, and Chemical Reaction," Chem. Eng. Prog. 46, 343 (1959)

52. Slattery, J. C., and Bird, R. B., "Calculations of the Diffusion Coefficient of Dilute Gases and of the Self-Diffusion Coefficient for Dense Gases," AIChE Jour, 4, 2 (1958)

53. Schwartz, C. E., and Smith, J. M., "Flow Distribution in Packed Beds," Ind. Eng. Chem. 45, 1209 (1953)

54. Skinner, J. L., Personal Communications

55. Toor, H. L., "Diffusion in Three Component Gas Mixtures," AIChE Jour, 3, 2, 198 (1957)

56. van Deemter, J. J., Bradler, and Lawrence, "Fluid Displacement in Capillaries," Chem. Eng. Sci. 5, 271 (1956)

57. van der Laan, E. Th., "Notes on the Diffusion-Type Model for Longitudinal Mixing in Flow," Comm. to the Editor, Chem. Eng. Sci. 7, 3 (1957)

58. van der Poel, C., "Effect of Lateral Diffusivity on Miscible Displacement in Horizontal Reservoirs, SPE Jour, Dec. 1962

59. Wilhelm, R. H., "Rate Processes in Chemical Reactors," Chem. Eng. Prog. 49, 3, 150 (1953)

# APPENDIX I

## SAMPLE CALCULATIONS

1. Determination of Porosity

Core: BE-1, Berea sandstone

Dimensions: 1.5 in. D x 4.203 in. L

Dry weight: 255.15 gm.

Bulk Bolume:

$$(1.5)^2 \frac{\pi}{4} \cdot 4.203 \cdot (2.54)^2 = 122 \text{ cc.}$$

Weight, saturated with water (1.00 gm/cc): 278.15 gm.

Weight of water:

$$\begin{array}{r} 278.15 \\ \underline{255.15} \\ 23.0 \end{array}$$ gm. or 23.0 cc.

Porosity, or fraction of bulk volume occupied by water:

$$\phi = \frac{23.0}{122} = 0.19, \text{ or } 19\%.$$

2. Determination of Electrical Resistivity Factor:

Core: BE-1, Berea sandstone

Dimensions: 1.5 in. D x 4.203 in. L

Porosity: 19%

Measured electrical resistance when saturated with 0.1 N KCl at 22.0°C: 1180 ohms

Conductivity of 0.1 N KCl @ 22.0°C: 0.01215 mho/cm

(from Chem. Rubber Handbook)

Resistance of 0.1 N KCl, "equivalent dimensions":

$$R = \frac{\text{length}}{\text{conductivity x c.s. area}} = \frac{4.203 \times 2.54}{11.4 \times 0.01215} = 77.5 \text{ ohms}$$

Resistivity factor: $F = \frac{1180}{77.5} = 15.2$

3. Determination of Permeability

Core: BE-1, Berea sandstone

Dimensions: 1.5 in. D x 4.203 in. L

Gas: Nitrogen

Darcy's Law for Gas Flow:

$$P_1^2 - P_2^2 = \frac{2L\mu' P_b Q}{KA}$$

P = atm. abs.
L = cm.
$\mu'$ = viscosity = 0.0176 cp. for Nitrogen
Q = cc/sec @ $P_b$ = 1 atm.
A = $cm^2$
K = permeability, Darcys

Flow rate = $Q = 0.0098 \frac{ft^3}{min} \frac{1 \text{ min}}{60 \text{ sec}} \times \frac{28400 \text{ cc}}{ft^3} = 4.63 \frac{cc}{sec}$.

$$A = \frac{\pi D^2}{4} = \frac{\pi}{4}(1.5 \times 2.54)^2 = 11.4 \text{ cm}^2$$

Inlet pressure $P_1$ = 3.4 psig = 1.23 atm. abs.

Outlet pressure $P_2$ = 0 psig = 1.0 atm. abs.

$$K = \frac{2L\mu P_b Q}{A(P_1^2 - P_2^2)} = \frac{2(2.54 \times 4.203)\text{cm}\,(0.0176)\text{cp}\,(1)\text{atm}\,(4.63)\text{cc/sec}}{(11.4)\text{cm}^2\,(1.23^2 - 1.0^2)\text{atm}^2}$$

$$= 0.3 \text{ d} = 300 \text{ md}.$$

4. Determination of the Turbulence Factor

Core: BO-3, Boise sandstone

Dimensions: 1.5 in. D x 3.20 in. L

Gas: Nitrogen

Integrated Flow Equation:

$$\frac{M(P_1^2-P_2^2)}{2zRT\mu'L}\frac{A}{W} = \frac{W}{A}\frac{\beta}{\mu'} + \frac{1}{K}$$

where M = mol. wt. = 28
P = pressure, atm. abs.
z = compressibility factor = 1.0
R = gas constant
T = absolute temperature
$\mu'$ = viscosity = 0.0176 cp.
L = length = 3.20 in.
A = c. s. area = 11.4 $cm^2$
W = mass flow rate
K = permeability, Darcy
$\beta$ = turbulence factor, $atm\text{-}sec^2/gm$ or $ft.^{-1}$

The quantity $\frac{M(P_1^2-P_2)^2}{2zRT\mu'L}\frac{A}{W}$ is plotted vs. $\frac{W}{A\mu'}$ in Figure I-1.

Intercept = $1/K = 0.7$

Permeability = $1/0.7 = 1.43$ Darcy

(may be checked by method of sample calculation No. 3)

Slope = 5.23 $atm\text{-}sec^2/gm = 1.72 \times 10^8$ $ft.^{-1}$

5. Calculation of the Molecular Diffusion Coefficient at Laboratory Conditions:

Nitrogen-argon system at 70°F, 14.7 psia.

Chapman-Enskog (rigid sphere) theory for ideal gases:

$$D_{o_{AB}} = \frac{0.0018583}{P\sigma_{AB}^2\Omega_{D_{AB}}}\sqrt{T^3\left(\frac{1}{M_A}+\frac{1}{M_B}\right)}$$

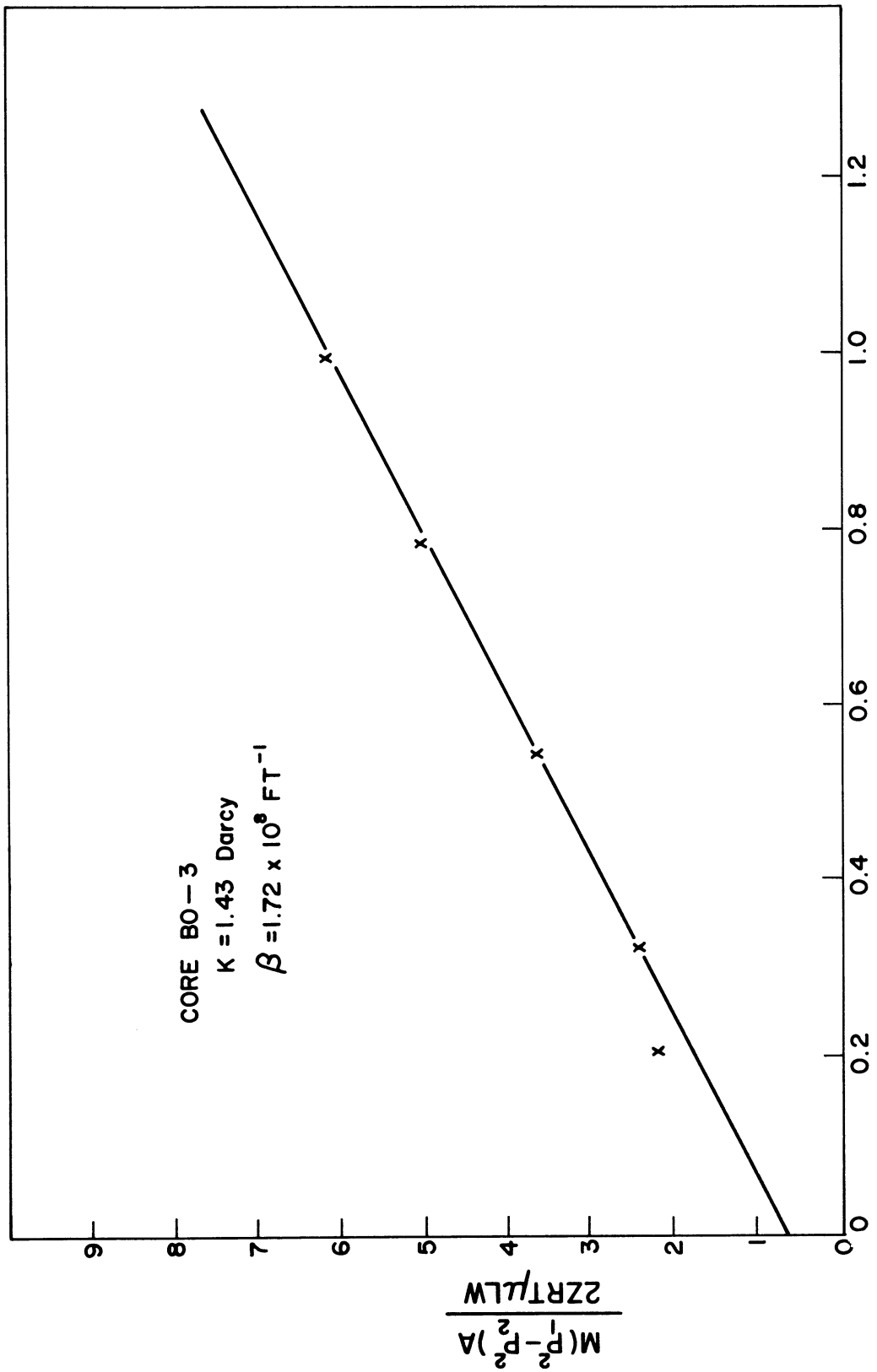


Figure I-1. Turbulence Factor Plot.

$M_A$ = mol. wt. argon = 39.94
$M_B$ = mol. wt. nitrogen = 28.02
T = 295°K.
P = 14.7 psia = 1.0 atm. abs.

Lennard-Jones Parameters[8]:

$$\sigma_{AB} = \tfrac{1}{2}(\sigma_A + \sigma_B) = \tfrac{1}{2}(3.418 + 3.681) = 3.505 \text{ Å}$$

$$\epsilon_{AB} = \sqrt{\epsilon_A \epsilon_B}$$

$$\left(\frac{\epsilon_A}{K}\right)_{Argon} = 124°K \quad , \quad \left(\frac{\epsilon_B}{K}\right)_{Nitrogen} = 91.5\ °K.$$

Hence $\Omega_{D_{AB}} = f(KT/\epsilon_{AB}) = f(3.24) = 0.929$

(tabulated function, ref. 8)

$D_o$ = 0.193 $cm^2/sec.$

For other pressures at 70°F, multiply by 14.7/P to find:

$D_o = 2.84/P$ (P = psia)

6. Determination of the "Characteristic Length" ($d_p\sigma$):

Core: BA-2, Bandera Sandstone

Porosity: 23.4%

See Figure 20a,

When $ud_p\sigma/D_o = 1.0$, then $0.5\left(\frac{ud_p\sigma}{D_o}\right)^m$ (the equation of the line fitting the data) is 0.5, and the corresponding value of the flow rate is determined to be 0.00135 cfm at 70°F, 14.7 psia.

$$u/D_o = \frac{v'}{60}\frac{1}{0.01225\ ft^2}\frac{14.7}{P_{avg}}\frac{P_{avg}}{2.84}\,30.4\frac{cm}{ft}\frac{1}{\phi}$$

$$= 215\, v'/\phi \text{ for nitrogen-argon (units } cm^{-1})$$

$$ud_p\sigma/D_o = 1.0 \times d_p\sigma = \frac{215 \times 0.00135}{0.234}$$

$$d_p\sigma = 0.475 \text{ cm.}$$

7. Determination of Effective Porosity for a Core Containing Wax in the Interstices:

Core: BA-2, Bandera sandstone

Dimensions: 1.5 in. D x 4.73 in. L.

Porosity (dry): 23.4%

Void volume: $\phi L \pi D^2/4 = (0.234)(4.73)(\pi)(1.5)^2/4 = 1.96\ in^3$.

Dry Weight: 294.225 gm.

After soaking in pentane-paraffin solution (prepared using 4.7 vol. % paraffin) and allowing the pentane to evaporate, weight: 295.490 gm.

Weight of paraffin in core: 1.265 gm.

Measured density of paraffin: 14.1 gm/in.$^3$

Volume of paraffin in core: 1.265/14.1 = 0.09 in.$^3$

Percent of pore space occupied: $100 \times \frac{0.09}{1.96} = 4.6\%$

Effective porosity: (1.00 - 0.046) x 23.4 = 22.3%

8. Evaluation of Dispersion Characteristics for a Typical Sample:

Core: BA-2, Bandera sandstone

A. Determine the $\sigma_t^2$ (variance) response to a 5.0 second square concentration wave input (argon on nitrogen) for cores BA-$2_A$ plus BA-$2_B$, length 2.10 inches.

See Data Sheet No. 1; recall

$$\sigma_t^2 = \frac{M_2'}{M_0'} - \left(\frac{M_1'}{M_0'}\right)^2 = \frac{100 C_E M_2}{M_0} - \left(\frac{10 M_1}{M_0}\right)^2 \qquad (31)$$

B. Determine the $\sigma_t^2$ response to a 5.0 second square wave input for cores BA-2 plus BA-$2_A$, length 5.87 inches.

See Data Sheet No. 2.

DATA SHEET NO. 1, $BA\text{-}2_A + BA\text{-}2_B$, $L = 2.10$ IN.

| RAW DATA | | | | | | COMPUTED DATA | |
|---|---|---|---|---|---|---|---|
| Rotameter reading | $M_o$ | $M_1$ | $M_2$ | $P_1$ psig | | $\sigma_t^2$ (sec$^2$) | Flow Rate, cfm @ 14.7psia, 70°F. |
| 7.5 | 69.97 | -11.34 | 26.57 | 1.9 | CE = 1.0 | 35.4 | 0.00165 |
| | 71.53 | - 9.27 | 27.59 | | | 36.8 | |
| | 126.6 | -12.46 | 47.91 | | | 36.8 | |
| 9.0 | 45.96 | 1.50 | 74.32 | 2.6 | CE = 0.1 | 16.1 | 0.0025 |
| | 48.46 | 0.32 | 77.70 | | | 16.1 | |
| | 47.7 | 3.01 | 75.7 | | | 15.5 | |
| 10.4 | 29.95 | 2.76 | 28.34 | 3.9 | | 8.60 | 0.00335 |
| | 25.54 | 1.86 | 22.72 | | | 8.27 | |
| | 30.89 | 2.37 | 26.65 | | | 8.05 | |
| 11.6 | 35.22 | 2.04 | 22.91 | 4.0 | | 6.22 | 0.0041 |
| | 34.96 | 1.76 | 22.99 | | | 6.33 | |
| | 35.54 | 5.17 | 31.12 | | | 6.64 | |
| | 35.04 | 4.23 | 29.04 | | | 6.84 | |
| 14.2 | 43.12 | - .31 | 16.96 | 5.9 | | 3.92 | 0.0059 |
| | 44.76 | .50 | 18.81 | | | 4.19 | |
| | 22.30 | -1.68 | 9.232 | | | 3.56 | |
| 17.2 | 33.04 | -4.31 | 18.69 | 7.3 | | 3.95 | 0.0080 |
| | 32.58 | -3.64 | 17.26 | | | 4.05 | |
| | 29.84 | -4.45 | 17.94 | | | 3.78 | |
| 20 | 25.84 | -4.74 | 15.54 | 9.1 | | 2.65 | 0.0097 |
| | 25.44 | -4.96 | 16.41 | | | 2.65 | |
| | 25.28 | -4.73 | 16.13 | | | 2.88 | |
| | 26.06 | -12.94 | 69.16 | | | 1.90 | |
| 18 | 30.81 | 4.68 | 16.50 | 11.2 | | 3.05 | 0.013 |
| (steel | 30.64 | 1.326 | 9.594 | | | 2.92 | |
| float) | 30.80 | -1.73 | 10.19 | | | 3.00 | |
| | 30.24 | -4.56 | 14.63 | | | 2.56 | |

DATA SHEET NO. 2, BA-2 + BA-2$_A$, L = 5.87"

| | RAW DATA | | | | | COMPUTED DATA | |
|---|---|---|---|---|---|---|---|
| Rotameter reading | $M_o$ | $M_1$ | $M_2$ | $P_1$ psig | | $\tau_t^2$ (sec$^2$) | Flow Rate, cfm @ 14.7 psia, 70°F. |
| 7.4 | 132.8 | 8.8 | 167.4 | 5.0 | CE = 1.0 | 126 | 0.0016 |
| | 66.56 | 3.24 | 84.42 | | | 128 | |
| | 19.86 | -11.41 | 29.58 | | | 116 | |
| | 40.28 | -10.0 | 53.54 | | | 127 | |
| 9.7 | 26.0 | - 5.49 | 11.74 | 8.0 | | 39.0 | 0.00285 |
| | 51.1 | -20.34 | 28.29 | | | 39.6 | |
| | 48.36 | 1.36 | 21.12 | | | 43.6 | |
| | 54.06 | 9.48 | 25.92 | | | 44.8 | |
| 11.0 | 43.22 | 19.12 | 22.2 | 9.8 | | 30.1 | 0.0037 |
| | 51.32 | 1.00 | 16.14 | | | 28.8 | |
| | 51.28 | - 1.66 | 15.50 | | | 30.1 | |
| 14.6 | 65.10 | 6.12 | 11.94 | 14.5 | | 17.4 | 0.0061 |
| | 66.10 | - 0.97 | 13.27 | | | 20.0 | |
| | 63.98 | - 0.74 | 11.30 | | | 17.7 | |
| | 66.12 | - 1.39 | 12.48 | | | 18.4 | |
| 16.0 | 62.65 | 2.54 | 10.62 | 16.5 | | 16.79 | 0.0070 |
| | 57.90 | 4.50 | 9.01 | | | 15.0 | |
| | 64.11 | 4.55 | 10.45 | | | 15.8 | |
| 18.2 | 56.38 | - 5.90 | 5.714 | 18.5 | | 9.05 | 0.0085 |
| | 62.36 | 0.13 | 71.06 | | CE = 0.1 | 11.38 | |
| | 57.92 | 3.49 | 64.00 | | | 10.69 | |
| | 61.08 | 1.57 | 52.46 | | | 11.74 | |
| 20.4 | 61.50 | 6.11 | 77.82 | 21 | | 11.66 | 0.010 |
| | 58.33 | 6.24 | 72.98 | | | 9.56 | |
| | 58.93 | 4.27 | 65.66 | | | 10.65 | |
| 19ss (steel float) | 57.59 | 0.12 | 47.28 | 26.5 | | 8.30 | 0.014 |
| | 57.54 | - 0.83 | 45.70 | | | 7.92 | |
| | 59.15 | - 0.58 | 48.94 | | | 8.24 | |

C. Determine correction factors for pressure (end effects data, L = 2.10 inches, Data Sheet No. 1):

$P_1$ = Psig @ inlet, L=2.10 in.
$P_2$ = Psig @ inlet, L=5.87 in.
$v'_m$ = flow rate, cfm @ 14.7 psia, 70°F.
$v'_c$ = the flow rate which would have corresponded to $\sigma_t^2$ (L = 2.10 in) if the inlet pressure had been $P_2$ instead of $P_1$.

$$v'_c = \left( \frac{P_2 + 14.7}{P_1 + 14.7} \right) v'_m \qquad (32)$$

| $v'_m$ | $P_1$ | $P_2$ | $v'_c$ |
|---|---|---|---|
| 0.00165 | 1.9 | 4.4 | 0.00173 |
| 0.0025 | 2.6 | 6.4 | 0.0028 |
| 0.00335 | 3.9 | 8.5 | 0.00375 |
| 0.0041 | 4.0 | 10.2 | 0.0048 |
| 0.0059 | 5.9 | 13.8 | 0.0072 |
| 0.0080 | 7.3 | 17.6 | 0.0102 |
| 0.0097 | 9.1 | 20.6 | 0.0126 |
| 0.0130 | 11.2 | 25.4 | 0.0174 |

Note: $P_2$ may be found from Figure I-2, "Inlet Pressure vs. Flow Rate," which is obtained from the data of Part B, Data Sheet No. 2.

D. Plot variance ( $\sigma_t^2$ ) vs. flow rate (v') for L = 5.87 inches (Data Sheet No. 2) and L = 2.10 inches (Data Sheet No. 1, $\sigma_t^2$ vs $v'_c$); See Figure I-3, "Variance vs. Flow Rate." Then "band" each set of points with the lines describing the maximum and minimum variances which could reasonably be ascribed to a given flow rate. (Note that $\sigma_t^2$ cannot be less than 2.1, the variance of a 5.0 second square wave. This gives a minimum value of $\sigma_t^2$ which each curve must assymtotically approach for high flow rates.) Thus the maximum and minimum values of $\Delta\sigma_t^2$ may be found for any given flow rate

in the range covered; these values characterize the mixing which occurs in a core of length $\Delta L = 5.87 - 2.10 = 3.77$ inches. E.g. for $v' = 0.01$ cfm at 14.7 psia, 70°F, the maximum value of $\Delta\sigma_t^2$ is approximately $11.5 - 2.8 = 8.7$ sec$^2$, and the minimum value is approximately $8.6 - 4.1 = 4.5$ sec$^2$.

E. The average flow pressure is determined as a function of flow rate and inlet pressure, $P_2$, by an integrated form of Darcy's Law (see Appendix II.)

$$P_{avg\ flowing} = \frac{2}{3}\left(\frac{P_2^3 - 14.7}{P_2^2 - 14.7}\right) \qquad (33)$$

These results are shown in Figure I-2.

F. For selected increments of flow rate, the dispersion parameter $De/D_o$ is computed; the results are shown in Figure 20a.

The example calculation shown here is for a flow rate of 0.002 cfm measured at 70°F, 14.7 psia.

1. For a flow rate of 0.002 cfm, the average flowing pressure is 17.7 psia (see Figure I-2)
2. The mean interstitial velocity is

$$u = \frac{v'}{60}\ \frac{1}{csa}\ \frac{14.7}{P_{avg}}\ \frac{1}{\phi}$$

$$= \frac{0.002}{60}\ \frac{1}{.01225}\ \frac{14.7}{17.7}\ \frac{1}{.234} = 0.00962\ \frac{ft}{sec.}$$

3. Core length $\Delta L = 3.77$ inches $= 0.314$ ft.
4. 1/res. time $= u/L = 0.00962/0.314 = 0.0306$ sec$^{-1}$
5. Max. value of $\Delta\sigma_t^2 = 67$
   Min. value of $\Delta\sigma_t^2 = 40$ } Figure I-3

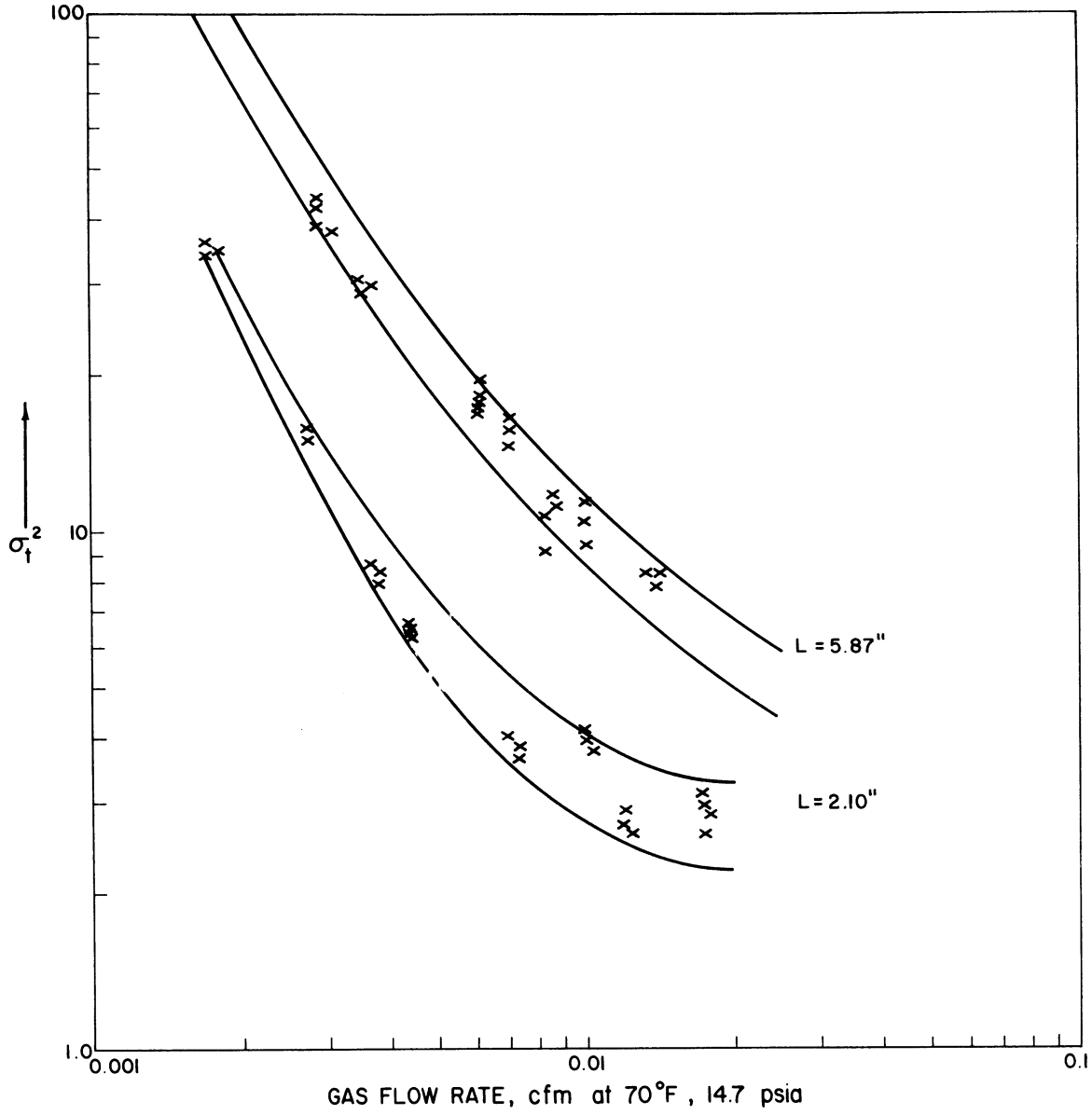


Figure I-2. Variance ($sec^2$) vs. Flow Rate (cfm), Core BA-2, $\phi$ = 23.4%, $\Delta L$ = 3.77", Bandera Sandstone.

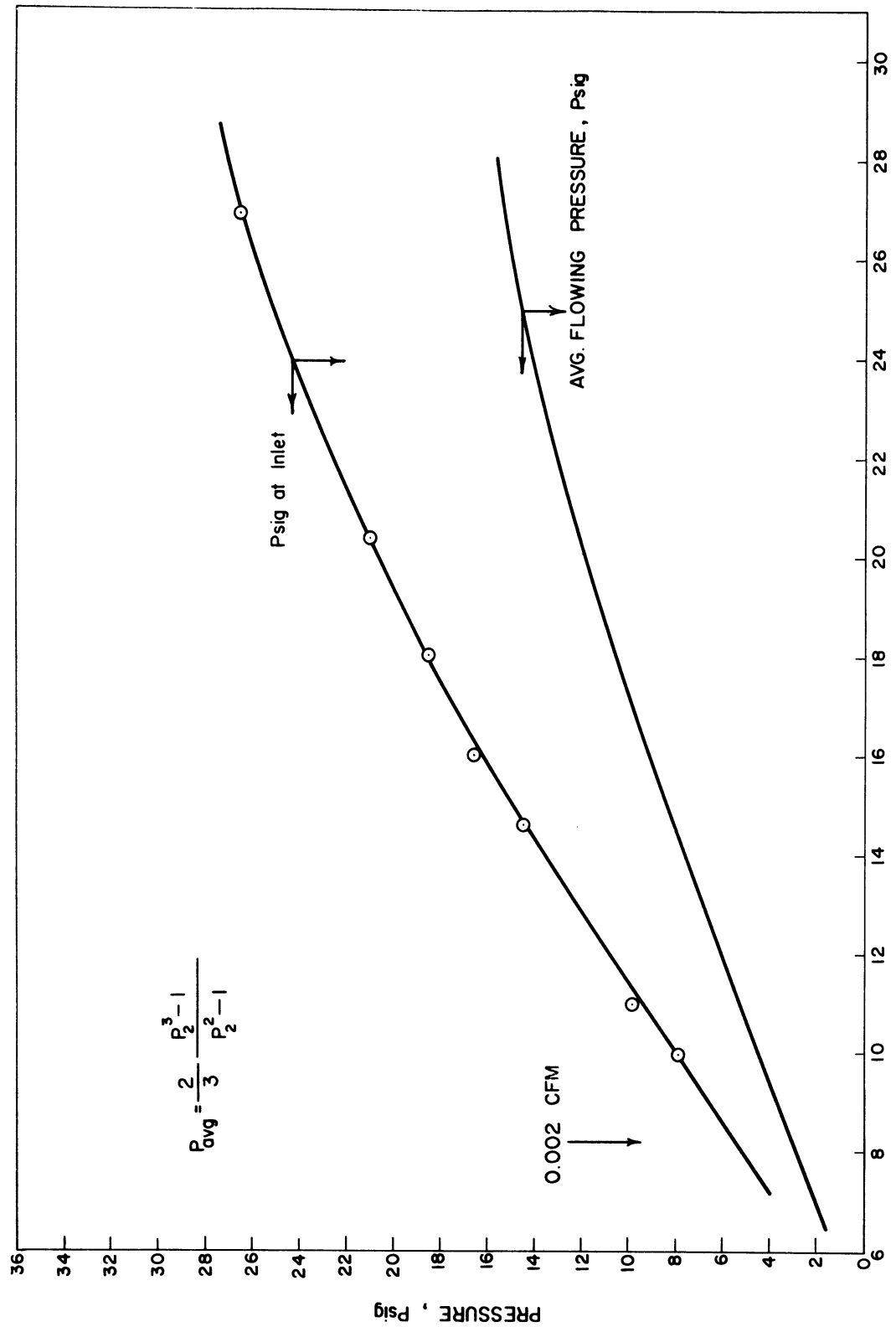


Figure I-3. Inlet Pressure vs. Flow Rate, Core BA-2 + BA-2A.

Max. $\Delta\sigma^2 = \Delta\sigma_t^2 (u/L)^2 = 9.4\times10^{-4} \times 67 = 0.0625$

Min. $\Delta\sigma^2 = \Delta\sigma_t^2 (u/L)^2 = 9.4\times10^{-4} \times 40 = 0.037$

6. $D_\ell = \frac{uL}{2}\Delta\sigma^2 = 0.00962 \frac{ft}{sec} \cdot 0.314\,ft \times 930 \frac{cm^2}{ft^2} \times \frac{\Delta\sigma^2}{2}$

$= 1.4\,\Delta\sigma^2$

$D_{\ell_{max}} = 0.0875\ cm^2/sec$

$D_{\ell_{min}} = 0.052\ cm^2/sec$

$D_o = 2.84/P_{avg} = 2.84/17.7 = 0.16\ cm^2/sec$

7.

$$\left(\frac{D_\ell}{D_o}\right)_{max} = \frac{0.0875}{0.16} = 0.55$$

$$\left(\frac{D_\ell}{D_o}\right)_{min} = \frac{0.052}{0.16} = 0.325$$

APPENDIX II

SUPPLEMENTARY CALCULATIONS

1. The Average Flowing Pressure of a Gas Through a Porous Medium, With Downstream Pressure of One Atmosphere, is Given By:

$$P_{avg} = \frac{2}{3}\left(\frac{P_{in}^3 - 1}{P_{in}^2 - 1}\right),$$

where $P_{in}$=inlet pressure (atm. abs.).

Darcy's Law for Gas Flow:

$$\frac{q}{A} = \frac{K}{\mu'}\left(-\frac{dP}{dL}\right)$$

or, in integrated form, with $P=P(x)$, $x=0$ at inlet:

$$Q = \frac{KA}{2x\mu' P_b}\left(P_{in}^2 - P^2\right)$$

$$y = Z\left(P_{in}^2 - P^2\right), \text{ where } Z = \frac{KA}{2Q\mu' P_b}$$

$$P = \left[P_{in}^2 - \frac{y}{Z}\right]^{1/2}$$

$$P_{avg} = \frac{1}{L}\int_0^L P(x)\,dx = \frac{1}{L}\int_0^L \left[P_{in}^2 - \frac{x}{Z}\right]^{1/2} dx$$

$$= \frac{2}{3}\frac{Z}{L}\left[P_{in}^3 - \left(P_{in}^2 - L/Z\right)^{3/2}\right]$$

But $L/Z = P_{in}^2 - P_{out}^2 = P_{in}^2 - 1$

$$\therefore P_{avg} = \frac{2}{3}\frac{1}{P_{in}^2 - 1}\left(P_{in}^3 - 1\right) = \frac{2}{3}\frac{P_{in}^3 - 1}{P_{in}^2 - 1}$$

2. The Relationship

$$\Delta\sigma_t^2 = \frac{M_2'}{m_0'} - \left(\frac{m_1'}{M_0'}\right)^2$$

Is Valid Even If $M_0$, $M_1$, and $M_2$ are Computed Beginning at $t' = t_0' \neq 0$, and if Estimated Values of $t_0'$ are not Accurate

$$\sigma_t^2 = \frac{\int_0^\infty C(t)(t-\mu^2)\,dt}{\int_0^\infty C(t)\,dt}$$

$$t' = t - t_0$$

where $t$ = real time
$t$ = 0 at pulse injection
$t_0$ = start of injection

$$\mu = \bar{t} = \int_0^\infty C(t)\, t\, dt \Big/ \int_0^\infty C(t)\, dt$$

Now, the integrals calculated by the computer program illustrated in Figure 13 are

$$M_0' = \int_0^\infty C(t)\, dt' = \int_0^\infty C(t)\, dt$$

$$M_1' = \int_0^\infty C(t)\, t'\, dt' = \int_0^\infty C(t)(t - t_0)\, dt$$
$$= \int_0^\infty C(t)\, t\, dt - t_0 \int_0^\infty C(t)\, dt = \int_0^\infty C(t)\, t\, dt - t_0 M_0'$$

$$M_2' = \int_0^\infty C(t)\, t'^2\, dt' = \int_0^\infty C(t)(t - t_0)^2\, dt$$
$$= \int_0^\infty C(t)\, t^2\, dt - 2t_0 \int_0^\infty C(t)\, t\, dt + t_0^2 \int_0^\infty C(t)\, dt$$

Therefore

$$\frac{M_1'}{M_0'} = \frac{\int_0^\infty C(t)\, t\, dt - t_0 M_0'}{M_0'} = \mu - t_0$$

$$\frac{M_2'}{M_0'} = \frac{\int_0^\infty C(t)\, t^2\, dt}{\int_0^\infty C(t)\, dt} - 2t_0 \frac{\int_0^\infty C(t)\, t\, dt}{\int_0^\infty C(t)\, dt} + t_0^2 \frac{\int_0^\infty C(t)\, dt}{\int_0^\infty C(t)\, dt}$$
$$= \frac{\int_0^\infty C(t)\, t^2\, dt}{\int_0^\infty C(t)\, dt} - 2t_0 \mu + t_0^2$$

Hence

$$\frac{M_2'}{M_0'} - \left(\frac{M_1'}{M_0'}\right)^2 = \frac{\int_0^\infty C(t)\, t^2\, dt}{\int_0^\infty C(t)\, dt} - 2t_0\mu + t_0^2 - (\mu - t_0)^2$$
$$= \frac{\int_0^\infty C(t)\, t^2\, dt}{\int_0^\infty C(t)\, dt} - \mu^2$$
$$= \frac{\int_0^\infty C(t)\, (t - \mu)^2\, dt}{\int_0^\infty C(t)\, dt} = \sigma_t^2$$

Q.E.D.

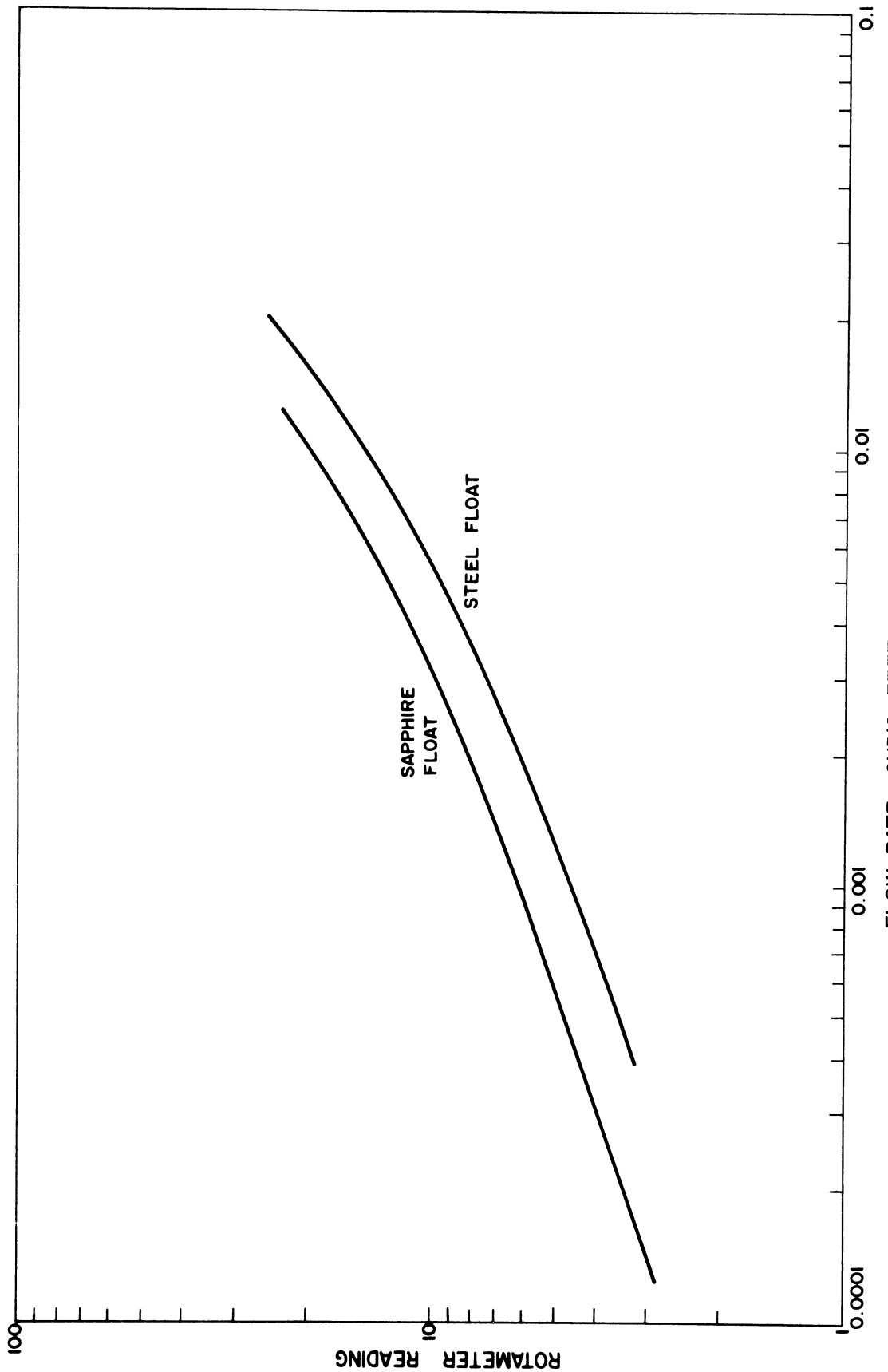


Figure II-1. Rotameter Calibration for Nitrogen at 70°F, 14.7 psia.

APPENDIX III

FIELD APPLICATIONS

The Analysis of a Simple Reservoir Problem

Assume that methane is to be displaced by ethane in a Boise sandstone formation at 2000 psia, 104°F. The sandstone contains interstitial water, which occupies 10% of the pore volume. Assume that there is no effect of overburden pressure or temperature on the electrical resistivity factor (an oversimplification according to Helander, ref. 31). An observed value of the molecular diffusion coefficient has been reported[7] to be $8.4 \times 10^{-4}$ $cm^2/sec$. The Boise sandstone (porosity 32%, permeability 260 md, electrical resistivity factor 9.5) is assumed to have the mixing properties of the sample labeled BO-2 in this manuscript, and it is desired to estimate the effective longitudinal dispersion coefficient at superficial flow rates of $3 \times 10^{-3}$ cm/sec and $3 \times 10^{-2}$ cm/sec.

From the tabulated results in Tables II and III, $m \cong 1.1$ and $d_p\sigma \cong 0.6$ cm in the equation

$$\frac{D_e}{D_o} = \frac{1}{F\Phi} + 0.5\left(\frac{u d_p \sigma}{D_o}\right)^m \qquad (9b)$$

(NOTE: Experimental values of the molecular diffusion coefficient should always be sought for systems of more than two components, since mathematical approximations are not only cumbersome but subject to considerable error.)

Peclet numbers are first computed, converting the given superficial velocities to interstitial velocities:

For $v = 3\times10^{-3}\ \frac{cm}{sec}$, $u = \frac{3\times10^{-3}}{0.32(1-0.1)} = 1.05\times10^{-3}\ \frac{cm}{sec}$

and

$$\mathrm{Pe} = \frac{u d_p \rho}{D_0} = \frac{1.05 \times 10^{-3} \times 0.6}{8.4 \times 10^{-4}} = 0.75$$

For $v = 3 \times 10^{-2}$ cm/sec , $\mathrm{Pe} = 7.5$

$$\frac{1}{F\phi} = \frac{1}{9.5 \times 0.32 \times 0.9} = 0.366$$ (approximate, since the value of the resistivity factor obtained for the dry core will be too low when an immobile phase is present.)

Hence

$$\frac{D_e}{D_0} \simeq 0.366 + 0.5\,\mathrm{Pe}^{1.1}$$

For $v = 3 \times 10^{-3}$ cm/sec

$$\frac{D_e}{D_0} = 0.366 + 0.5\,(0.75)^{1.1} = 0.73$$

$$D_e = 0.73\,(8.4 \times 10^{-4}) = \underline{6.1 \times 10^{-4}\ \mathrm{cm^2/sec}}$$

For $v = 3 \times 10^{-2}$ cm/sec

$$\frac{D_e}{D_0} = 0.366 + 0.5\,(7.5)^{1.1} = 5.0$$

$$D_e = 5.0\,(8.4 \times 10^{-4}) = \underline{42 \times 10^{-4}\ \mathrm{cm^2/sec}}$$